NASA Technical Memorandum 89435

Two-Dimensional Aerodynamic Characteristics of the OLS/TAAT Airfoil

Michael E. Watts and Jeffrey L. Cross
Ames Research Center
Moffett Field, California

Kevin W. Noonan
Aerostructures Directorate
USAARTA-AVSCOM
Langley Research Center
Hampton, Virginia

NASA
National Aeronautics
and Space Administration

Scientific and Technical Information Division

1988

SYMBOLS

C_p static-pressure coefficient, $C_p = \dfrac{p - p_\infty}{(1/2)\rho V_\infty^2}$

c airfoil chord, in.

c_d section profile-drag coefficient, $c_d = \sum\limits_{\text{wake}} c_d' \dfrac{\Delta h}{c}$

c_d' point-drag coefficient,

$$c_d' = 2 \left(\frac{p}{p_\infty}\right)^{6/7} \left[\frac{(p_t/p)^{2/7} - 1}{(p_{t,\infty}/p_\infty)^{2/7} - 1}\right]^{1/2} \left\{\left(\frac{p_t}{p_{t,\infty}}\right)^{1/7} - \left[\frac{(p_t/p_\infty)^{2/7} - 1}{(p_{t,\infty}/p_\infty)^{2/7} - 1}\right]^{1/2}\right\}$$

c_l section lift coefficient, $c_l = c_n \cos(\alpha) - (c_d - c_n \sin(\alpha))\tan(\alpha)$

c_m section pitching-moment coefficient about quarter-chord

c_n section normal-force coefficient, $c_n = \sum\limits_{\text{u.s.}} C_p(\Delta x/c) + \sum\limits_{\text{l.s.}} C_p(\Delta x/c)$

h height of wake-survey probe tubes from given reference plane, in.

M Mach number

P pressure, psi

p static pressure, psi

Q dynamic pressure, psi

R_n Reynolds number based on airfoil chord and free-stream conditions

t airfoil thickness, in.

v velocity, ft/sec

x airfoil abscissa, in.

z airfoil ordinate, in.

α_c angle of attack corrected for lift-interference effects, deg

ρ density, slugs/ft^3

Subscripts:

t total

∞ free stream

PRECEDING PAGE BLANK NOT FILMED

PAGE __ii__ INTENTIONALLY BLANK

TWO-DIMENSIONAL AERODYNAMIC CHARACTERISTICS OF THE OLS/TAAT AIRFOIL

Michael E. Watts, Jeffrey L. Cross, and Kevin W. Noonan*

Ames Research Center

SUMMARY

Two flight tests have been conducted that obtained extensive pressure data on a modified AH-1G rotor system. These two tests, the Operational Loads Survey (OLS) and the Tip Aerodynamics and Acoustics Test (TAAT) used the same rotor set. In the analysis of these data bases, accurate two-dimensional airfoil data is invaluable, for not only does it allow comparison studies between two- and three-dimensional flow, but it also provides accurate tables of the airfoil characteristics for use in comprehensive rotorcraft analysis codes. To provide this two-dimensional data base, a model of the OLS/TAAT airfoil was tested over a Reynolds number range from 3×10^6 to 7×10^6 and between Mach numbers of 0.34 to 0.88 in the NASA Langley Research Center's 6- by 28-Inch Transonic Tunnel. The two-dimensional airfoil data is presented as chordwise pressure coefficient plots, as well as lift, drag, and pitching-moment coefficient plots and tables.

INTRODUCTION

Two flight tests have been conducted that obtained extensive pressure data on a modified AH-1G rotor system. These two tests, the Operational Loads Survey (OLS) and the Tip Aerodynamics and Acoustics Test (TAAT) used the same rotor set. In the analysis of these data bases, accurate two-dimensional airfoil data is invaluable, for not only does it allow comparison studies between two- and three-dimensional flow, but it also provides accurate tables of the airfoil characteristics for use in comprehensive rotorcraft analysis codes. To provide this two-dimensional data base, a model of the OLS/TAAT airfoil was tested over a Reynolds number range from 3×10^6 to 7×10^6 and between Mach numbers of 0.34 to 0.88 in the NASA Langley Research Center's 6- by 28-Inch Transonic Tunnel by the Langley Research Center's staff in 1983. The authors would like to acknowledge the support of Mr. Gene J. Bingham at Langley Research Center for his assistance with the conduct of this test.

The two-dimensional airfoil data is presented here so that it will be available for future correlation with the flight data available in the OLS/TAAT data base. The data is presented as chordwise pressure coefficient plots, as well as lift-, drag-, and pitching-moment-coefficient plots and tables.

TEST FACILITY

This test was conducted at the Langley Research Center's 6- by 28-Inch Transonic Tunnel. The pertinent tunnel specifications, obtained from references 1 and 2, are presented in table I, and drawings of the tunnel are presented in figures 1 and 2. The wind tunnel has solid sidewalls with a slotted floor and ceiling. The slots consist of four longitudinal half slots along the junction of the tunnel's floor, ceiling, and sidewalls. The slots provide the tunnel with a 5% openness ratio with the flow that passes through the slots reentering the main flow aft of the model. This bypass process is controlled by a set of flaps located 12.75 in. downstream from the test section center. The rectangular test section extends from 38 in. upstream of the center to 44.25 in. downstream. The sidewalls of the test tection house 9.5-in. diam turntables that support the model. The tunnel gets its supply of dry, compressed air from the 26-in. Transonic Blowdown Tunnel situated below the 6- by 28-Inch Tunnel.

The tunnel has four primary control systems that regulate Mach number, stagnation pressure, model angle of attack, and flow control. The tunnel Mach number is controlled by two sliding choker doors located downstream of the test section. The stagnation pressure is controlled with a valve control system that allows for constant Reynolds number testing. The turntables are controlled, as are the primary controls, by a closed-loop servovalve system. The flap system, mentioned earlier, is manually operated using an electrical drive system.

*Aerostructures Directorate, U.S. Army Aviation Research and Technology Activity, Langley Research Center, Hampton, Virgina.

TEST SET-UP AND INSTRUMENTATION

The wind tunnel instrumentation system has the capability of measuring a total of 64 channels of pressure measurements. These pressure measurements are broken into four primary groupings of measurements. The first set consists of model static pressure orifices and are generally aligned in a chordwise array so as to measure the static pressure distribution characteristics of that airfoil. The model static pressure measurements are used in the calculations of the section lift and pitching-moment coefficients. The second instrumentation set is a traversing survey probe which measures the pressure in the flow aft of the model. The airfoil drag measurements are obtained with the use of the pressures measured by this traversing rake (fig. 3). The rake can be traversed from 10 in. above to 10 in. below tunnel centerline. The computation of drag requires the use of static pressure measured downstream of the model by the third set of instrumentation. A fourth set of instrumentation is used to measure free-stream total and static pressures.

The model tested was a symmetrical airfoil known as the OLS/TAAT airfoil, which is a slightly modified Bell 540 airfoil. The 540 was the standard airfoil used on the rotor of the AH-1 series of helicopters. The OLS/TAAT airfoil was obtained by adding a 0.1-in.-thick glove to the basic 540, and extending the trailing edge to obtain a blade thickness ratio of 9.71%. The full-scale airfoil coordinates are presented in appendix A. The 6-in. chord model was constructed out of stainless steel, and contained a pressure tap at the leading edge with 22 pressure tap locations on each of the top and bottom surface for a total of 45 ports. The exact chordwise pressure tap locations are presented in table II. The model was constructed to contour tolerances of $\pm 5.0 \times 10^{-4}$ in.

PRESENTATION OF RESULTS

Table III presents the test conditions that were obtained during this investigation arranged by Mach and corrected angle of attack. To produce the airfoil sectional normal force and pitching moment coefficients, the pressure coefficient data have been integrated about the airfoil, using a spline integration routine. The airfoil sectional drag coefficients have been calculated from the rake array data using the standard 6- by 28-Inch Tunnel data processing computational procedure. The lift coefficient has been obtained from the drag and normal force coefficients. The nondimensional aerodynamic coefficient results are presented in the figures called out in table IV and the tabular results are presented in table V. The tabular results are grouped by Mach number and angle of attack. Through each angle of attack sweep the Mach number and Reynolds number shifted slightly; However, the values given in these figures are the nominal values during each sweep.

TWO DIMENSIONALITY OF FLOW

The results of a previous investigation of rotorcraft airfoils in the Langley Research Center's 6- by 28-Inch Transonic Tunnel (ref. 3) have shown that the indicated maximum normal-force coefficient is reduced by tunnel-wall boundary-layer influences. This reduction is characteristic of two-dimensional wind tunnels without proper sidewall boundary-layer control and occurs because the tunnel-wall boundary layer is thicker than that of the airfoil; therefore, initial separation begins at the tunnel wall.

Although it is not possible to determine precisely the affected Mach number range or the loss in maximum normal-force coefficient of the airfoils reported herein, a comparison of the NACA 0012 data measured in this facility with 0.05 open slots with unpublished data from two other facilities has been useful in indicating the magnitude of these losses. The maximum normal-force coefficients measured in the Langley Research Center's Low-Turbulence Pressure Tunnel and the United Technologies Research Center 8-Foot Subsonic/Transonic Wind Tunnel at similar Reynolds numbers and at a Mach number of 0.36 are higher than that from the Langley Research Center's 6- by 28-Inch Transonic Tunnel by about 0.15. The difference between the data from the Langley Research Center's 6- by 28-Inch Transonic Tunnel and the United Technologies Research Center's data decreased to 0.05 at a Mach number of about 0.53. Incremental values for other airfoils may vary slightly because of specific configuration influences.

An investigation conducted in the Office National d'Études et de Recherches Aérospatiale (ONERA) R1 Ch wind tunnel (ref. 4) has shown that the tunnel sidewall boundary layer can affect the normal-force coefficients at all angles of attack (that is, with either attached or separated boundary layers). In this investigation, the sidewall boundary layer thickness was varied by applying sidewall suction upstream of the model while the Mach number and Reynolds number were held constant. Generally, an increase in sidewall boundary layer thickness resulted in a decrease in the normal-force coefficient at a given angle of attack; the trend reversed at Mach numbers greater than 0.85 with a supercritical airfoil.

CORRECTION FOR LIFT INTERFERENCE

The corrections for lift interference, which have been applied to the angles of attack, were obtained from references 5 and 6. The basic equations for the correction are

$$\alpha_c = \alpha + \Delta\alpha$$

where

$$\Delta\alpha = \frac{-c_n}{8}\left(\frac{c}{36.195}\right)\left(\frac{1}{k+1}\right)\left(\frac{180}{\pi}\right)$$

$$k = \frac{a}{h} K$$

where a is the slot spacing and h is the semiheight of the tunnel. The slotted-wall boundary condition coefficient k for the present tunnel configuration is 0.4211K. A value of 3.5 was selected for the slotted-wall performance coefficient K, based on the data and discussion presented in reference 6. These substitutions yield a correction given by the equation

$$\Delta\alpha = -c_n c(0.0800)$$

where c is in centimeters, α is in degrees, and the constant of 0.08 is in degrees per centimeter.

CONCLUSION

An investigation was conducted in the Langley Research Center's 6- by 28-Inch Transonic Wind Tunnel to determine the two-dimensional aerodynamic characteristics of the OLS/TAAT airfoil. The tests were conducted at Reynolds numbers of 3.0×10^6 to 7.0×10^6, typical of full scale R_n at a Mach number range from 0.34 to 0.88. The results of this investigation are presented as both chordwise-pressure coefficient plots, and integrated lift, drag and pitching-moment coefficient plots.

APPENDIX A

Appendix A contains the upper surface ordinates of the OLS/TAAT full scale airfoil in inches. The x dimension is distance along the chord mean line with 0.0 being the leading edge and z is the distance from the mean line. The airfoil is symmetrical, therefore the lower surface ordinates are the negative of the z value.

TABLE A1.– OLS/TAAT FULL SCALE AIRFOIL COORDINATES

X (In.)	Z (In.)	X (In.)	Z (In.)
0.0	0.0	4.42296	1.34029
0.12969	0.33318	4.52340	1.34556
0.24679	0.44944	4.62383	1.35049
0.35811	0.53187	4.72425	1.35510
0.46632	0.59781	4.82465	1.35939
0.57262	0.65363	4.92505	1.36337
0.67767	0.70244	5.02544	1.36704
0.78185	0.74604	5.12582	1.37042
0.88538	0.78554	5.22618	1.37351
0.98843	0.82172	5.32654	1.37531
1.09110	0.85512	5.42690	1.37885
1.19346	0.88613	5.52724	1.38111
1.29558	0.91508	5.62757	1.38311
1.39750	0.94222	5.72790	1.38486
1.49925	0.96772	5.82822	1.38636
1.60085	0.99177	5.92854	1.38760
1.70233	1.01448	6.02884	1.38861
1.80371	1.03598	6.12914	1.38939
1.90499	1.07571	6.22944	1.38994
2.10731	1.09409	6.32973	1.39026
2.20837	1.11157	6.43001	1.39036
2.30937	1.12820	6.53029	1.39024
2.41032	1.14404	6.63056	1.38992
2.51122	1.15913	6.73082	1.38938
2.61208	1.17350	6.83108	1.38865
2.71290	1.18720	6.93134	1.38771
2.81368	1.20026	7.03159	1.38658
2.91443	1.21271	7.13184	1.38526
3.01515	1.22457	7.23208	1.38375
3.11585	1.23587	7.33231	1.38206
3.21651	1.24663	7.43255	1.38018
3.31715	1.25687	7.53277	1.37813
3.41777	1.26662	7.63300	1.37590
3.51837	1.27589	7.73322	1.37351
3.61894	1.28470	7.83343	1.37094
3.71950	1.29306	7.93364	1.36821
3.82004	1.30099	8.03385	1.36532
3.92057	1.30851	8.13406	1.36227
4.02107	1.31562	8.23426	1.35907
4.12157	1.32234	8.33446	1.35571
4.22204	1.32869	8.43465	1.35220
4.32251	1.33466	8.53484	1.34854

TABLE A1.– CONTINUED

X (In.)	Z (In.)	X (In.)	Z (In.)
8.63503	1.34473	13.63853	1.04460
8.73521	1.34079	13.73853	1.03803
8.83539	1.33670	13.83853	1.03145
8.93557	1.33247	13.93853	1.02488
9.03574	1.32811	14.03853	1.01831
9.13592	1.32361	14.13853	1.01173
9.23608	1.31898	14.23853	1.00516
9.33625	1.31423	14.33853	0.99859
9.43641	1.30934	14.43853	0.99202
9.53658	1.29920	14.53853	0.98544
9.73689	1.29394	14.63853	0.97887
9.83704	1.28857	14.73853	0.97230
9.93719	1.28308	14.83853	0.96572
10.03734	1.27747	14.93853	0.95915
10.13749	1.27174	15.03853	0.95258
10.23763	1.26591	15.13853	0.94600
10.33778	1.25996	15.23853	0.93943
10.43792	1.25391	15.33853	0.93286
10.53805	1.24775	15.43853	0.92628
10.63819	1.24148	15.53853	0.91971
10.73832	1.23511	15.63853	0.91314
10.83845	1.22864	15.73853	0.90656
10.89478	1.22495	15.83853	0.89999
10.93853	1.22208	15.93853	0.89342
11.03853	1.21550	16.03853	0.88684
11.13853	1.20893	16.13850	0.88027
11.23853	1.20236	16.23849	0.87370
11.33853	1.19578	16.33850	0.86713
11.43853	1.18921	16.43851	0.86055
11.53853	1.18264	16.53850	0.85398
11.63853	1.17606	16.63850	0.84741
11.73853	1.16949	16.73849	0.84083
11.83853	1.16292	16.83850	0.83426
11.93853	1.15634	16.93851	0.82769
12.03853	1.14977	17.03850	0.82111
12.13853	1.14320	17.13850	0.81454
12.23853	1.13662	17.23849	0.80797
12.33853	1.13005	17.33850	0.80139
12.43853	1.12348	17.43851	0.79482
12.53853	1.11691	17.53850	0.78825
12.63853	1.11033	17.63850	0.78167
12.73853	1.10376	17.73849	0.77510
12.83853	1.09719	17.83850	0.76853
12.93853	1.09061	17.93851	0.76195
13.03853	1.08404	18.03850	0.75538
13.13853	1.07747	18.13850	0.74881
13.23853	1.07089	18.23849	0.74224
13.33853	1.06432	18.33850	0.73566
13.43853	1.05775	18.43851	0.72909
13.53853	1.05117	18.53850	0.72252

TABLE A1.– CONCLUDED

X (In.)	Z (In.)	X (In.)	Z (In.)
18.63850	0.71594	23.63850	0.38728
18.73849	0.70937	23.73849	0.38071
18.83850	0.70280	23.83850	0.37414
18.93851	0.69622	23.93851	0.36756
19.03850	0.68965	24.03850	0.36099
19.13850	0.68308	24.13850	0.35442
19.23849	0.67650	24.23849	0.34784
19.33850	0.66993	24.33850	0.34127
19.43851	0.66336	24.43851	0.33470
19.53850	0.65678	24.53850	0.32813
19.63850	0.65021	24.63850	0.32155
19.73849	0.64364	24.73849	0.31498
19.83850	0.63706	24.83850	0.30841
19.93851	0.63049	24.93851	0.30183
20.03850	0.62392	25.03850	0.29526
20.13850	0.61734	25.13850	0.28869
20.23849	0.61077	25.23849	0.28211
20.33850	0.60420	25.33850	0.27554
20.43851	0.59762	25.43851	0.26897
20.53850	0.59105	25.53850	0.26239
20.63850	0.58448	25.63850	0.25582
20.73849	0.57791	25.73851	0.24925
20.83850	0.57133	25.83850	0.24267
20.93851	0.56476	25.93851	0.23610
21.03850	0.55819	26.03850	0.22953
21.13850	0.55161	26.13850	0.22295
21.23849	0.54504	26.23851	0.21638
21.33850	0.53847	26.33850	0.20981
21.43851	0.53189	26.43851	0.20323
21.53850	0.52532	26.53850	0.19666
21.63850	0.61875	26.63850	0.19009
21.73849	0.51217	26.73851	0.18351
21.83850	0.50560	26.83850	0.17694
21.93851	0.49903	26.93851	0.17037
22.03850	0.49245	27.03850	0.16380
22.13850	0.48588	27.13850	0.15722
22.23849	0.47931	27.23851	0.15065
22.33850	0.47273	27.33850	0.14408
22.43851	0.46616	27.43851	0.13750
22.53850	0.45959	27.53850	0.13093
22.63350	0.45302	27.63850	0.12438
22.73849	0.44044	27.73851	0.11778
22.83850	0.43967	27.83850	0.11121
22.93851	0.43330	27.93851	0.10464
23.03850	0.42672	28.13850	0.09149
23.13850	0.42014	28.23851	0.08492
23.23849	0.41358	28.33850	0.07834
23.33850	0.40700	28.43851	0.07177
23.43851	0.40043	28.53850	0.06520
23.53850	0.39380	28.63850	0.05862

REFERENCES

1. Ladson, Charles L.: Description and Calibration of the Langley 6- by 28-Inch Transonic Tunnel. NASA TN D-8070, 1975.
2. Sewell, W. G.: Description of Recent Changes in the Langley 6- by 28-Inch Transonic Tunnel. NASA TM-81947, 1981.
3. Noonan, Kevin W.; and Bingham, Gene J.: Two-Dimensional Aerodynamic Characteristics of Several Rotorcraft Airfoils at Mach Numbers From 0.35 to 0.90. NASA TM X-73990, 1977.
4. Bernard-Guelle, Rene: Influence of Wind Tunnel Wall Boundary Layers on Two Dimensional Transonic Tests. NASA TT F-17,255, 1976.
5. Barnwell, Richard W.: Design and Performance Evaluation of Slotted Walls for Two Dimensional Wind Tunnels, NASA TM-78648, 1978.
6. Davis, Don D., Jr.; and Moore, Dewey: Analytical Study of Blockage- and Lift-Interference Corrections for Slotted Tunnels Obtained by the Substitution of an Equivalent Homogeneous Boundary for the Discrete Slots. NACA RM L53E07b, 1953.

TABLE I.– LANGLEY 6- BY 28-INCH TRANSONIC WIND TUNNEL CHARACTERISTICS

Tunnel Size	6- by 28-in.
Speed Range	0.3 to 1.2 Mach
Temperature Range	Ambient
Reynolds Number	4.0 to 25x10^6 /foot
Dynamic Pressure	256 to 5387 lb/ft^2
Stagnation Pressure	30 to 90 psia
Model Size	up to 6-in. chord
Test Medium	Air
Run Time	30 to 300 sec.

TABLE II.– COORDINATES OF PRESSURE TAP LOCATIONS ON 6-IN. MODEL

ORIFICE	x/c	z/c	ORIFICE	x/c	z/c
1	0.0000	0.0000			
2	0.0095	-0.0165	24	0.0096	0.0166
3	0.0297	-0.0271	25	0.0297	0.0270
4	0.0493	-0.0331	26	0.0497	0.0333
5	0.0664	-0.0369	27	0.0667	0.0370
6	0.0995	-0.0422	28	0.0997	0.0423
7	0.1501	-0.0469	29	0.1494	0.0469
8	0.2002	-0.0486	30	0.1995	0.0487
9	0.2498	-0.0486	31	0.2498	0.0486
10	0.3004	-0.0470	32	0.2999	0.0471
11	0.3501	-0.0446	33	0.3499	0.0446
12	0.4001	-0.0413	34	0.4001	0.0414
13	0.4500	-0.0381	35	0.4497	0.0381
14	0.5002	-0.0349	36	0.4998	0.0349
15	0.5502	-0.0317	37	0.5497	0.0316
16	0.6001	-0.0284	38	0.5996	0.0283
17	0.6502	-0.0250	39	0.6499	0.0250
18	0.7001	-0.0218	40	0.6999	0.0218
19	0.7504	-0.0185	41	0.7501	0.0185
20	0.8003	-0.0152	42	0.7995	0.0152
21	0.9000	-0.0087	43	0.8996	0.0086
22	0.9203	-0.0073	44	0.9200	0.0073
23	0.9752	-0.0036	45	0.9746	0.0037

TABLE III.– TEST CONDITIONS

Mach No.	α_c	Run No.	Test Point	p_∞	p Ref.	P_t	Q_∞	R_n x10^6	Temp. °F
0.338	-3.51	2	15	55.77	55.09	60.34	4.45	4.70	57.34
0.339	-1.78	2	14	55.19	54.54	59.76	4.44	4.63	61.18
0.346	0.02	1	2	55.29	54.60	60.06	4.63	4.63	70.57
0.332	0.02	19	135	57.12	56.26	61.65	4.41	4.68	61.51
0.345	1.87	19	136	55.79	55.09	60.57	4.64	4.81	57.32
0.336	1.87	1	3	55.81	55.09	60.34	4.41	4.57	66.92
0.343	3.61	19	137	54.85	54.24	59.50	4.51	4.71	56.76
0.345	5.36	19	138	55.26	54.61	60.00	4.60	4.76	57.93
0.339	7.13	1	6	55.57	54.83	60.19	4.48	4.64	63.85
0.339	7.16	19	139	55.41	54.77	59.99	4.45	4.69	57.26
0.337	8.06	1	7	55.52	54.79	60.06	4.41	4.61	62.43
0.336	8.95	1	8	55.45	54.72	59.97	4.39	4.62	60.33
0.338	9.92	1	9	55.57	54.81	60.13	4.44	4.67	58.40
0.337	10.90	1	10	55.49	54.71	60.04	4.42	4.69	56.41
0.340	11.97	1	11	55.44	54.66	60.06	4.49	4.75	53.91
0.391	-3.51	4	30	54.11	53.41	60.14	5.80	5.28	61.75
0.389	-1.68	4	29	54.34	53.67	60.33	5.77	5.22	65.70
0.390	-0.05	4	28	54.06	53.37	60.04	5.76	5.19	67.41
0.394	0.00	3	18	54.00	53.32	60.09	5.86	5.24	67.02
0.389	1.69	3	19	54.35	53.68	60.33	5.75	5.31	58.44
0.391	3.43	3	20	54.07	53.42	60.09	5.79	5.39	53.41
0.392	5.24	3	21	54.16	53.48	60.20	5.81	5.49	46.94
0.391	7.05	3	22	54.15	53.46	60.16	5.78	5.56	41.25
0.392	7.94	3	23	54.21	53.50	60.27	5.83	5.65	36.76
0.391	8.84	3	24	54.22	53.48	60.25	5.81	5.69	33.42
0.391	9.99	3	25	54.05	53.30	60.04	5.77	5.73	28.28

TABLE III.– CONTINUED

Mach No.	α_c	Run No.	Test Point	p_∞	p Ref.	P_t	Q_∞	R_n x10^6	Temp. °F
0.438	-3.43	6	45	52.74	51.98	60.16	7.08	5.99	49.55
0.445	-1.70	6	44	52.69	51.99	60.36	7.30	6.00	56.02
0.437	0.00	5	32	52.63	51.89	60.01	7.04	5.78	62.64
0.434	1.70	5	33	52.75	52.02	60.02	6.94	5.79	59.57
0.437	3.53	5	34	52.58	51.85	59.94	7.02	5.85	56.87
0.438	5.31	5	35	52.73	51.97	60.17	7.09	5.94	53.55
0.440	7.19	5	36	52.36	51.57	59.79	7.08	5.98	49.05
0.440	8.07	5	38	52.54	51.73	60.00	7.11	6.10	42.70
0.435	8.94	5	39	52.80	51.98	60.14	7.00	6.12	39.18
0.433	9.95	5	40	52.83	51.97	60.07	6.92	6.14	35.68
0.430	11.01	5	41	52.79	51.90	59.96	6.85	6.18	30.77
0.496	-3.52	7	49	50.48	49.68	59.74	8.71	6.52	53.74
0.491	-3.50	22	150	51.02	50.28	60.17	8.62	6.43	59.03
0.491	-1.78	7	48	51.30	50.53	60.50	8.67	6.49	57.52
0.491	-1.71	21	147	50.92	50.22	60.04	8.60	6.41	59.43
0.496	0.01	21	146	51.08	50.26	60.44	8.81	6.44	63.59
0.485	0.00	22	149	50.94	50.26	59.84	8.39	6.27	63.14
0.498	1.81	22	151	50.62	49.87	59.96	8.79	6.55	54.60
0.496	3.42	22	152	50.82	50.06	60.13	8.75	6.63	49.99
0.491	5.19	22	153	51.05	50.26	60.18	8.61	6.64	45.95
0.491	7.05	22	154	50.99	50.19	60.13	8.61	6.71	41.69
0.488	7.13	7	54	51.45	50.63	60.55	8.58	6.84	35.42
0.491	8.00	22	155	51.03	50.20	60.16	8.61	6.80	37.02
0.486	8.06	7	55	51.23	50.39	60.20	8.47	6.85	31.25
0.487	8.95	22	156	50.94	50.08	59.93	8.47	6.81	32.46
0.487	9.08	7	56	51.26	50.38	60.27	8.49	6.95	26.61
0.488	10.00	22	157	50.82	49.93	59.82	8.48	6.90	27.65

TABLE III.– CONTINUED

Mach No.	α_c	Run No.	Test Point	p_∞	p Ref.	P_t	Q_∞	R_n x10^6	Temp. °F
0.541	-3.50	8	61	49.31	48.39	60.17	10.10	6.96	57.39
0.545	-1.80	8	60	49.07	48.31	60.04	10.19	6.95	59.31
0.530	-0.03	8	59	49.79	48.92	60.29	9.79	6.56	75.84
0.548	-0.03	8	62	48.94	48.17	60.04	10.30	7.06	54.65
0.542	1.78	8	63	49.28	48.48	60.20	10.15	7.10	50.54
0.535	3.61	8	64	49.82	48.98	60.55	10.00	7.13	47.28
0.535	5.34	8	65	49.37	48.50	59.98	9.89	7.15	42.15
0.533	7.17	8	66	49.39	48.44	59.92	9.81	7.16	39.92
0.534	8.17	8	67	49.37	48.37	59.95	9.85	7.25	36.28
0.586	-3.45	9	72	47.47	46.65	59.90	11.41	7.41	54.35
0.600	-1.81	9	71	47.09	46.32	60.05	11.86	7.51	56.32
0.586	-0.07	9	70	47.68	46.92	60.14	11.44	7.32	60.57
0.594	-0.01	9	73	47.28	46.53	60.03	11.68	7.53	52.60
0.589	1.77	9	74	47.60	46.82	60.19	11.56	7.55	49.85
0.583	3.45	9	76	47.72	46.93	60.05	11.34	7.66	40.23
0.586	5.28	9	77	47.56	46.71	60.01	11.43	7.86	32.03
0.582	7.17	9	78	47.67	46.72	59.96	11.30	7.89	28.40
0.638	-3.52	10	82	45.83	44.95	60.29	13.07	7.87	56.13
0.635	-1.66	10	81	45.57	44.75	59.79	12.87	7.76	57.09
0.639	-0.03	10	80	46.15	45.31	60.73	13.18	7.83	61.44
0.641	0.02	10	83	45.90	45.09	60.52	13.21	8.00	52.26
0.643	1.77	10	84	45.79	44.98	60.46	13.24	8.12	47.16
0.642	3.51	10	85	45.77	44.90	60.41	13.22	8.20	42.82
0.638	5.27	10	86	45.55	44.59	59.92	12.99	8.26	35.12
0.635	7.24	10	87	45.85	44.76	60.15	12.95	8.37	30.31

TABLE III.– CONTINUED

Mach No.	α_c	Run No.	Test Point	p_∞	p Ref.	P_t	Q_∞	R_n x10^6	Temp. °F
0.686	-3.44	12	93	44.25	43.22	60.64	14.59	8.29	56.41
0.687	-1.71	12	92	43.73	42.82	59.93	14.43	8.16	58.39
0.683	-0.01	12	91	44.19	43.28	60.35	14.41	8.08	63.49
0.695	0.06	12	94	43.86	42.89	60.55	14.82	8.44	51.73
0.687	1.78	12	95	44.02	43.11	60.37	14.55	8.49	45.58
0.690	3.49	12	96	43.76	42.76	60.19	14.60	8.58	41.50
0.686	5.29	12	97	44.23	43.08	60.61	14.58	8.74	35.52
0.737	-3.42	13	102	41.78	40.65	59.91	15.86	8.65	51.47
0.747	-1.72	13	101	41.63	40.67	60.30	16.27	8.68	56.06
0.731	-0.02	13	100	42.83	41.80	61.12	16.03	8.61	59.73
0.736	0.00	13	103	41.94	40.99	60.11	15.90	8.79	46.30
0.735	1.71	13	104	42.16	41.14	60.37	15.94	8.92	42.12
0.732	3.45	13	105	42.20	41.08	60.24	15.81	9.01	36.50
0.736	4.34	13	106	41.94	40.75	60.09	15.88	9.17	30.04
0.781	-3.41	14	110	40.12	38.97	60.00	17.11	8.81	57.38
0.791	-1.64	14	109	39.96	38.97	60.39	17.51	8.86	60.46
0.789	-0.07	14	108	39.46	38.58	59.50	17.19	8.62	65.09
0.785	1.66	14	111	40.36	39.38	60.59	17.39	8.97	55.32
0.783	2.54	14	112	40.45	39.39	60.63	17.35	9.11	49.15
0.781	3.39	14	113	40.16	39.03	60.05	17.13	9.15	43.10
0.822	-3.29	15	117	38.83	37.58	60.53	18.37	9.25	51.78
0.829	-1.73	15	116	38.17	37.08	59.89	18.35	9.10	55.50
0.829	-0.05	15	115	38.50	37.49	60.43	18.53	9.05	61.39
0.828	1.64	15	118	38.42	37.34	60.22	18.43	9.39	45.29
0.825	2.47	15	119	38.67	37.49	60.43	18.41	9.53	40.11
0.825	3.44	15	120	38.66	37.39	60.41	18.40	9.64	35.66

TABLE III.– CONCLUDED

Mach No.	α_c	Run No.	Test Point	p_∞	p Ref.	P_t	Q_∞	R_n x10^6	Temp. °F
0.876	-3.49	18	131	36.30	34.95	59.86	19.51	9.65	42.10
0.881	-1.65	18	130	36.51	35.28	60.50	19.83	9.56	50.67
0.887	1.64	18	132	36.23	35.00	60.43	19.96	9.93	36.83
0.873	2.54	18	133	36.79	35.52	60.43	19.61	10.10	27.88

TABLE IV.– TABLE OF FIGURES OF COEFFICIENT RESULTS

Mach	α_c	Figure Number for C_p versus x/c	Figure Number for c_l, c_d, & c_m versus α_c
0.34	-3.5 → 12.0	4	16
0.39	-3.5 → 10.0	5	17
0.44	-3.4 → 11.0	6	18
0.49	-3.5 → 10.0	7	19
0.54	-3.5 → 8.2	8	20
0.59	-3.5 → 7.2	9	21
0.64	-3.5 → 7.2	10	22
0.69	-3.4 → 5.3	11	23
0.74	-3.4 → 4.3	12	24
0.78	-3.4 → 3.4	13	25
0.83	-3.3 → 3.4	14	26
0.88	-3.5 → 2.5	15	27

TABLE V.– DERIVED AERODYNAMIC COEFFICIENTS

Mach	α_c	c_n	c_l	c_d	$c_{m1/4}$
0.338	-3.51	-0.4591	-0.4594	0.0077	0.0034
0.339	-1.78	-0.2263	-0.2261	0.0077	0.0033
0.346	0.02	0.0001	0.0001	0.0072	0.0037
0.332	0.02	-0.0013	-0.0013	0.0067	0.0030
0.345	1.87	0.2398	0.2397	0.0074	0.0039
0.336	1.87	0.2407	0.2405	0.0073	0.0037
0.343	3.61	0.4670	0.4674	0.0080	0.0039
0.345	5.36	0.6939	0.6962	0.0089	0.0052
0.339	7.13	0.9111	0.9172	0.0085	0.0061
0.339	7.16	0.9205	0.9264	0.0107	0.0066
0.337	8.06	1.0315	1.0403	0.0105	0.0102
0.336	8.95	1.1314	1.1433	0.0132	0.0131
0.338	9.92	1.1906	1.2053	0.0193	0.0128
0.337	10.90	1.2044	1.2177	0.0457	-0.0079
0.340	11.97	1.1551	1.1594	0.1006	-0.0691
0.391	-3.51	-0.4470	-0.4474	0.0077	0.0018
0.389	-1.68	-0.2163	-0.2162	0.0063	0.0024
0.390	-0.05	-0.0041	-0.0041	0.0068	0.0026
0.394	0.00	0.0049	0.0049	0.0070	0.0026
0.389	1.69	0.2213	0.2212	0.0066	0.0029
0.391	3.43	0.4487	0.4490	0.0080	0.0036
0.392	5.24	0.6822	0.6842	0.0097	0.0059
0.391	7.05	0.9110	0.9166	0.0108	0.0095
0.392	7.94	1.0013	1.0090	0.0145	0.0115
0.391	8.84	1.0550	1.0642	0.0225	0.0119
0.391	9.99	1.0779	1.0865	0.0454	-0.0034
0.438	-3.43	-0.4497	-0.4501	0.0072	0.0009
0.445	-1.70	-0.2155	-0.2154	0.0074	0.0017
0.437	0.00	0.0073	0.0073	0.0067	0.0023
0.434	1.70	0.2310	0.2309	0.0064	0.0027
0.437	3.53	0.4620	0.4625	0.0073	0.0034
0.438	5.31	0.6916	0.6939	0.0074	0.0061
0.440	7.19	0.9194	0.9252	0.0120	0.0113
0.440	8.07	0.9727	0.9788	0.0254	0.0123
0.435	8.94	1.0008	1.0072	0.0373	0.0028
0.433	9.95	1.0178	1.0207	0.0723	-0.0154
0.430	11.01	1.0356	1.0343	0.1066	-0.0423

TABLE V.– CONTINUED

Mach	α_c	c_n	c_l	c_d	$c_{m1/4}$
0.496	-3.52	-0.4655	-0.4659	0.0074	-0.0002
0.491	-3.50	-0.4554	-0.4558	0.0068	-0.0001
0.491	-1.78	-0.2307	-0.2306	0.0067	0.0012
0.491	-1.71	-0.2253	-0.2252	0.0069	0.0012
0.485	0.00	0.0096	0.0096	0.0060	0.0022
0.496	0.01	0.0084	0.0084	0.0069	0.0021
0.498	1.81	0.2527	0.2526	0.0070	0.0028
0.496	3.42	0.4639	0.4642	0.0074	0.0039
0.491	5.19	0.7092	0.7114	0.0085	0.0081
0.491	7.05	0.8980	0.9022	0.0212	0.0148
0.488	7.13	0.8910	0.8960	0.0155	0.0142
0.491	8.00	0.9430	0.9461	0.0442	0.0059
0.486	8.06	0.9470	0.9505	0.0415	0.0074
0.487	8.95	0.9713	0.9720	0.0714	-0.0106
0.487	9.08	0.9561	0.9562	0.0751	-0.0111
0.488	10.00	0.9765	0.9741	0.0994	-0.0316
0.541	-3.50	-0.4844	-0.4849	0.0068	-0.0018
0.545	-1.80	-0.2383	-0.2382	0.0064	0.0006
0.530	-0.03	-0.0028	-0.0028	0.0065	0.0017
0.548	-0.03	0.0018	0.0018	0.0064	0.0015
0.542	1.78	0.2506	0.2505	0.0066	0.0028
0.535	3.61	0.5078	0.5084	0.0070	0.0054
0.535	5.34	0.7248	0.7269	0.0111	0.0107
0.533	7.17	0.8894	0.8917	0.0374	0.0105
0.534	8.17	0.9246	0.9252	0.0620	-0.0096
0.586	-3.45	-0.4814	-0.4819	0.0067	-0.0030
0.600	-1.81	-0.2378	-0.2377	0.0066	0.0003
0.586	-0.07	0.0014	0.0014	0.0066	0.0014
0.594	-0.01	0.0085	0.0085	0.0064	0.0015
0.589	1.77	0.2616	0.2615	0.0065	0.0031
0.583	3.45	0.5153	0.5158	0.0075	0.0087
0.586	5.28	0.7390	0.7406	0.0162	0.0168
0.582	7.17	0.8751	0.8763	0.0459	-0.0009

TABLE V.– CONCLUDED

Mach	α_c	c_n	c_l	c_d	$c_{m1/4}$
0.638	-3.52	-0.5075	-0.5080	0.0087	-0.0067
0.635	-1.66	-0.2356	-0.2355	0.0065	-0.0005
0.639	-0.03	0.0069	0.0069	0.0065	0.0014
0.641	0.02	0.0103	0.0103	0.0067	0.0012
0.643	1.77	0.2787	0.2786	0.0065	0.0046
0.642	3.51	0.5188	0.5192	0.0106	0.0103
0.638	5.27	0.7483	0.7482	0.0349	0.0146
0.635	7.24	0.8683	0.8656	0.0759	-0.0227
0.686	-3.44	-0.5477	-0.5475	0.0193	-0.0109
0.687	-1.71	-0.2575	-0.2574	0.0064	-0.0020
0.683	-0.01	0.0072	0.0072	0.0063	0.0015
0.695	0.06	0.0095	0.0095	0.0063	0.0005
0.687	1.78	0.2920	0.2919	0.0066	0.0056
0.690	3.49	0.5526	0.5523	0.0220	0.0121
0.686	5.29	0.7320	0.7299	0.0567	-0.0119
0.737	-3.42	-0.5564	-0.5550	0.0399	0.0053
0.747	-1.72	-0.2827	-0.2825	0.0121	-0.0054
0.731	-0.02	0.0106	0.0106	0.0066	0.0013
0.736	0.00	0.0005	0.0005	0.0065	0.0000
0.735	1.71	0.3071	0.3068	0.0121	0.0076
0.732	3.45	0.5738	0.5723	0.0427	-0.0007
0.736	4.34	0.6688	0.6662	0.0590	-0.0319
0.781	-3.41	-0.5786	-0.5764	0.0548	0.0474
0.791	-1.64	-0.2835	-0.2830	0.0204	0.0009
0.789	-0.07	0.0059	0.0059	0.0088	0.0016
0.785	1.66	0.3153	0.3147	0.0241	-0.0003
0.783	2.54	0.4896	0.4884	0.0377	-0.0154
0.781	3.39	0.6022	0.6001	0.0529	-0.0440
0.822	-3.29	-0.5925	-0.5897	0.0659	0.0826
0.829	-1.73	-0.3810	-0.3800	0.0379	0.0367
0.829	-0.05	0.0209	0.0209	0.0200	-0.0010
0.828	1.64	0.3645	0.3636	0.0351	-0.0332
0.825	2.47	0.5309	0.5294	0.0469	-0.0586
0.825	3.44	0.6279	0.6248	0.0694	-0.0817
0.876	-3.49	-0.5507	-0.5477	0.0649	0.0950
0.881	-1.65	-0.3637	-0.3626	0.0446	0.0923
0.887	1.64	0.3856	0.3841	0.0605	-0.0966
0.873	2.54	0.5222	0.5196	0.0701	-0.1035

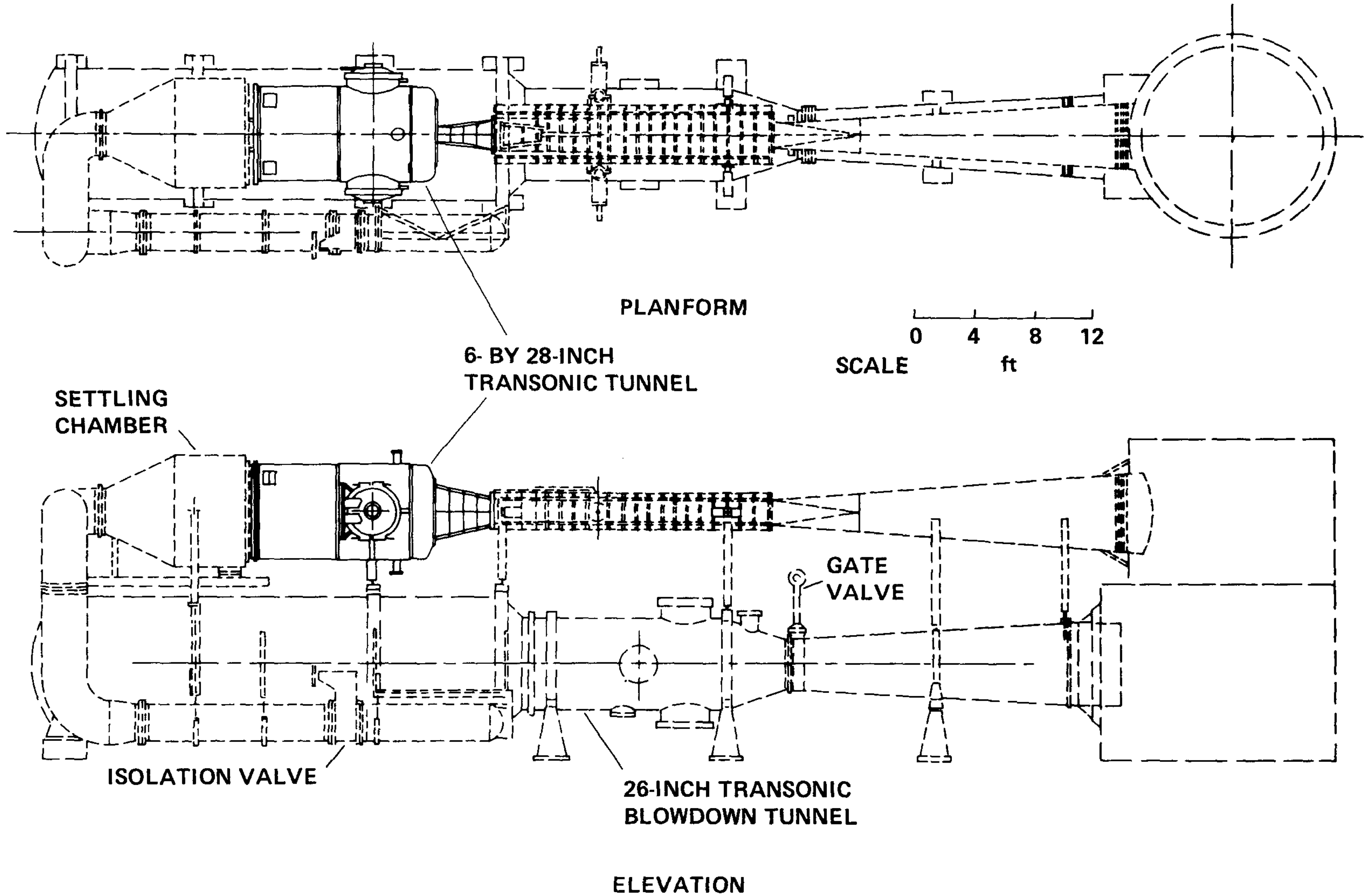

Figure 1.– Assembly drawing of the Langley Research Center's 6- by 28-Inch Transonic Tunnel.

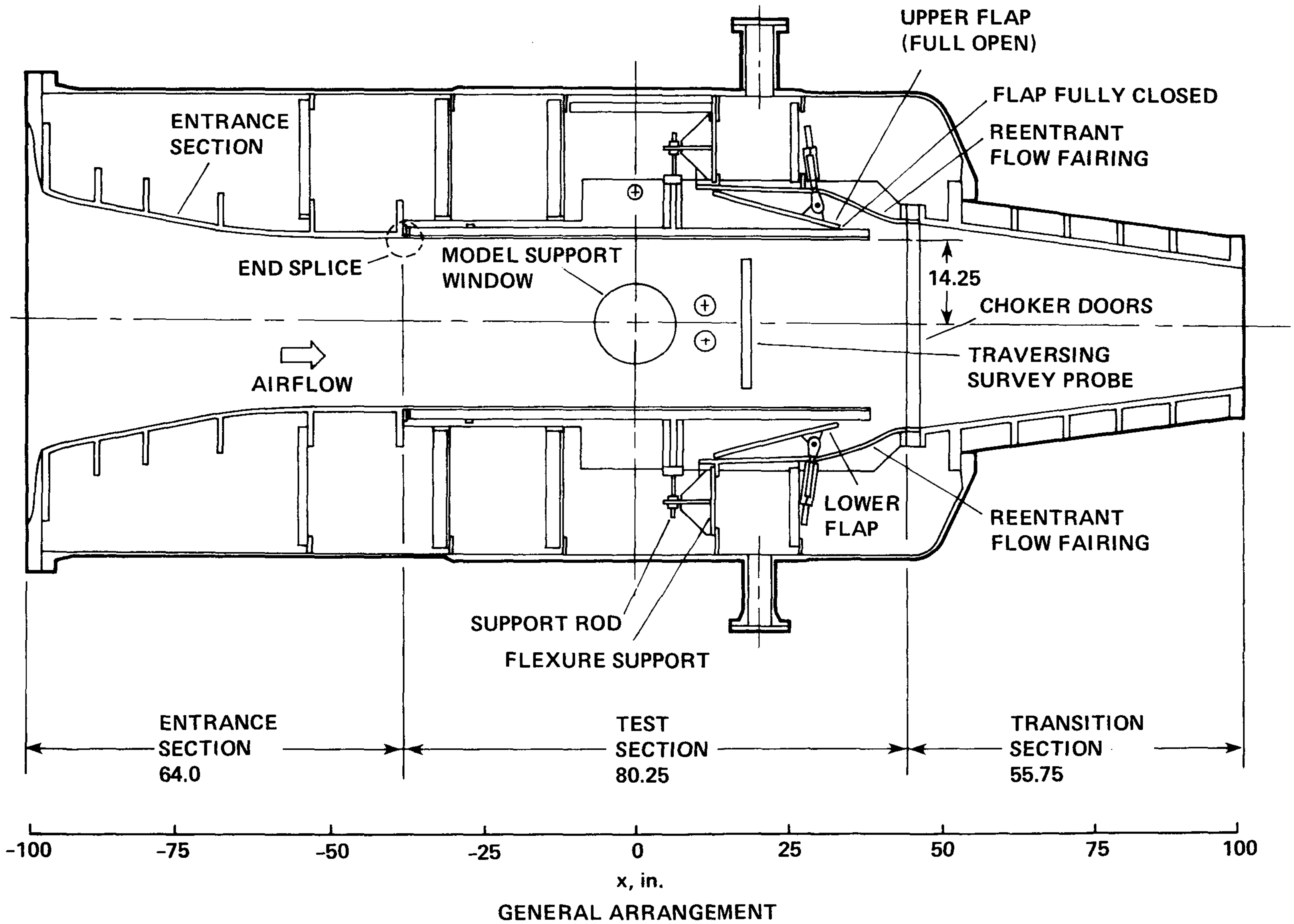

Figure 2.– Cross section drawing of side view of Langley Research Center's 6- by 28-Inch Transonic Tunnel (in.).

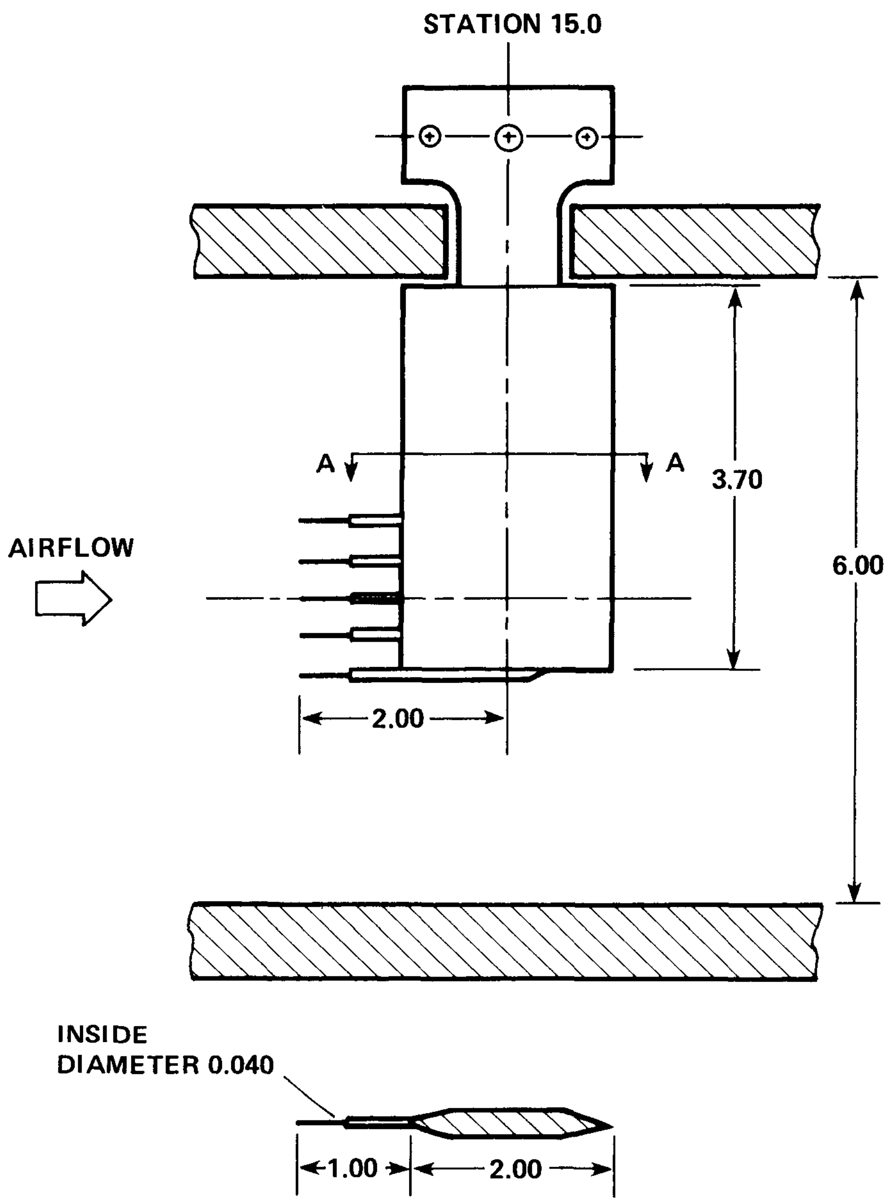

Figure 3.– Details of multitube probe used on traversing survey mechanism (in.).

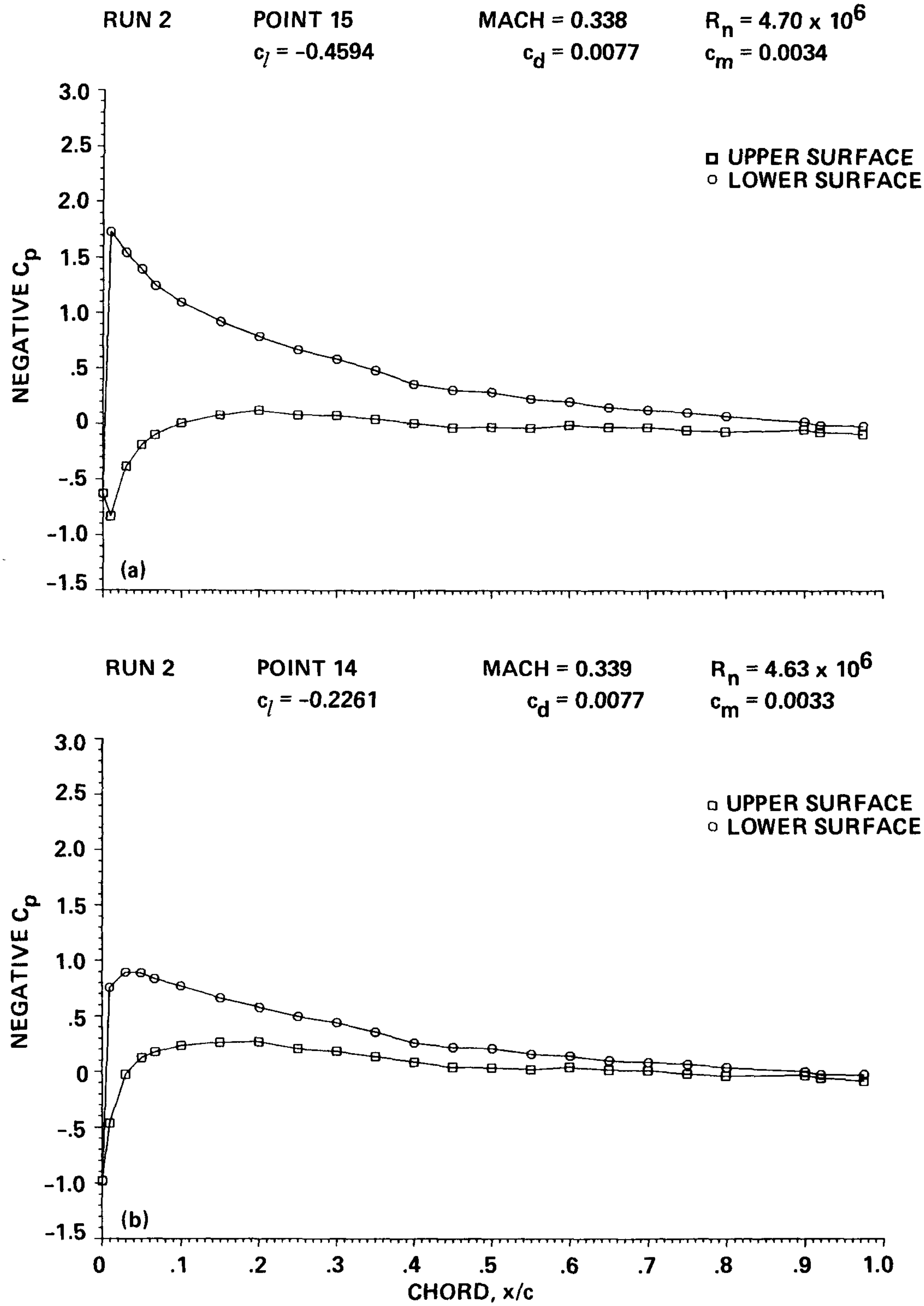

Figure 4.– Chordwise pressure distribution of the OLS/TAAT airfoil, $M = 0.34$; (a) $\alpha_c = -3.51°$, (b) $\alpha_c = -1.78°$.

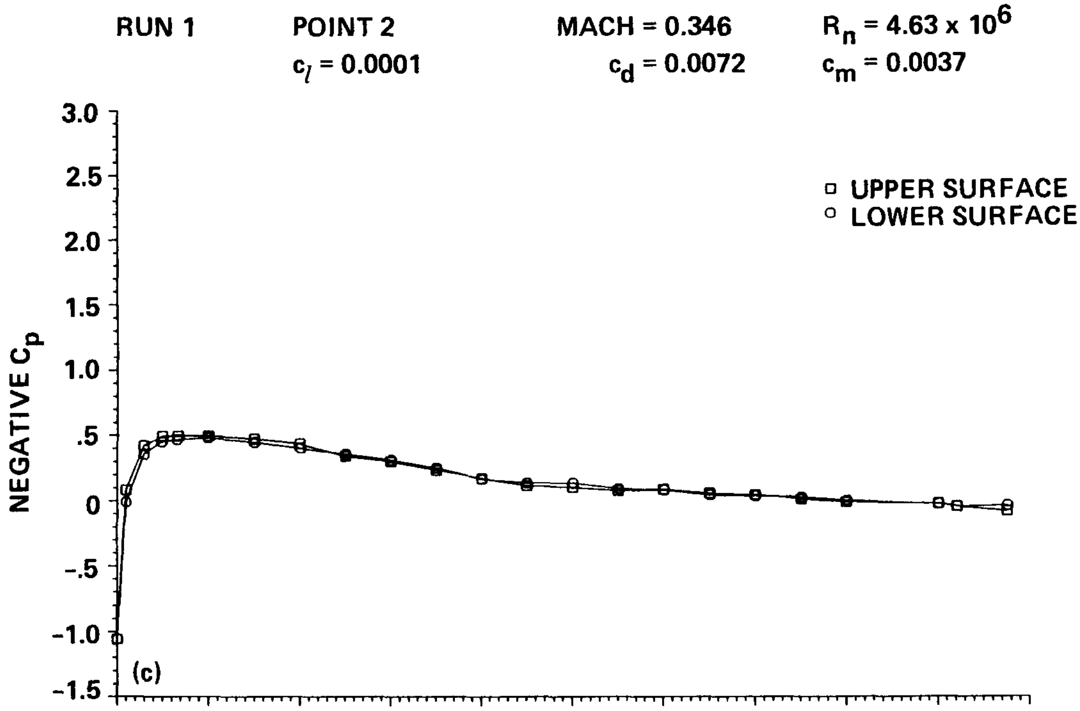

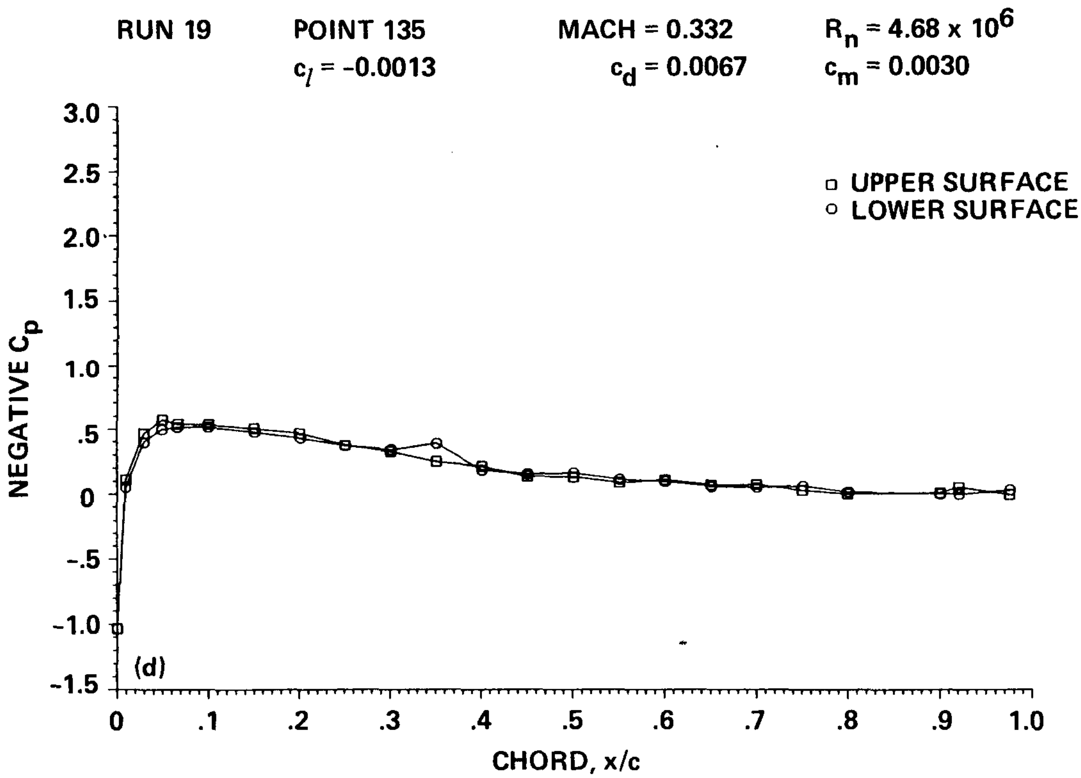

Figure 4.– Continued; (c) $\alpha_c = 0.02°$, (d) $\alpha_c = 0.02°$.

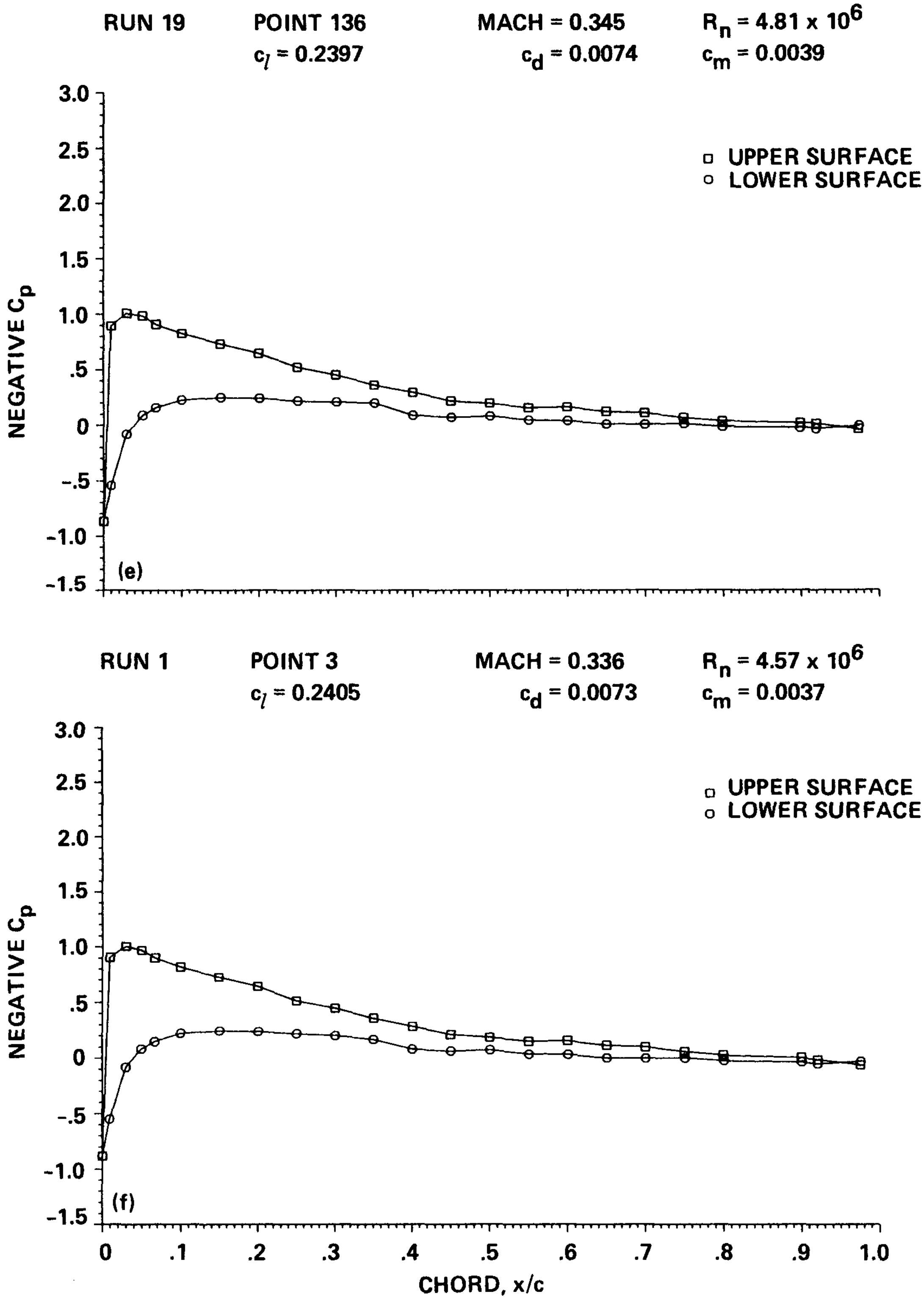

Figure 4.– Continued; (e) $\alpha_c = 1.87°$, (f) $\alpha_c = 1.87°$.

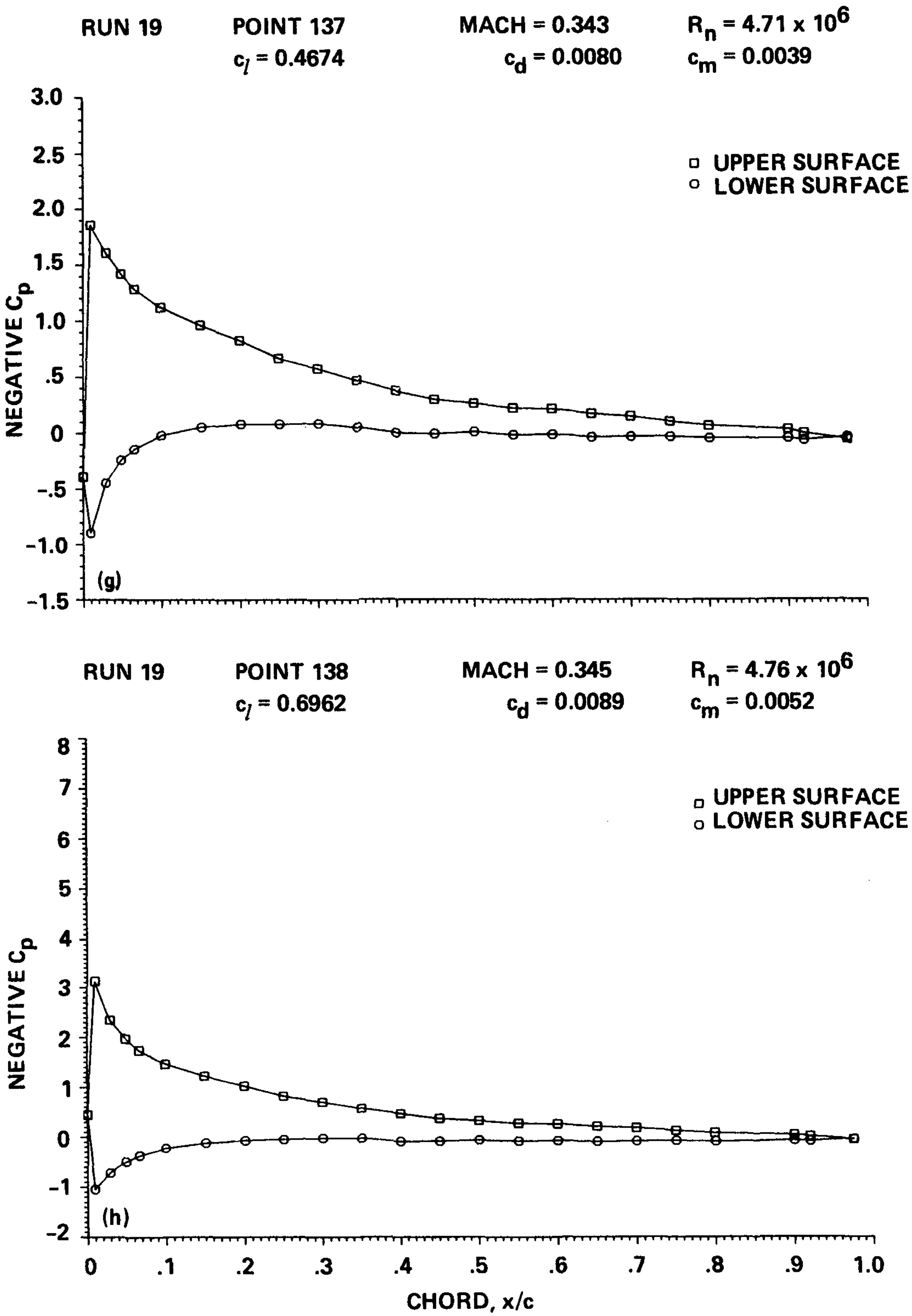

Figure 4.- Continued; (g) $\alpha_c = 3.61°$, (h) $\alpha_c = 5.36°$.

RUN 1 POINT 6 MACH = 0.339 $R_n = 4.64 \times 10^6$

$c_l = 0.9172$ $c_d = 0.0085$ $c_m = 0.0061$

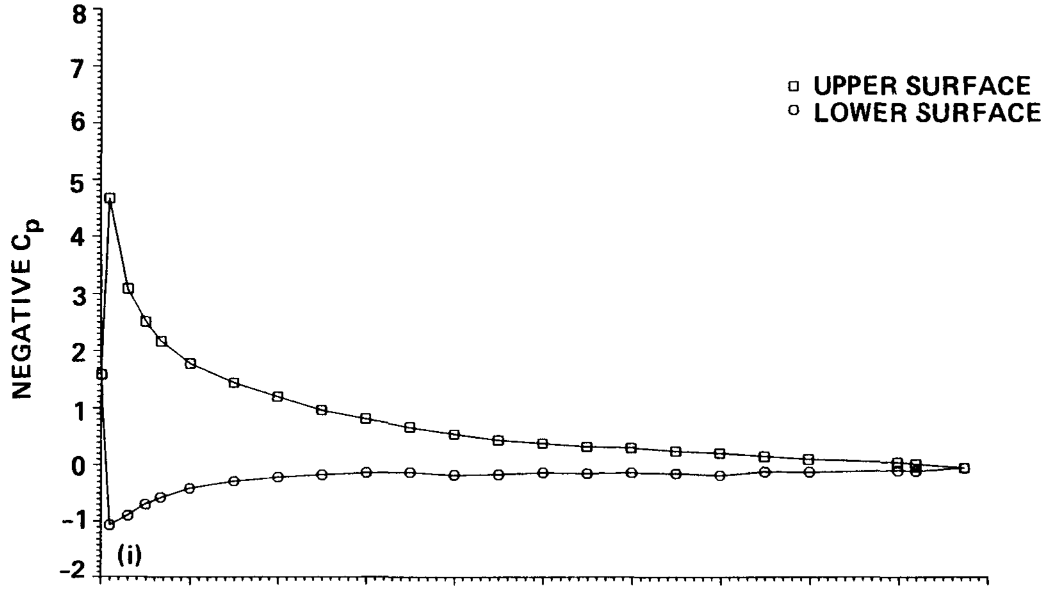

RUN 19 POINT 139 MACH = 0.339 $R_n = 4.69 \times 10^6$

$c_l = 0.9264$ $c_d = 0.0107$ $c_m = 0.0066$

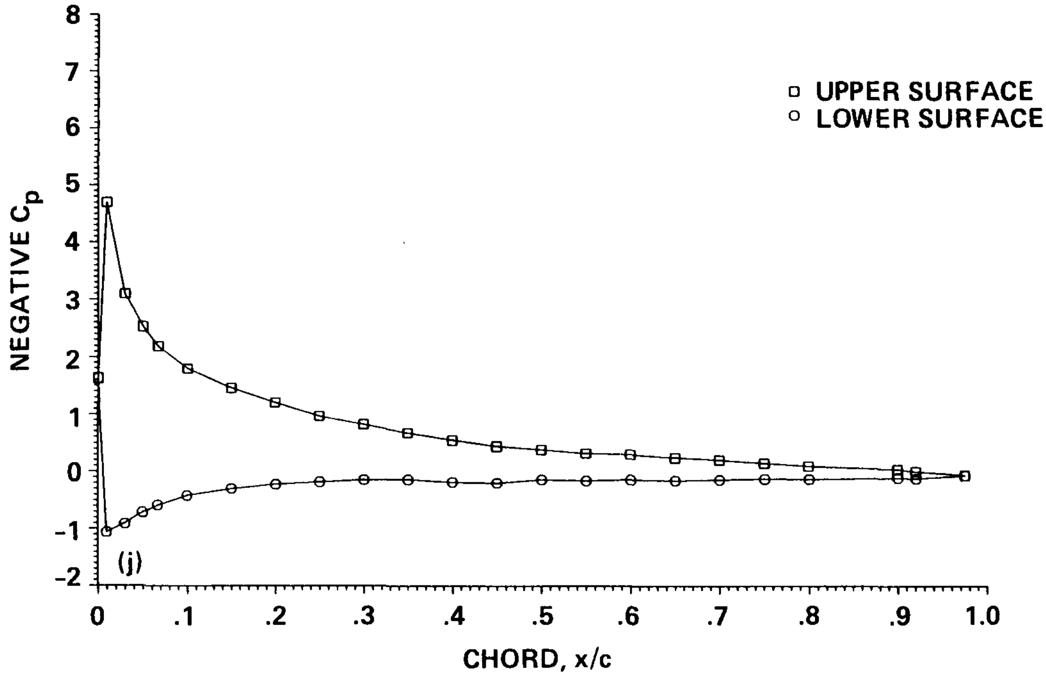

Figure 4.– Continued; (i) $\alpha_c = 7.13°$, (j) $\alpha_c = 7.16°$.

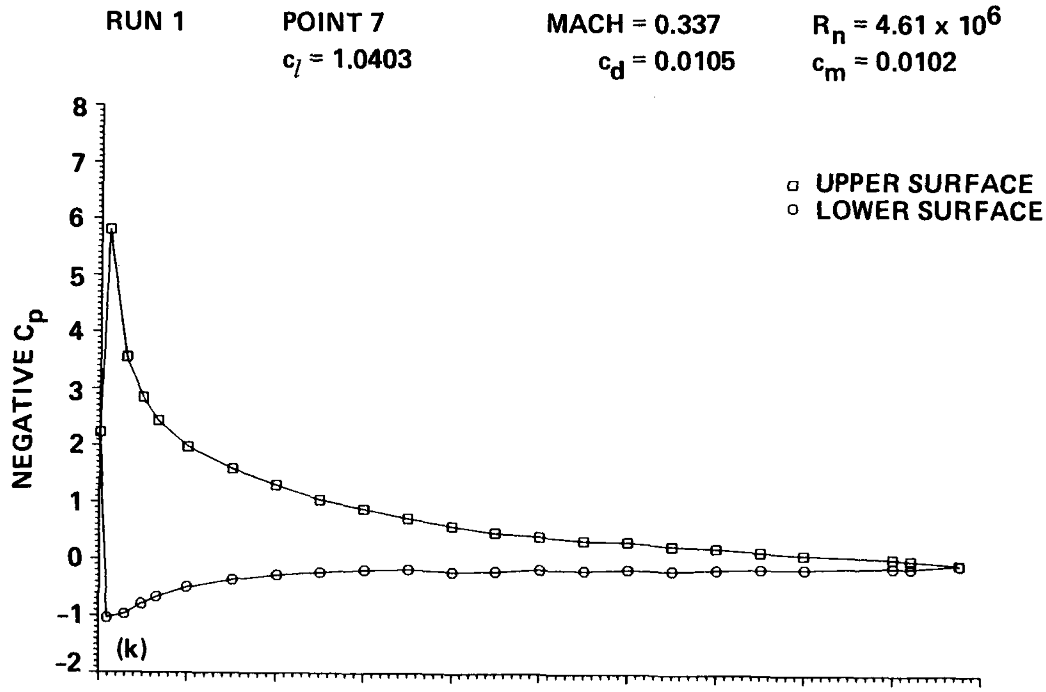

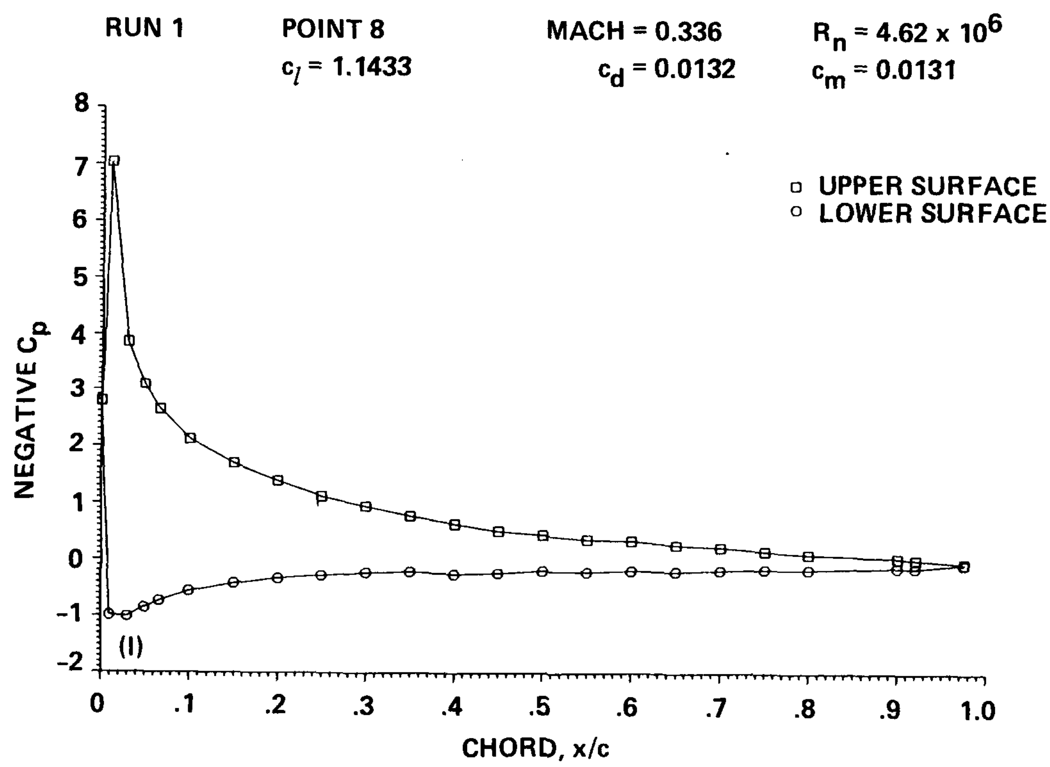

Figure 4.– Continued; (k) $\alpha_c = 8.06°$, (l) $\alpha_c = 8.95°$.

RUN 1 POINT 9 MACH = 0.338 $R_n = 4.67 \times 10^6$
$c_l = 1.2053$ $c_d = 0.0193$ $c_m = 0.0128$

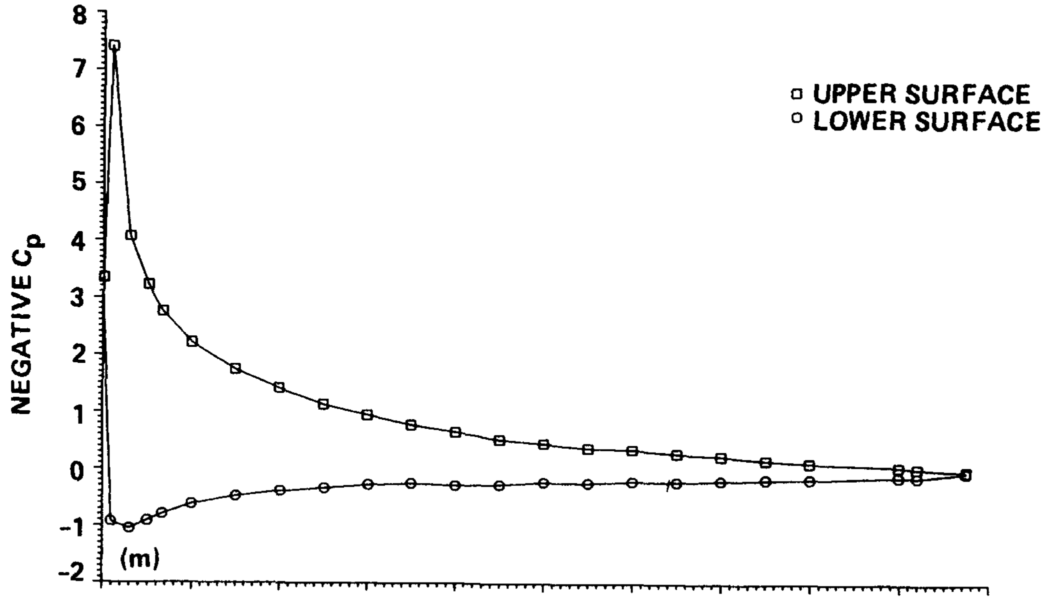

RUN 1 POINT 10 MACH = 0.337 $R_n = 4.69 \times 10^6$
$c_l = 1.2177$ $c_d = 0.0457$ $c_m = -0.0079$

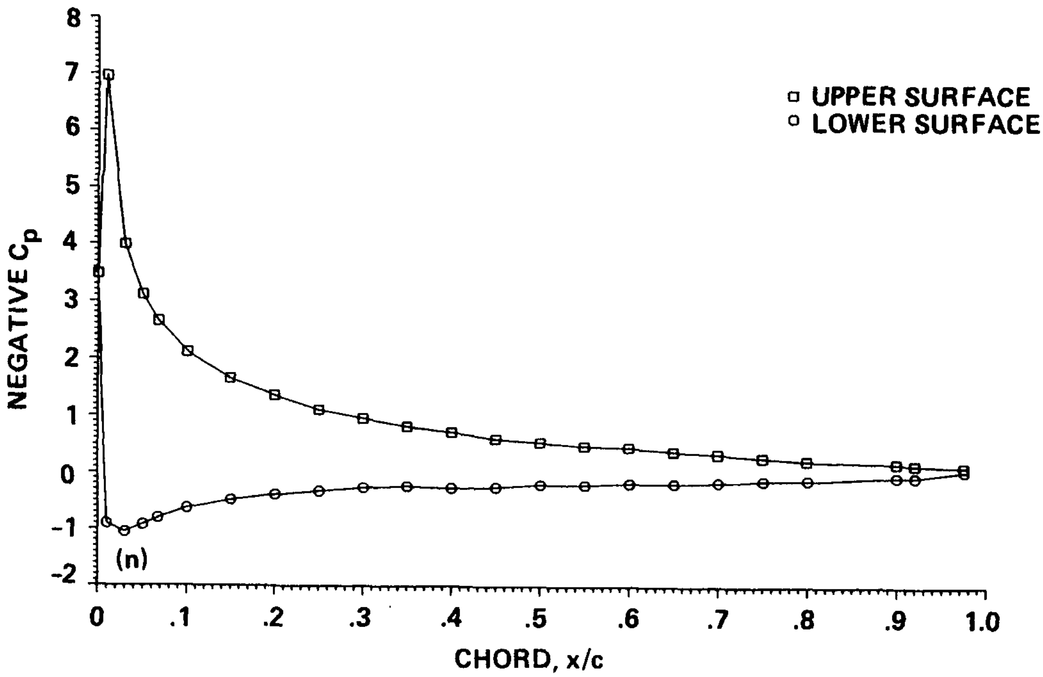

Figure 4.– Continued; (m) $\alpha_c = 9.92°$, (n) $\alpha_c = 10.90°$.

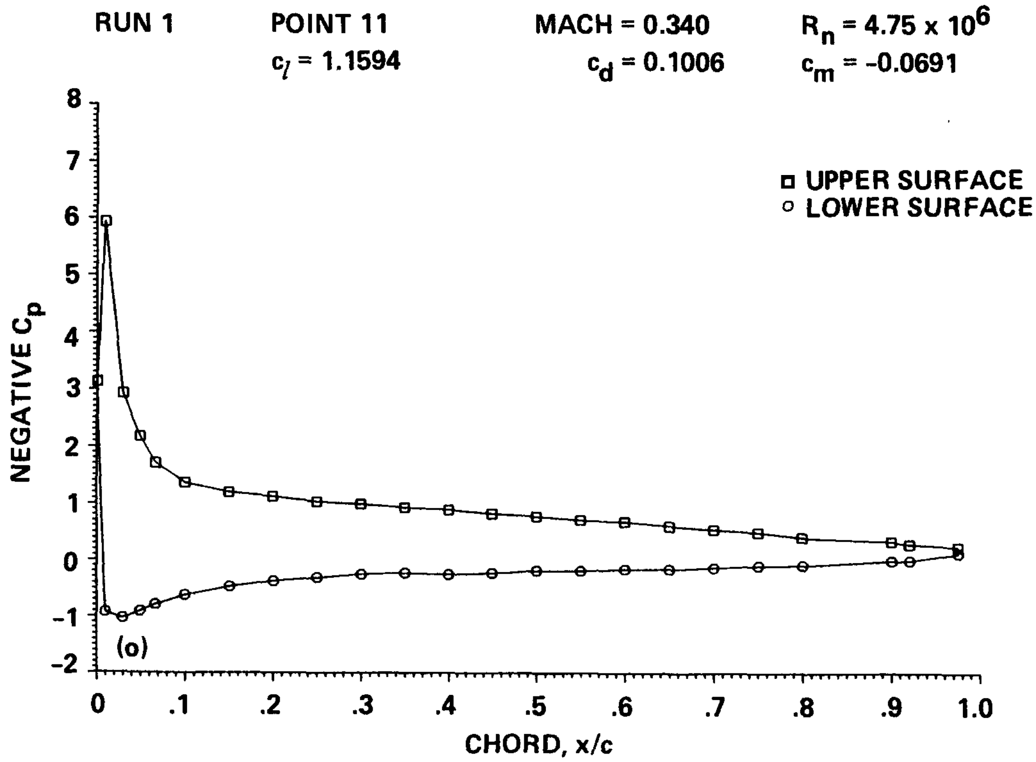

Figure 4.– Concluded; (o) $\alpha_c = 11.97°$.

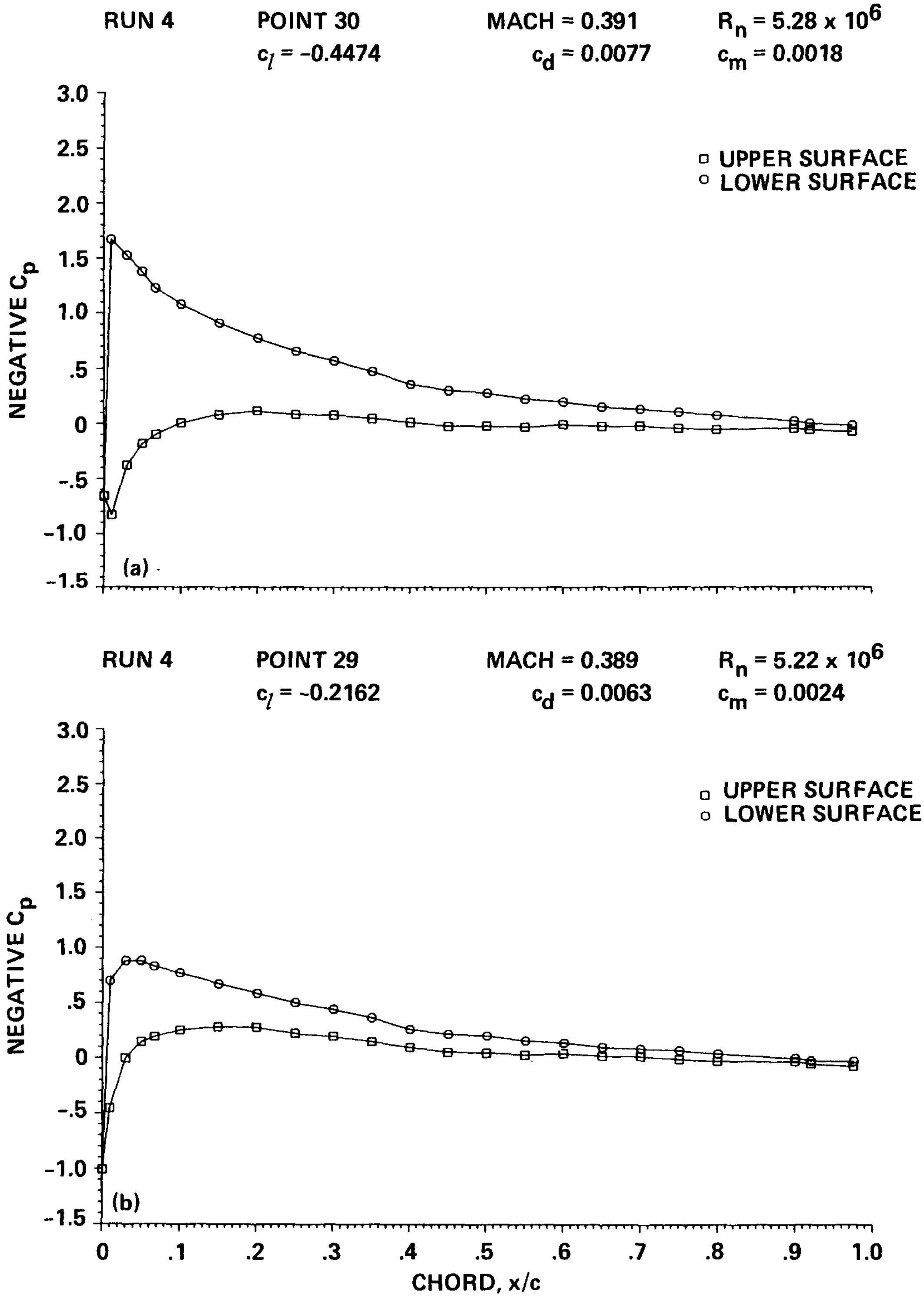

Figure 5.– Chordwise pressure distribution of the OLS/TAAT airfoil, $M = 0.39$; (a) α_c = -3.51°, (b) α_c = -1.68°.

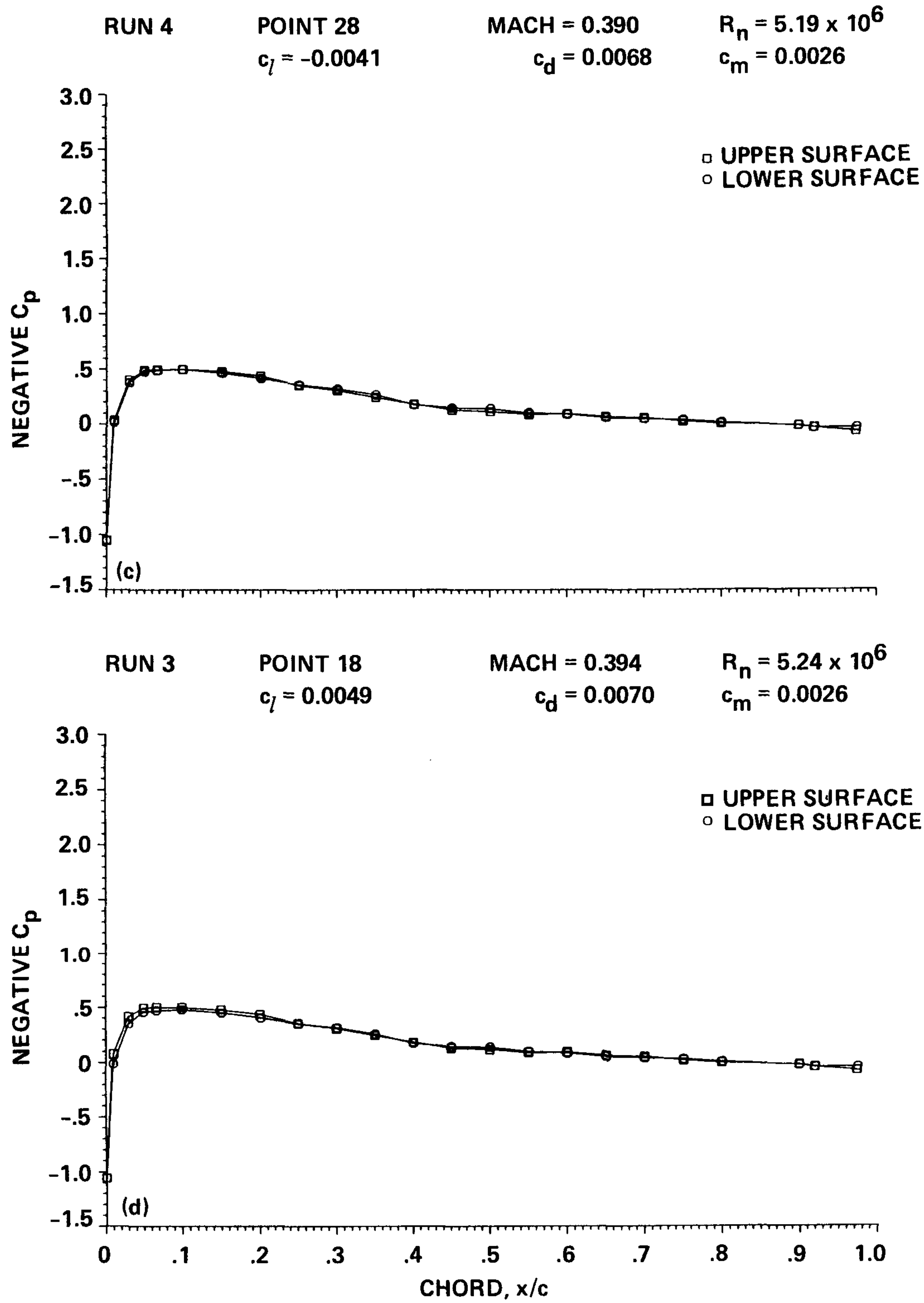

Figure 5.– Continued; (c) $\alpha_c = -0.05°$, (d) $\alpha_c = 0.00°$.

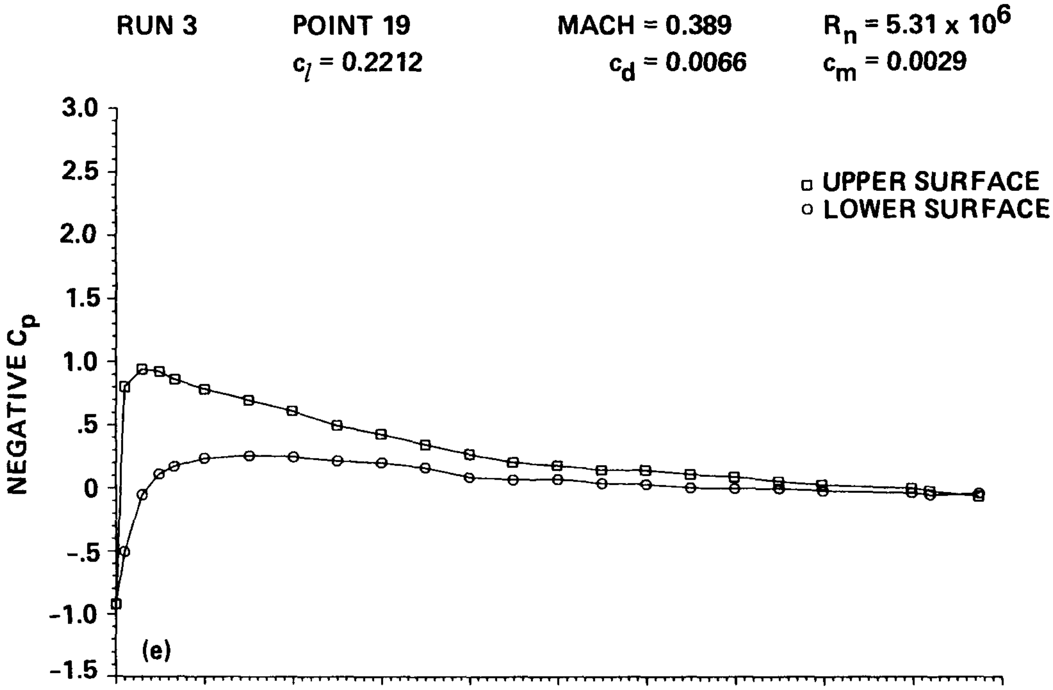

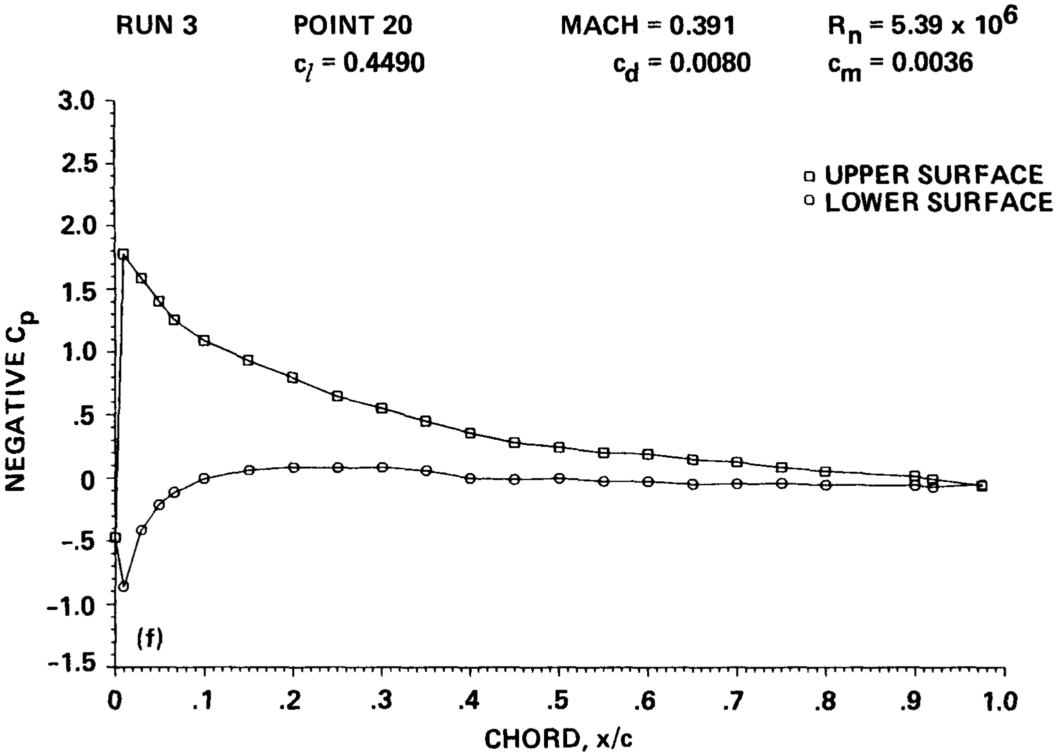

Figure 5.– Continued; (e) $\alpha_c = 1.69°$, (f) $\alpha_c = 3.43°$.

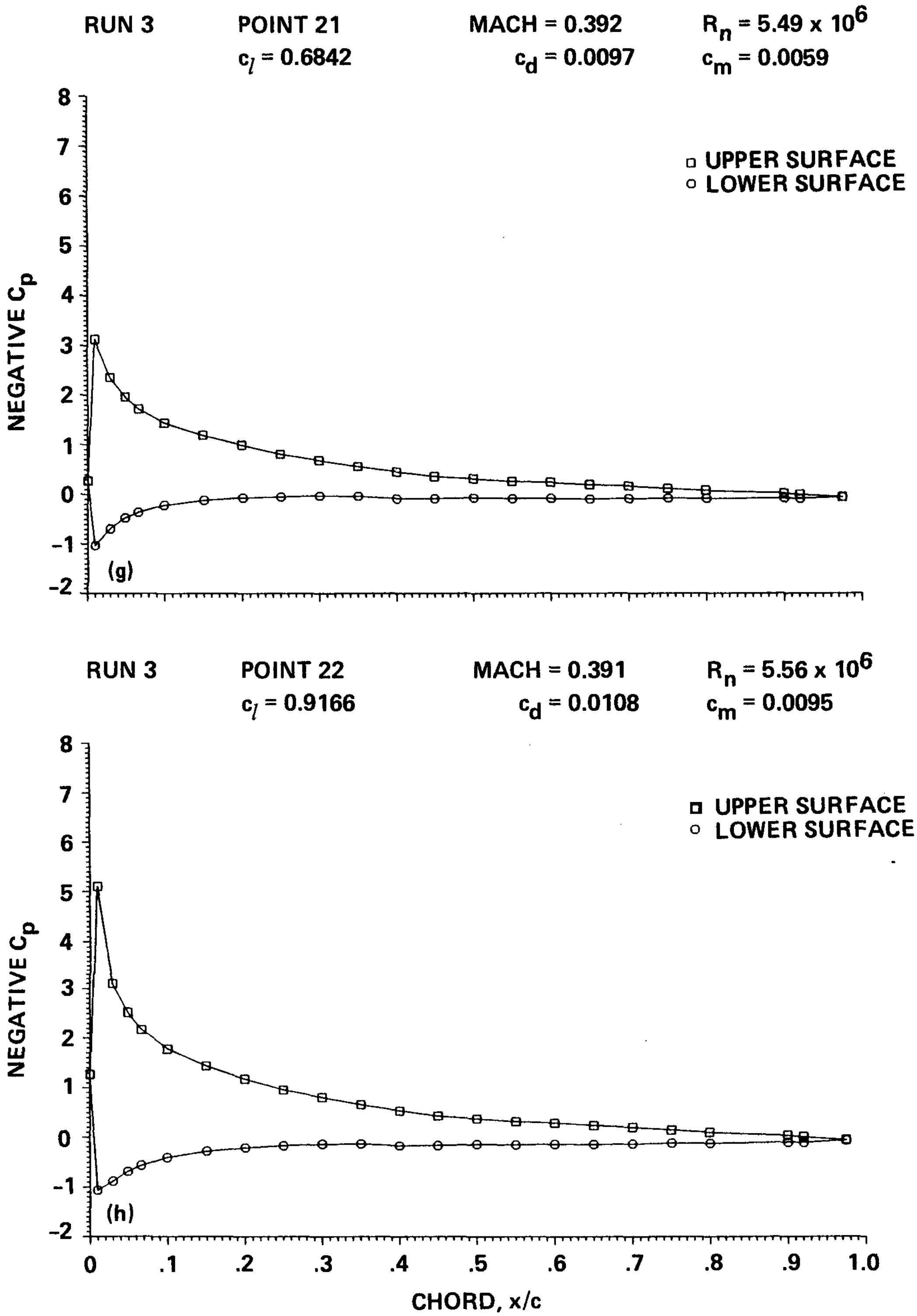

Figure 5.– Continued; (g) $\alpha_c = 5.24°$, (h) $\alpha_c = 7.05°$.

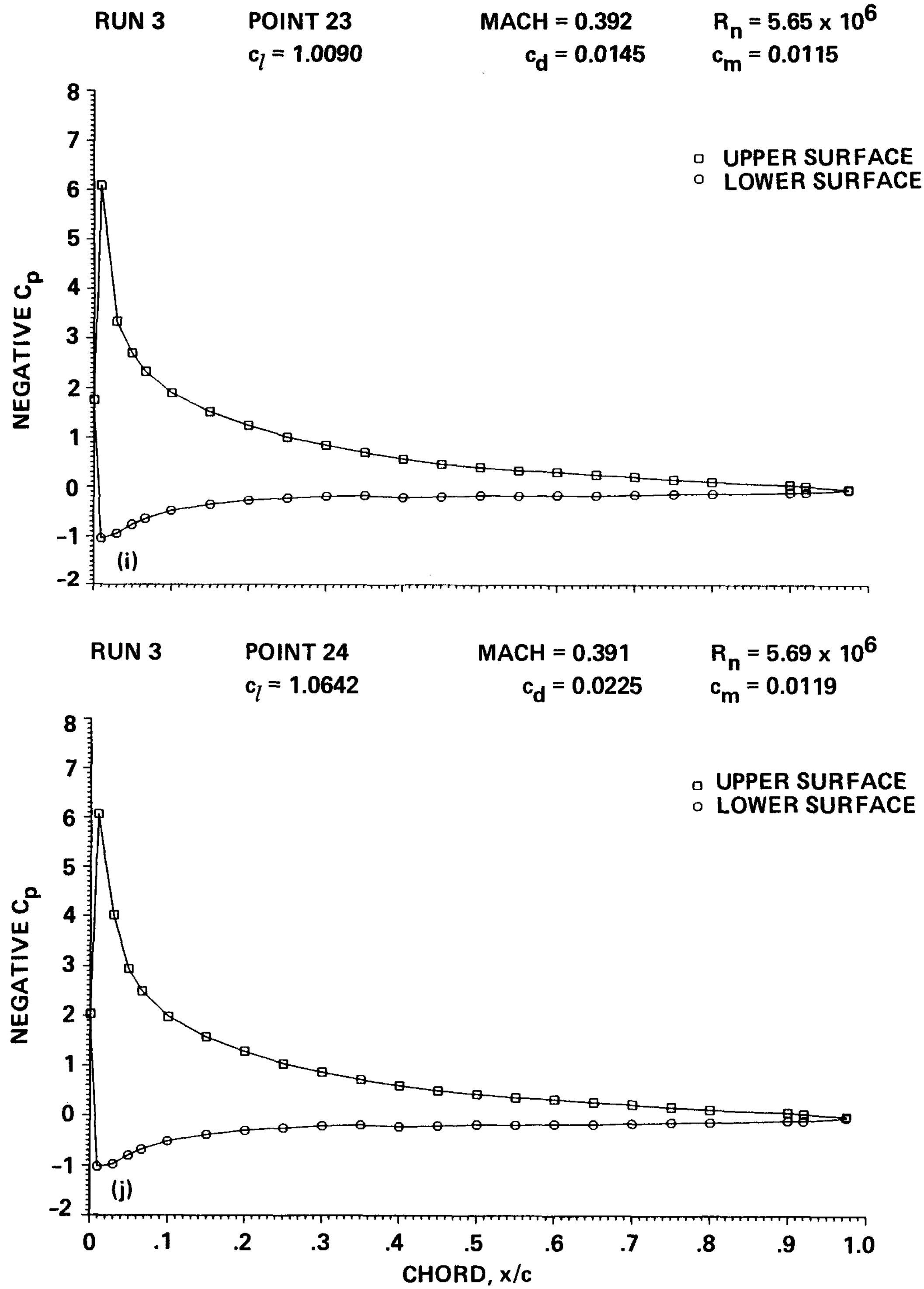

Figure 5.– Continued; (i) $\alpha_c = 7.94°$, (j) $\alpha_c = 8.84°$.

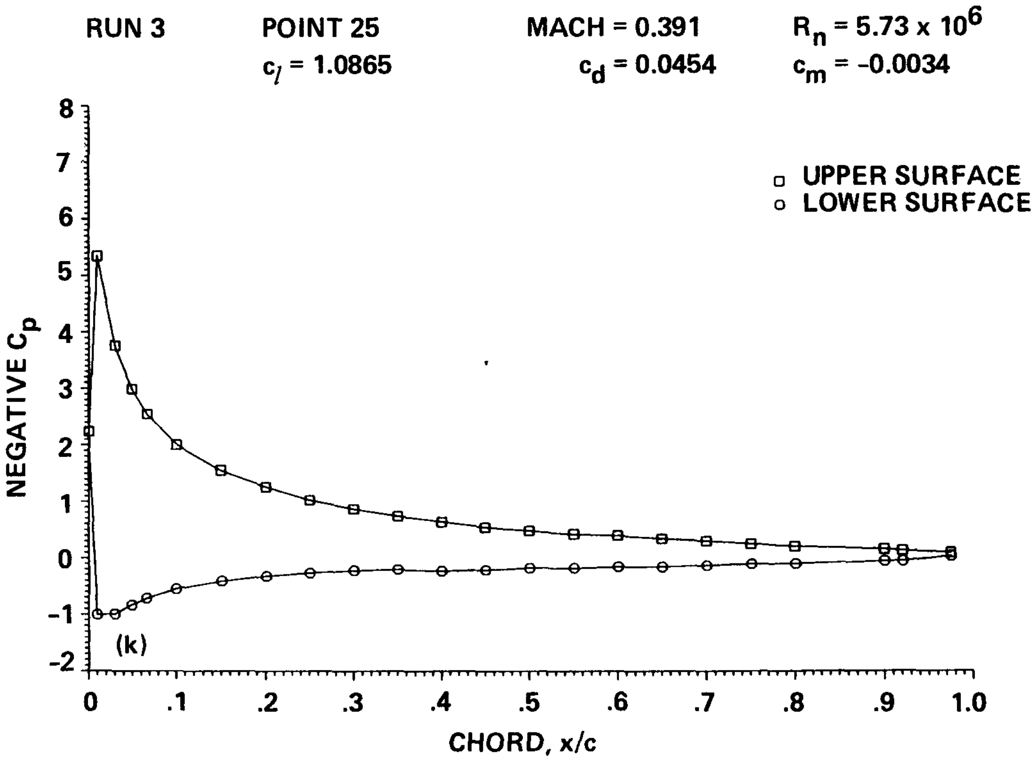

Figure 5.– Concluded; (k) $\alpha_c = 9.99°$.

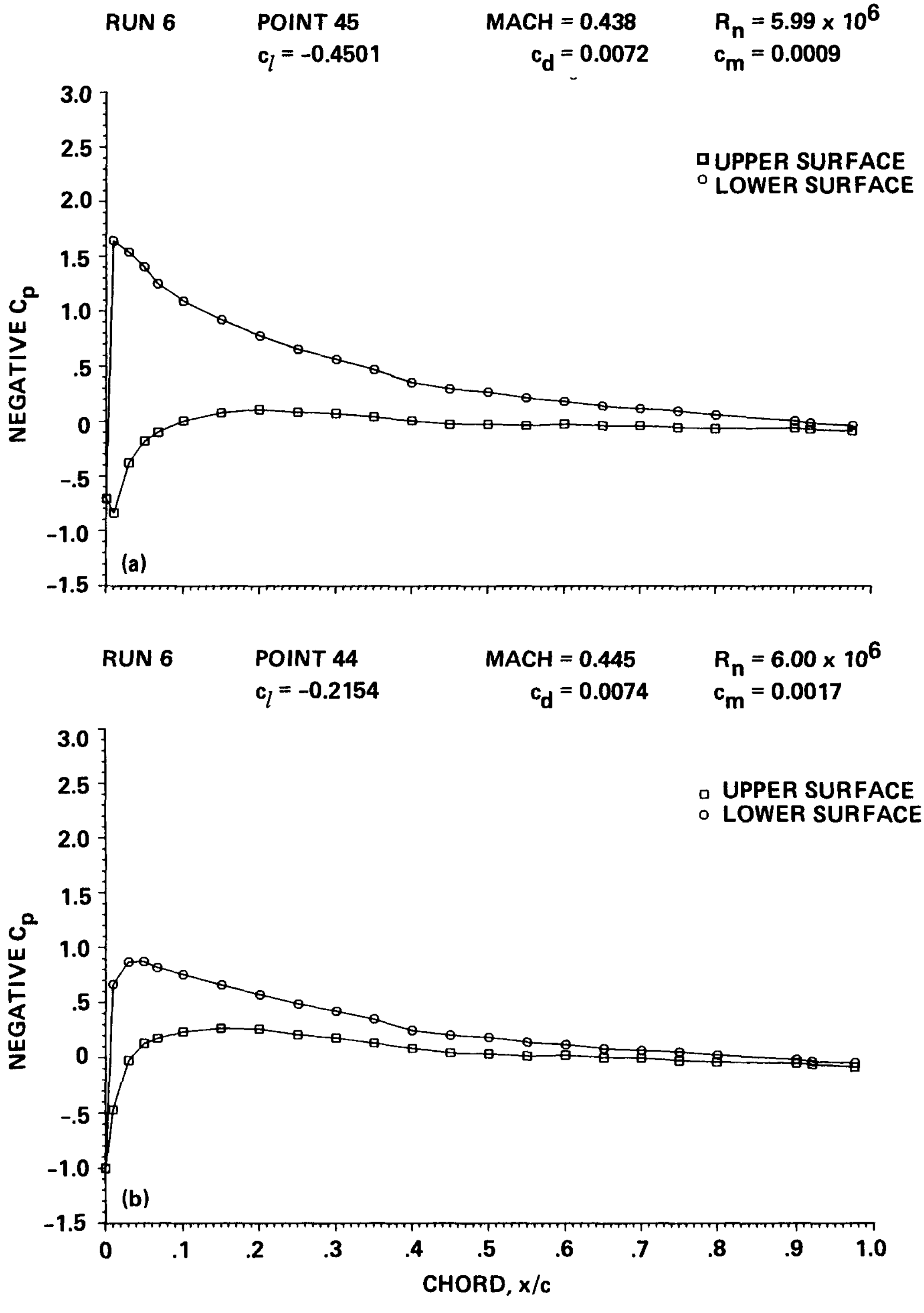

Figure 6.– Chordwise pressure distribution of the OLS/TAAT airfoil, $M = 0.44$; (a) $\alpha_c = -3.43°$, (b) $\alpha_c = -1.70°$.

RUN 5 POINT 32 MACH = 0.437 $R_n = 5.78 \times 10^6$

$c_l = 0.0073$ $c_d = 0.0067$ $c_m = 0.0023$

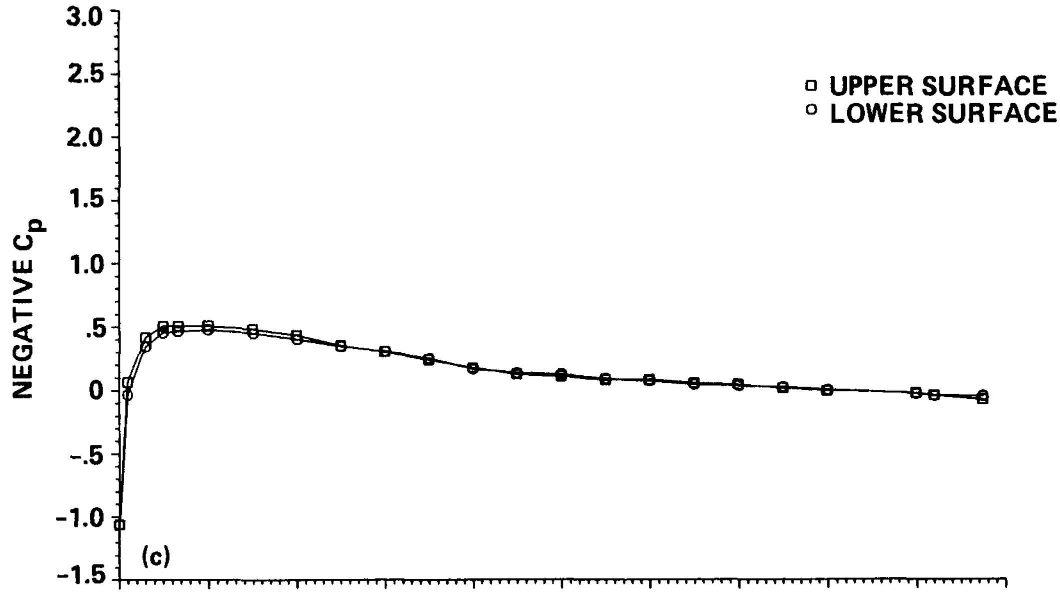

RUN 5 POINT 33 MACH = 0.434 $R_n = 5.79 \times 10^6$

$c_l = 0.2309$ $c_d = 0.0064$ $c_m = 0.0027$

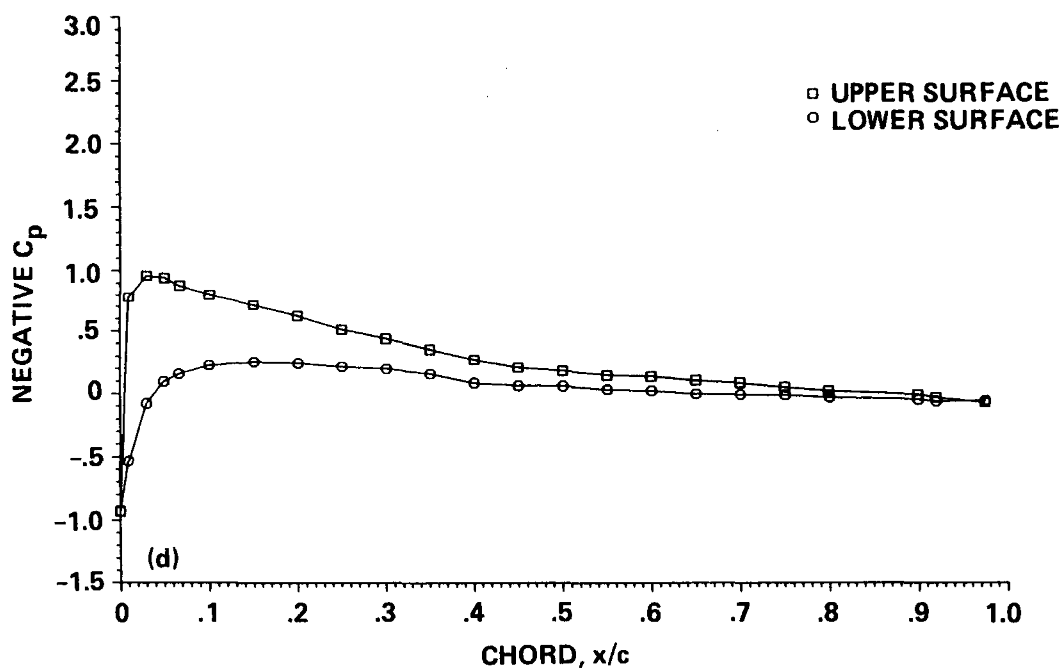

Figure 6.– Continued; (c) $\alpha_c = 0.00°$, (d) $\alpha_c = 1.70°$.

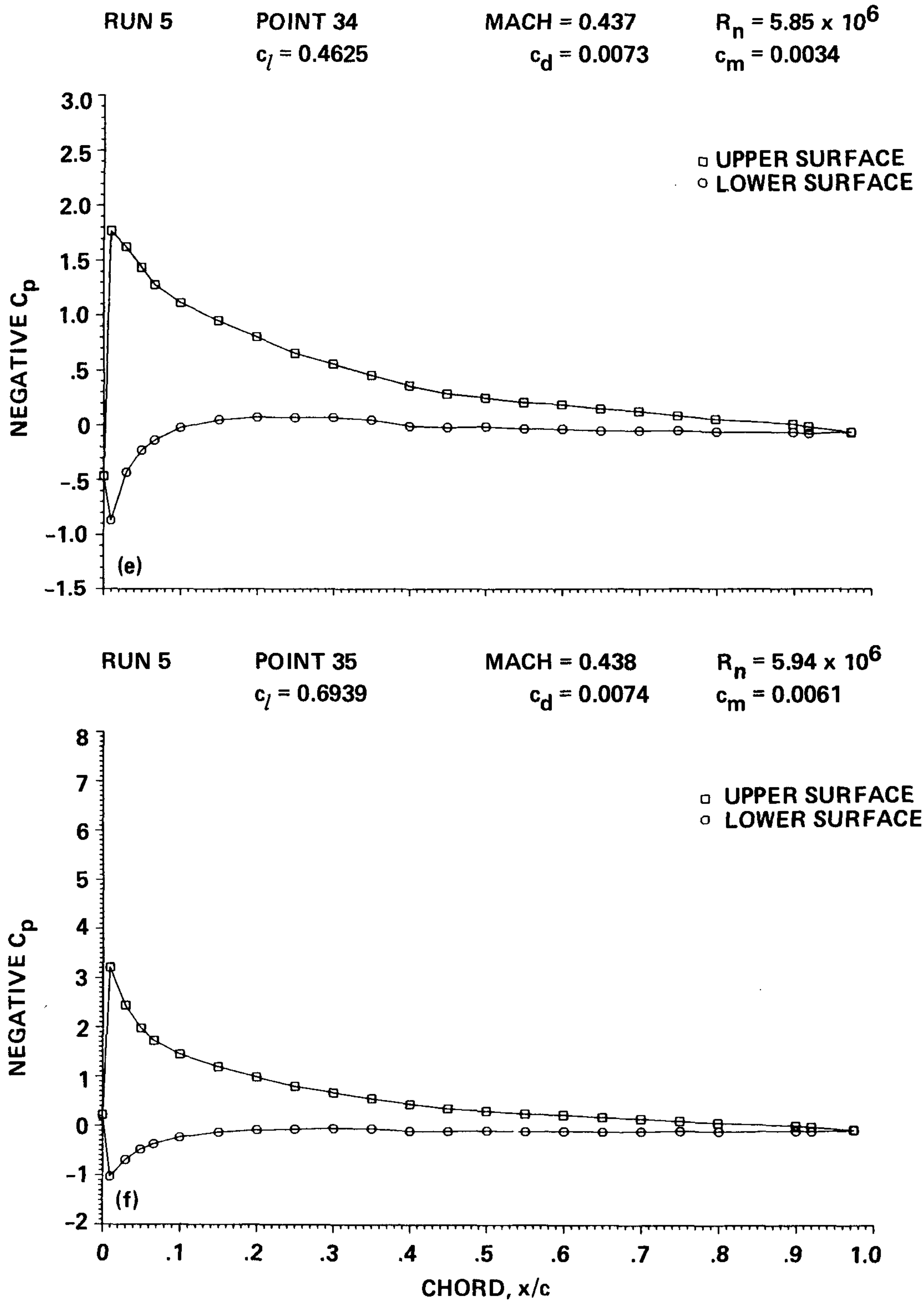

Figure 6.– Continued; (e) $\alpha_c = 3.53°$, (f) $\alpha_c = 5.31°$.

RUN 5 POINT 36 MACH = 0.440 $R_n = 5.98 \times 10^6$

$c_l = 0.9252$ $c_d = 0.0120$ $c_m = 0.0113$

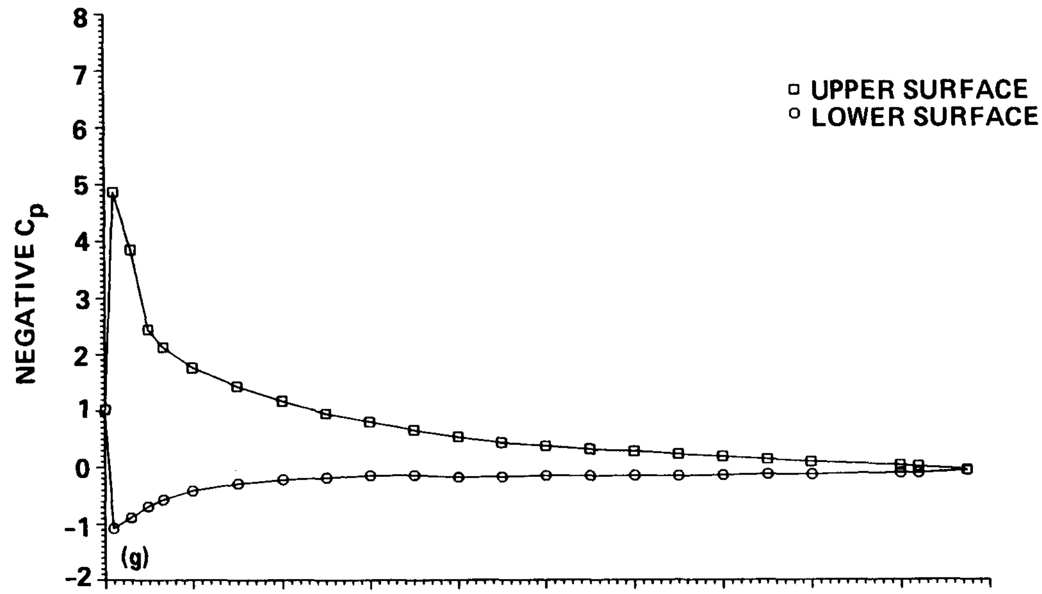

RUN 5 POINT 38 MACH = 0.440 $R_n = 6.10 \times 10^6$

$c_l = 0.9788$ $c_d = 0.0254$ $c_m = 0.0123$

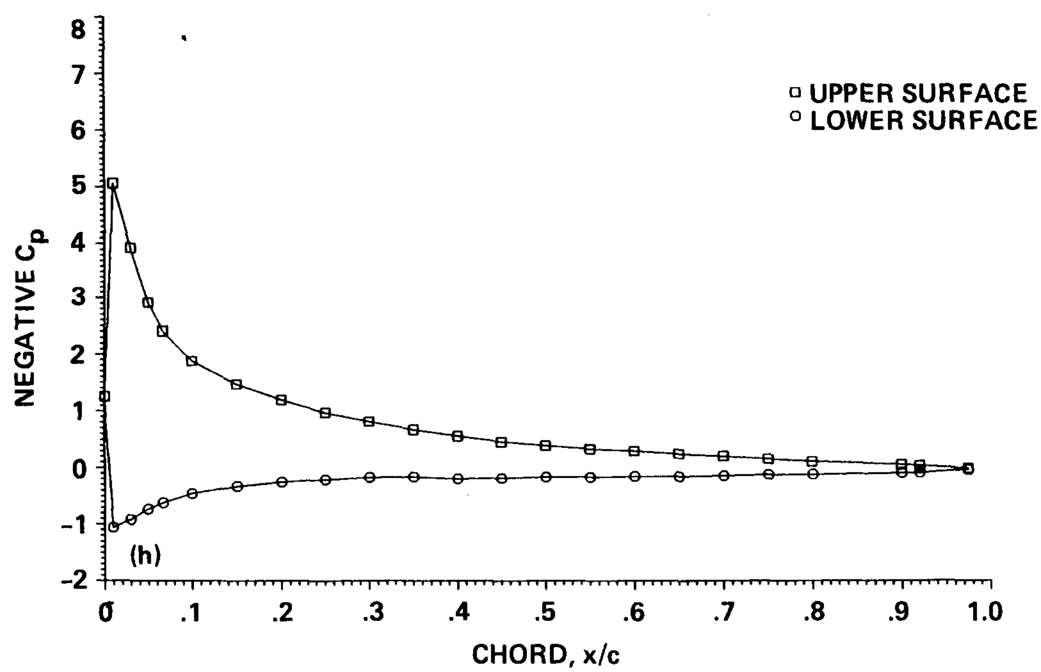

Figure 6.– Continued; (g) $\alpha_c = 7.19°$, (h) $\alpha_c = 8.07°$.

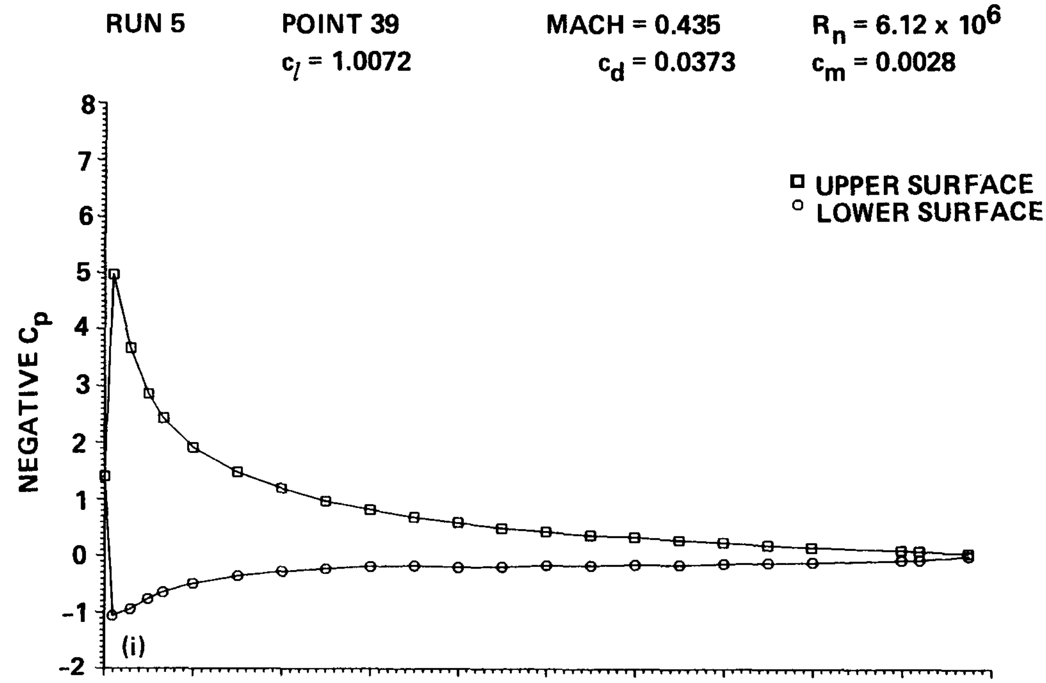

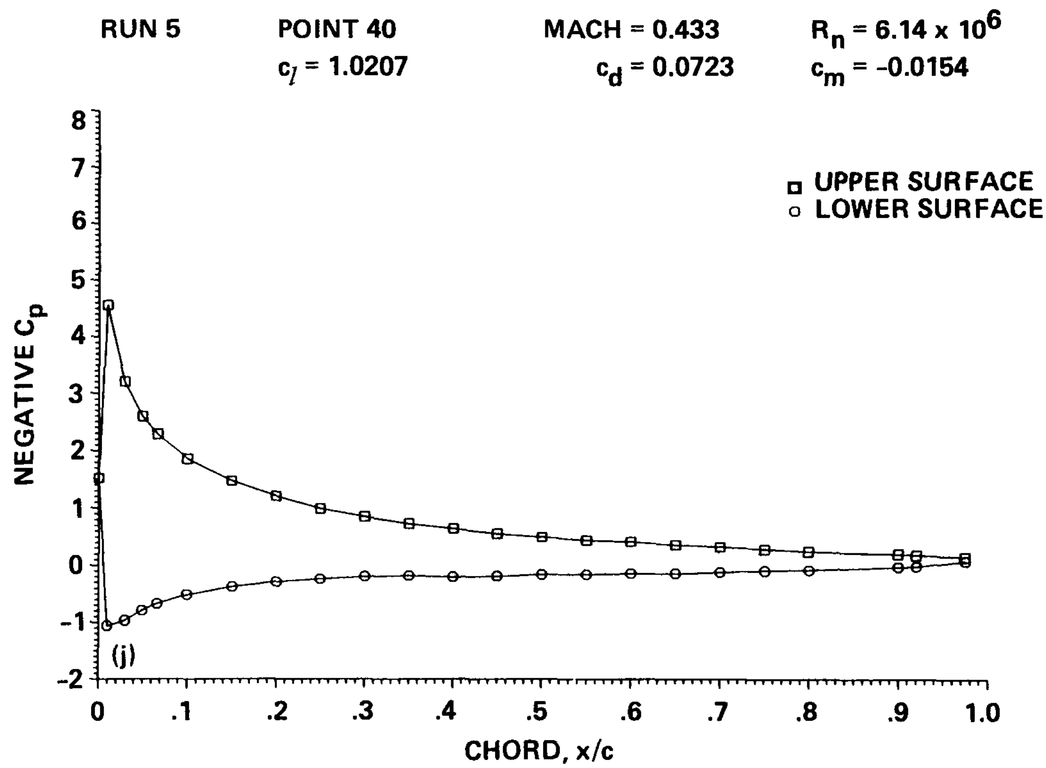

Figure 6.- Continued; (i) $\alpha_c = 8.94°$, (j) $\alpha_c = 9.95°$.

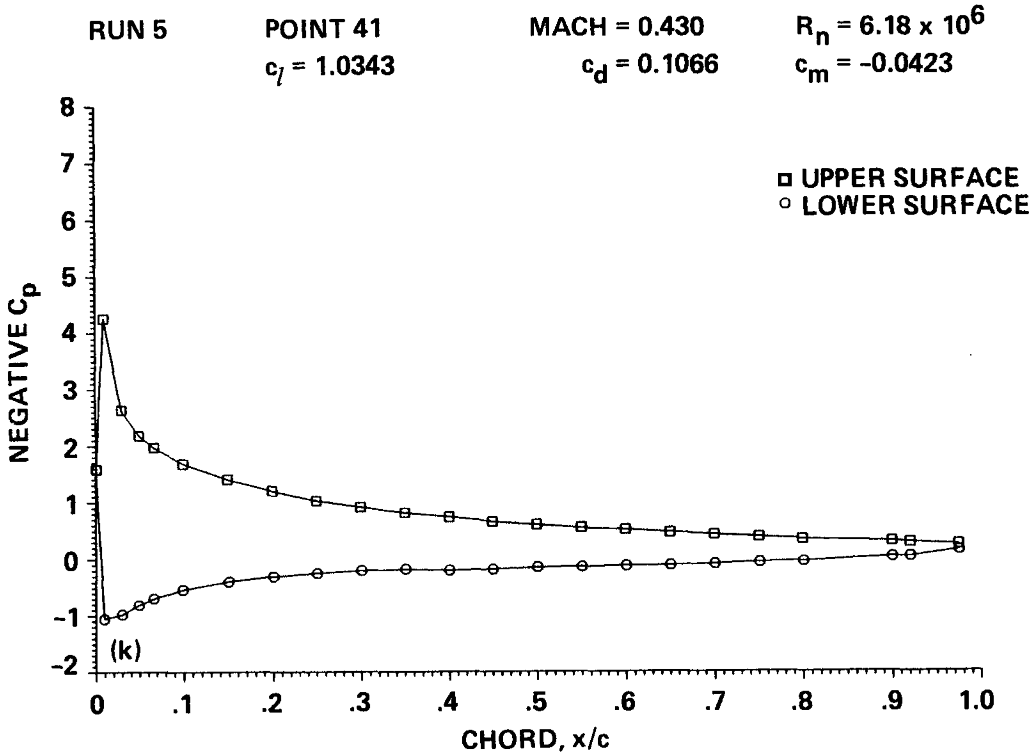

Figure 6.– Concluded; (k) $\alpha_c = 11.01°$.

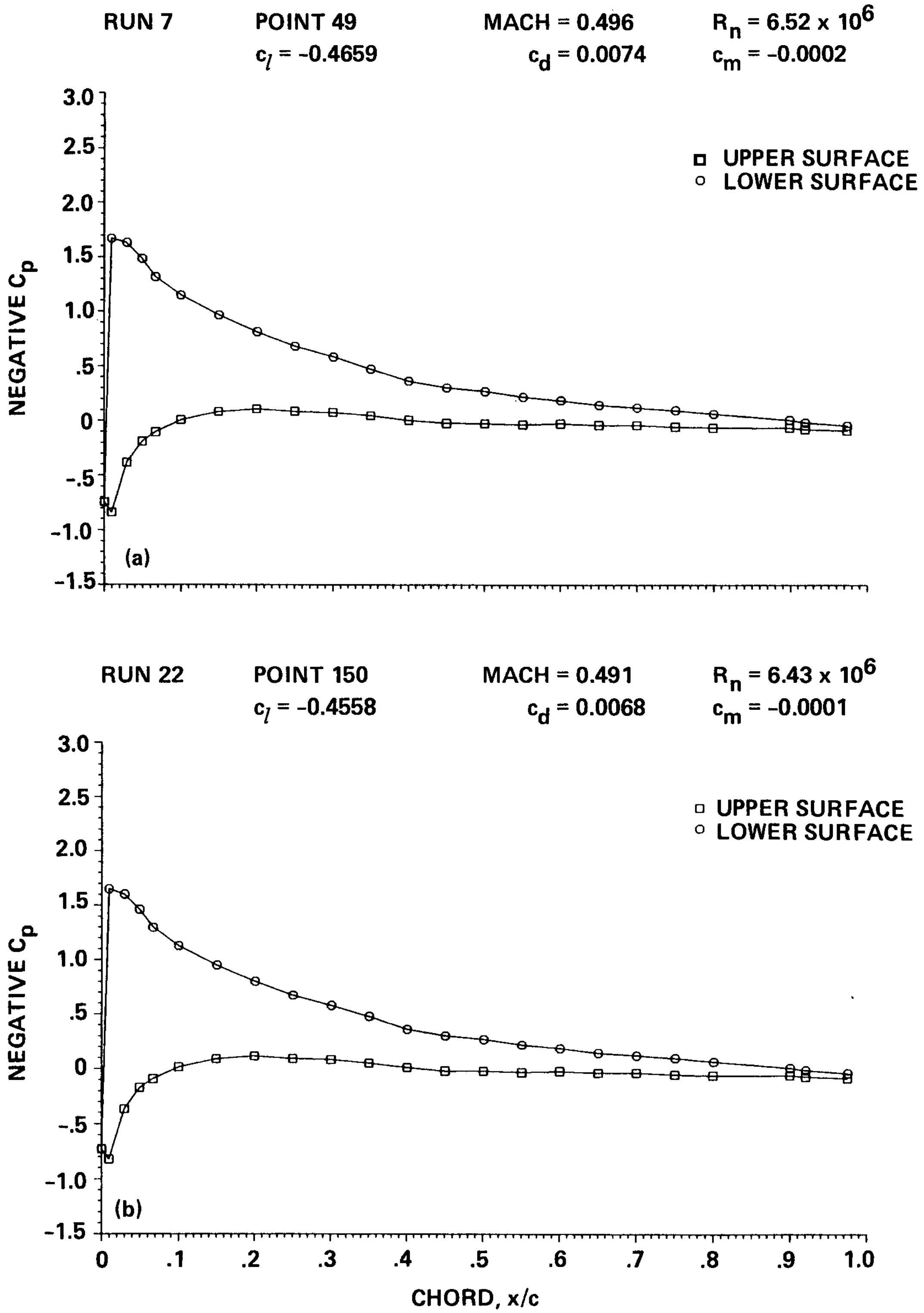

Figure 7.– Chordwise pressure distribution of the OLS/TAAT airfoil, $M = 0.49$; (a) $\alpha_c = -3.52°$, (b) $\alpha_c = -3.50°$.

RUN 7 POINT 48 MACH = 0.491 $R_n = 6.49 \times 10^6$

$c_l = -0.2306$ $c_d = 0.0067$ $c_m = 0.0012$

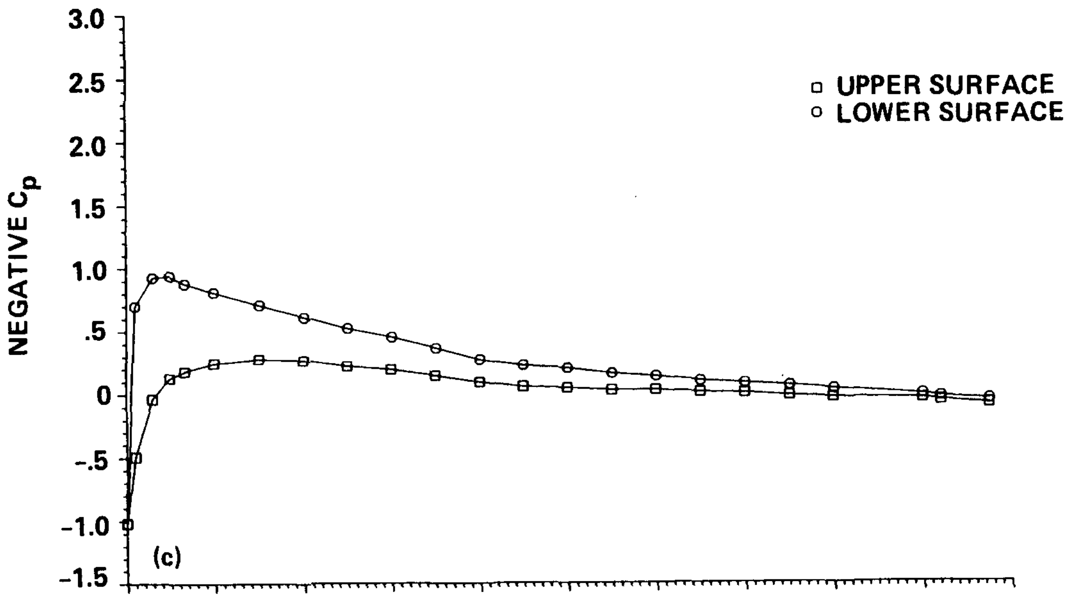

RUN 21 POINT 147 MACH = 0.491 $R_n = 6.41 \times 10^6$

$c_l = -0.2252$ $c_d = 0.0069$ $c_m = 0.0012$

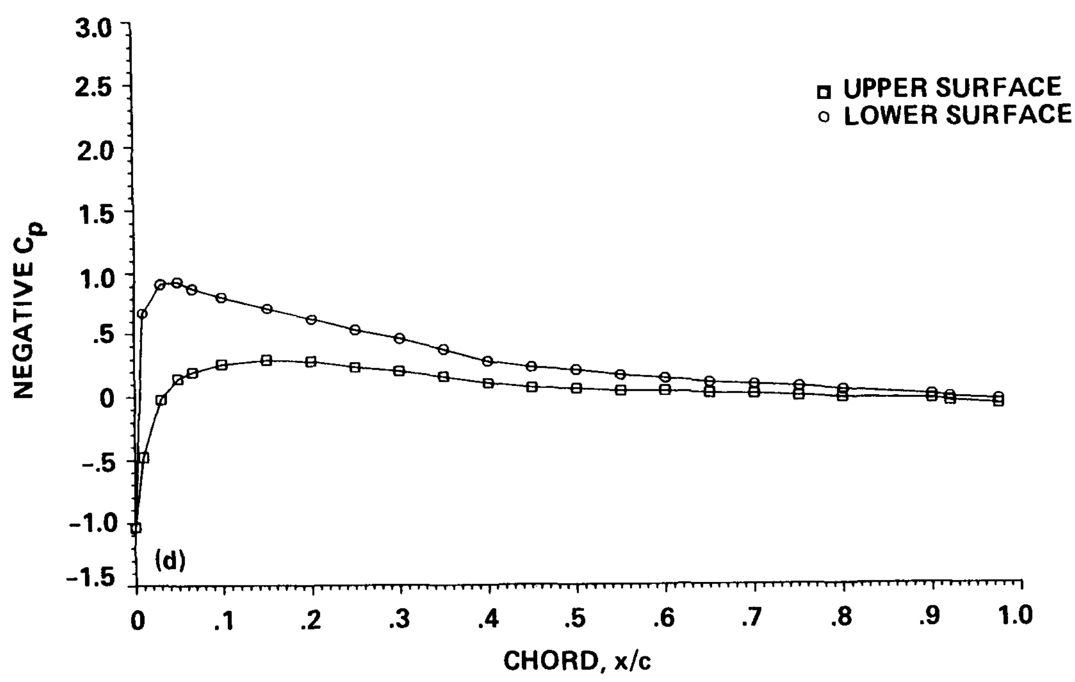

Figure 7.– Continued; (c) $\alpha_c = -1.78°$, (d) $\alpha_c = -1.71°$.

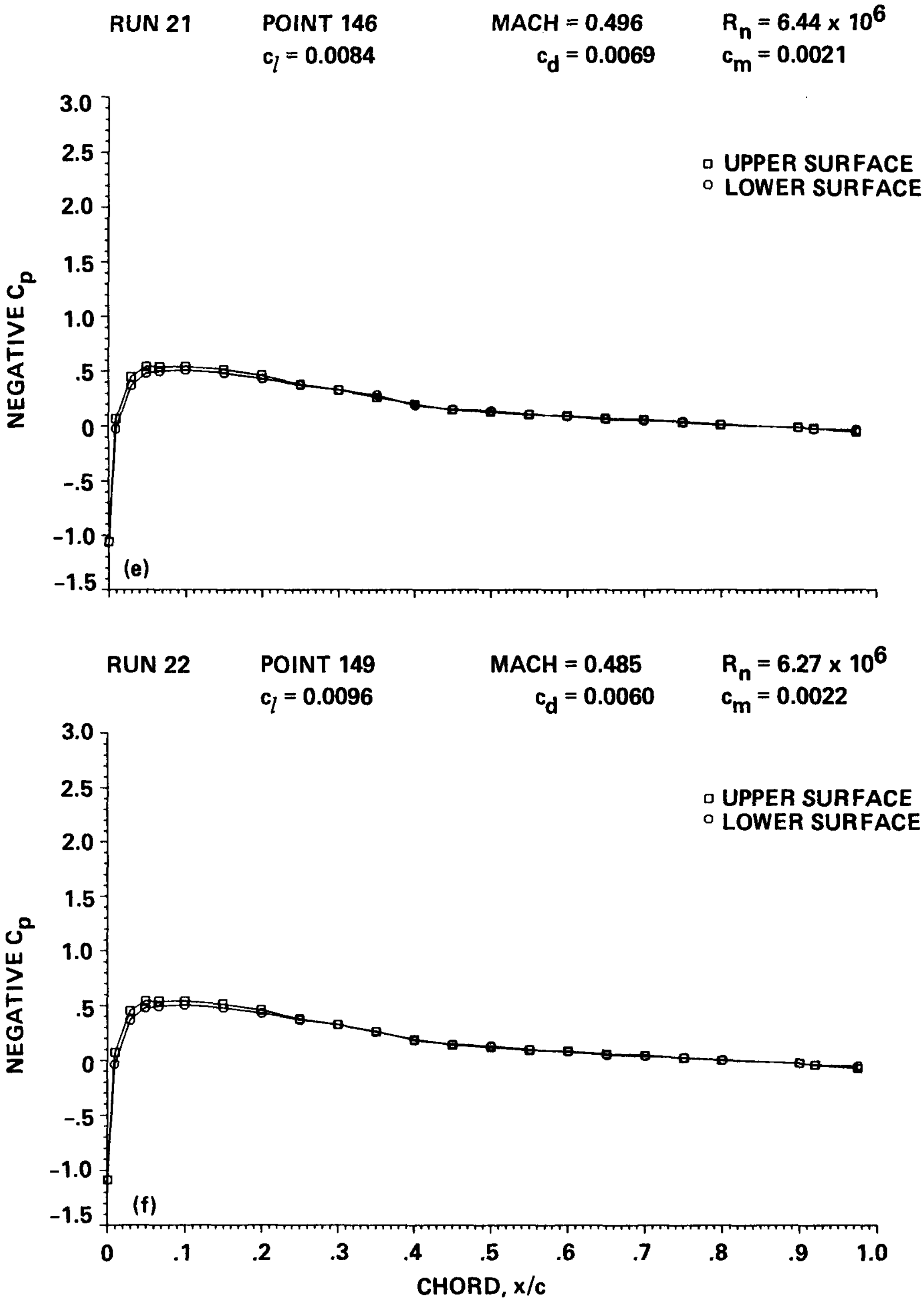

Figure 7.- Continued; (e) $\alpha_c = 0.01°$, (f) $\alpha_c = 0.00°$.

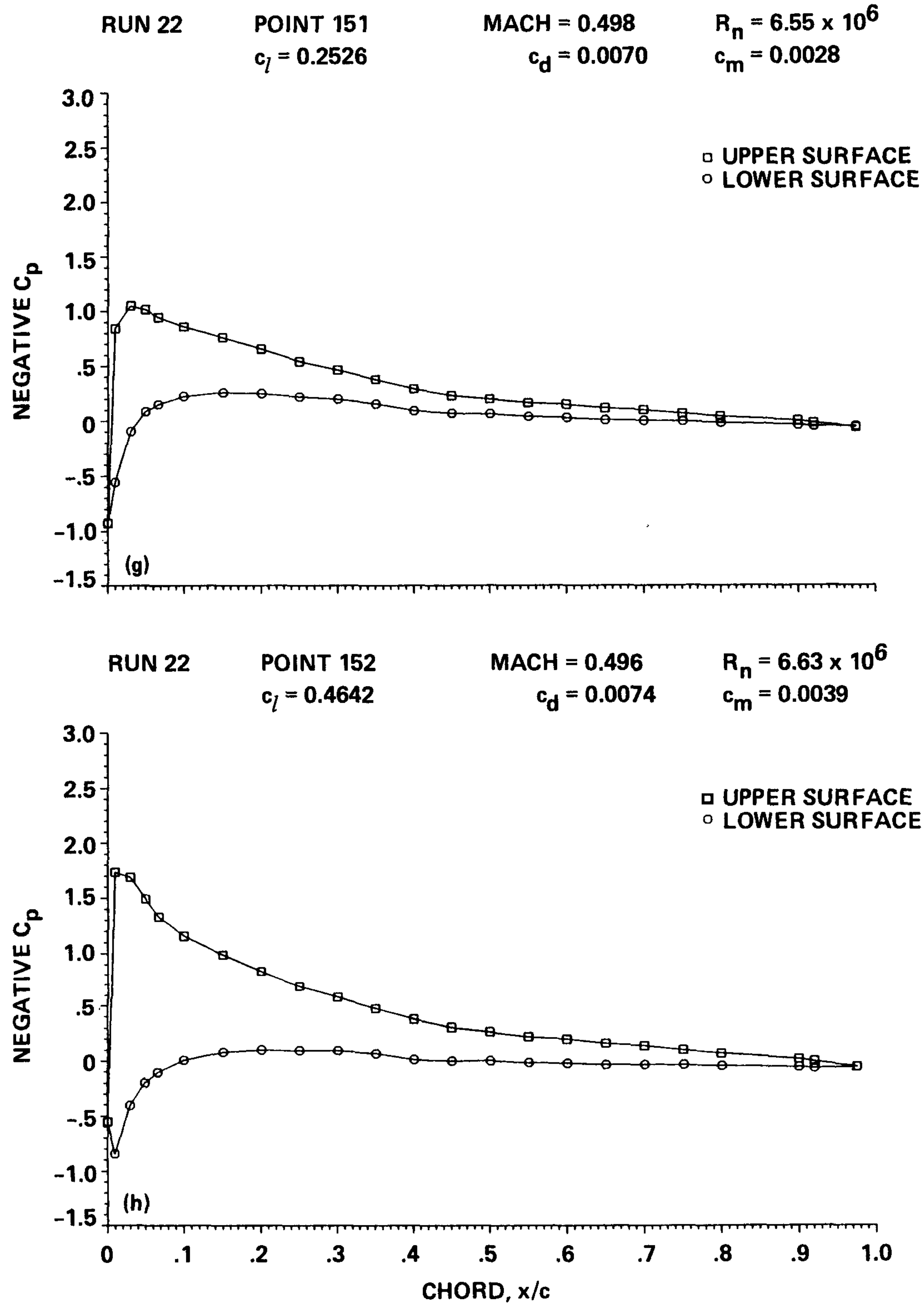

Figure 7.– Continued; (g) α_c = 1.81°, (h) α_c = 3.42°.

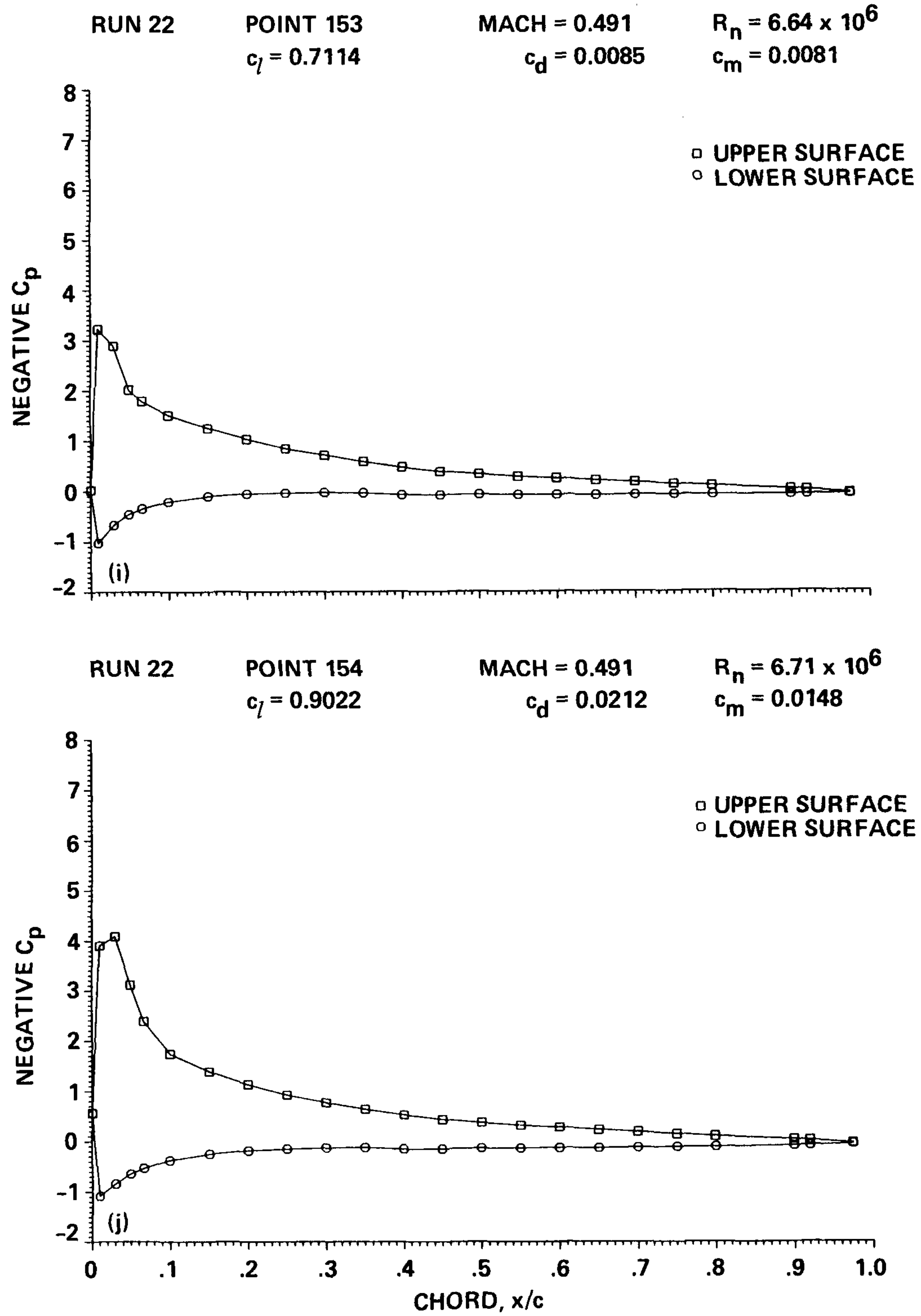

Figure 7.– Continued; (i) $\alpha_c = 5.19°$, (j) $\alpha_c = 7.05°$.

RUN 7 POINT 54 MACH = 0.488 $R_n = 6.84 \times 10^6$

$c_l = 0.8960$ $c_d = 0.0155$ $c_m = 0.0142$

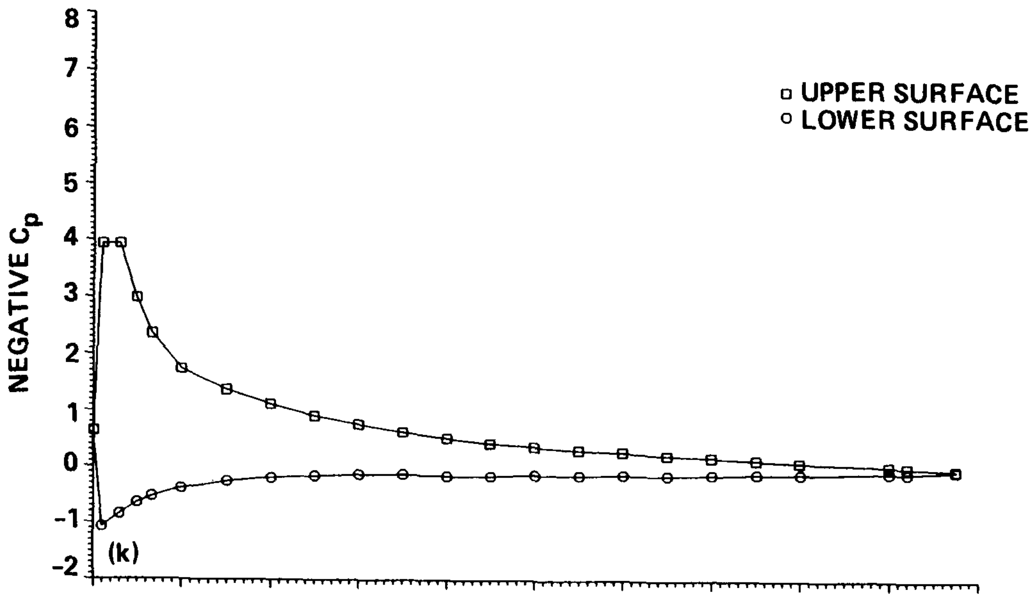

RUN 22 POINT 155 MACH = 0.491 $R_n = 6.80 \times 10^6$

$c_l = 0.9461$ $c_d = 0.0442$ $c_m = 0.0059$

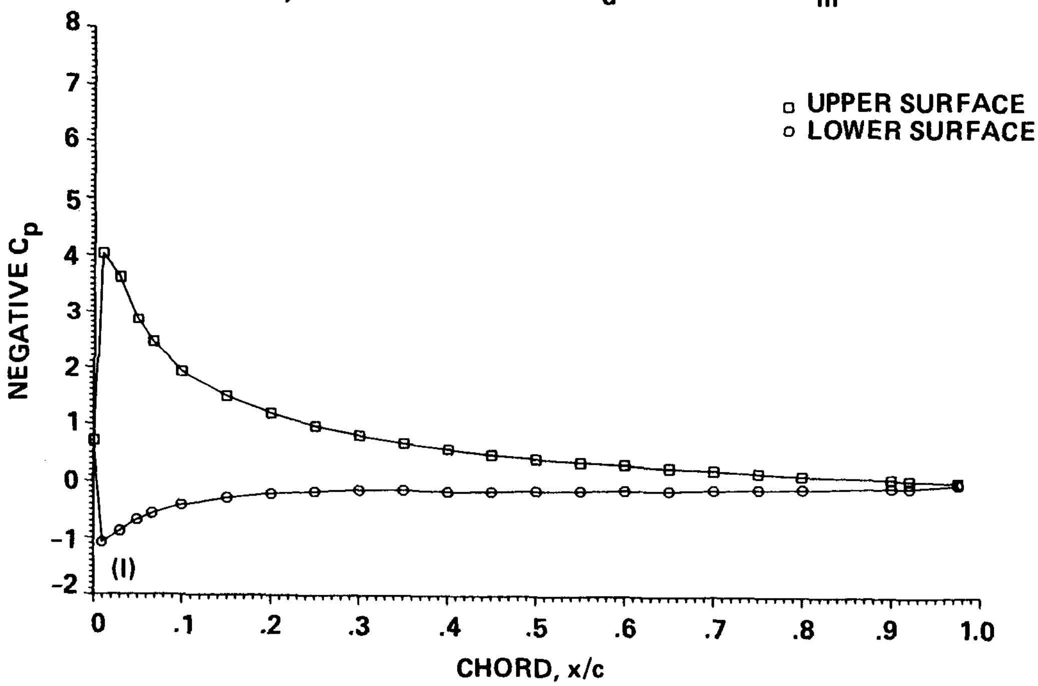

Figure 7.– Continued; (k) $\alpha_c = 7.13°$, (l) $\alpha_c = 8.00°$.

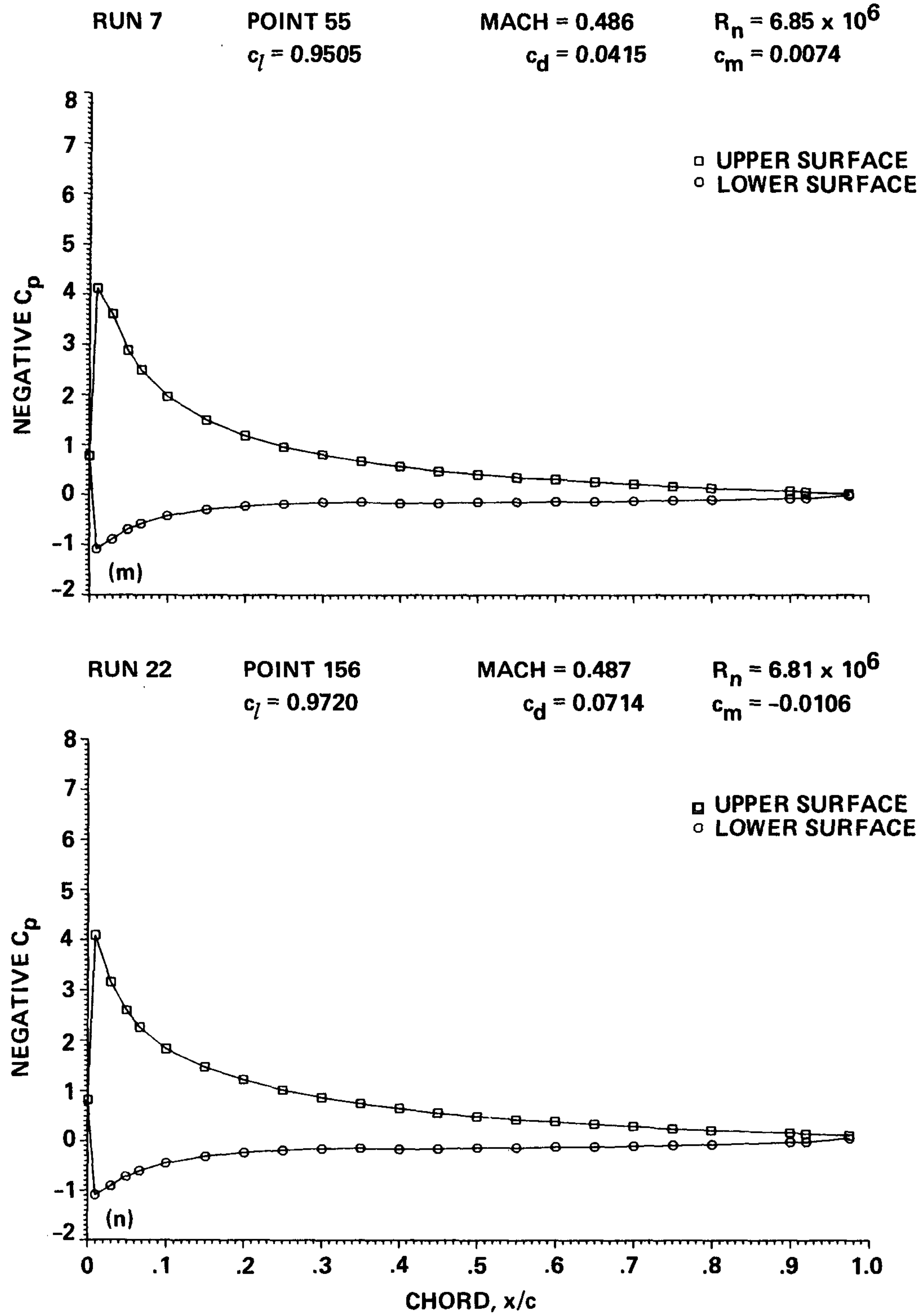

Figure 7.– Continued; (m) $\alpha_c = 8.06°$, (n) $\alpha_c = 8.95°$.

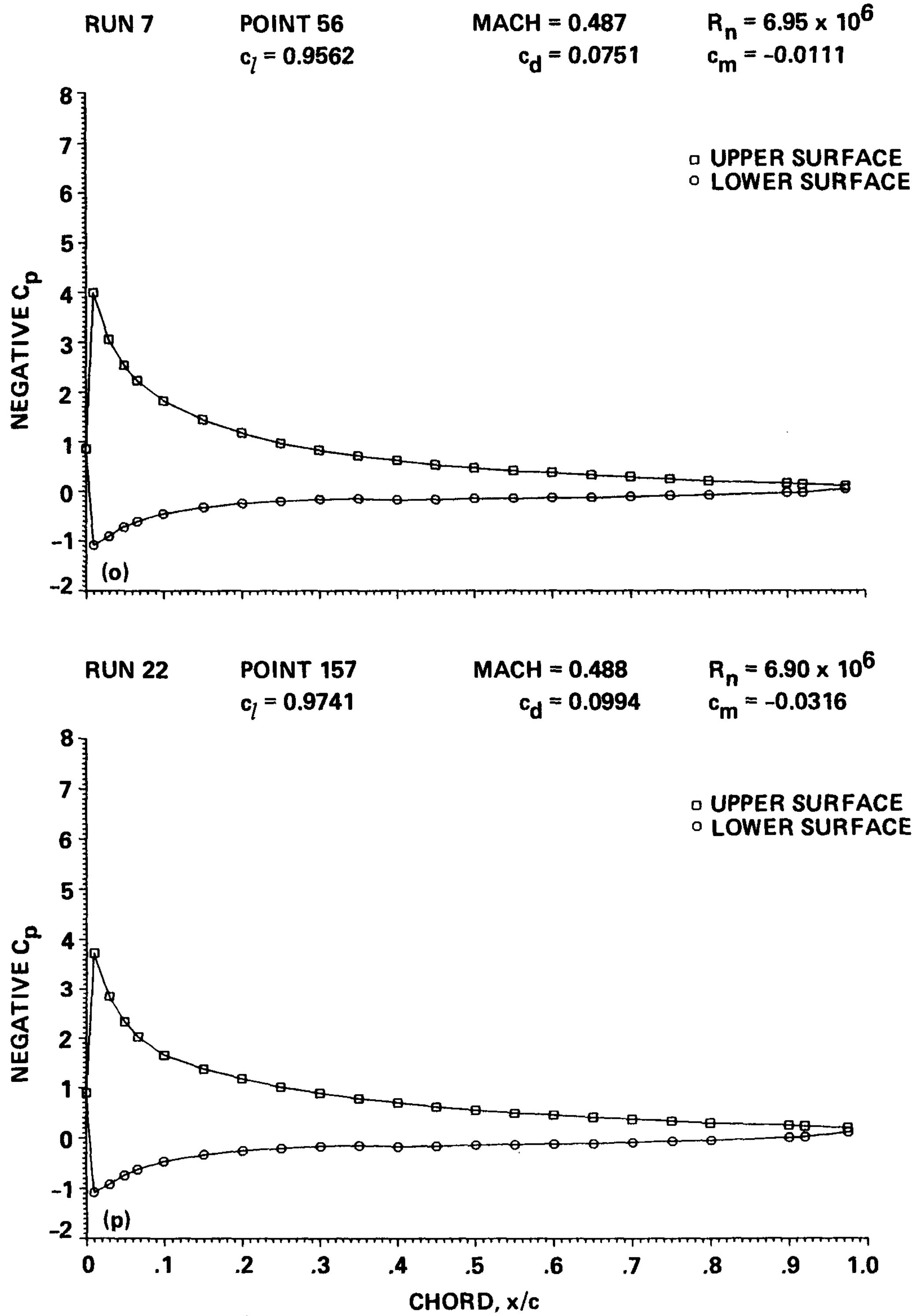

Figure 7.– Concluded; (o) $\alpha_c = 9.08°$, (p) $\alpha_c = 10.00°$.

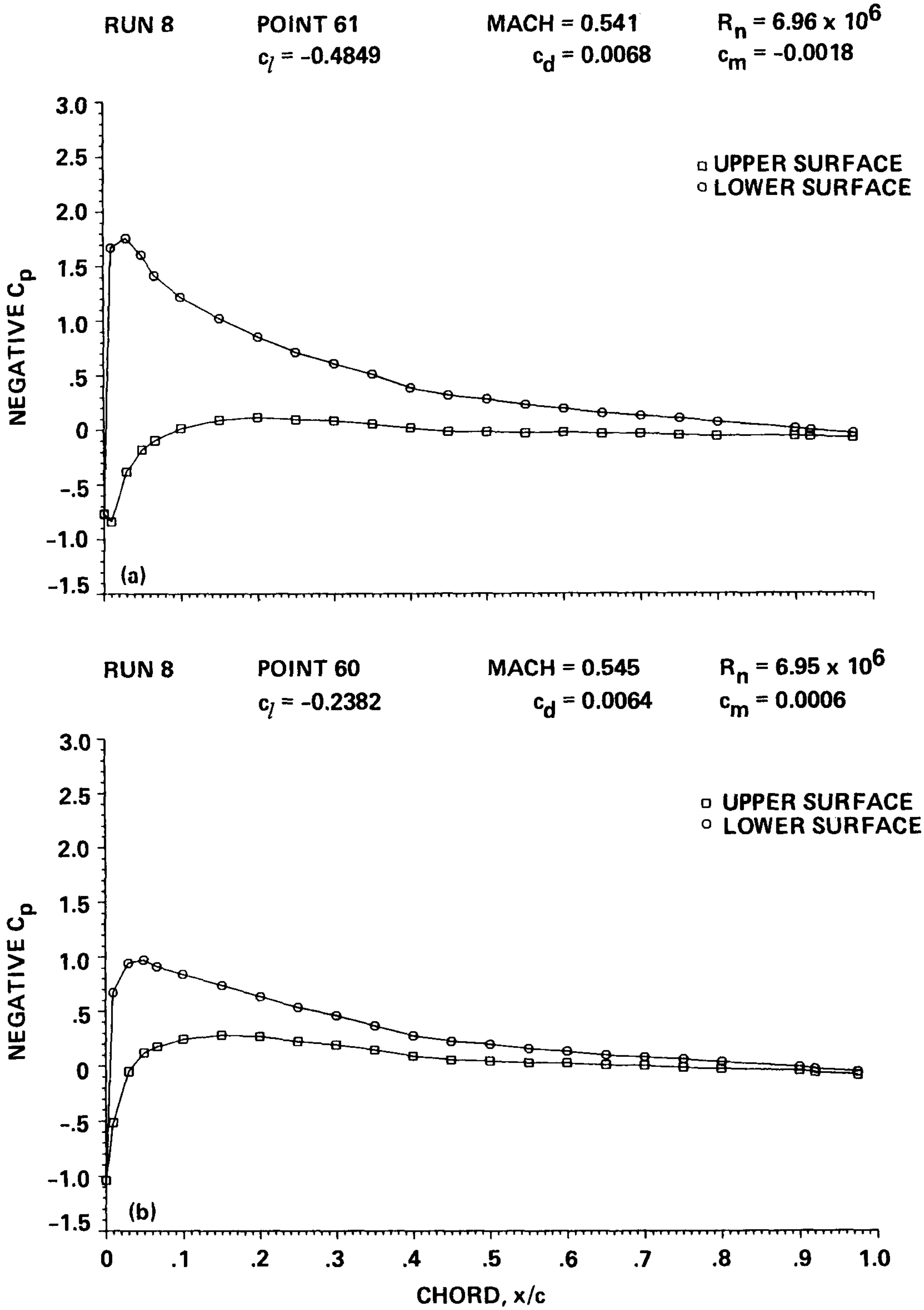

Figure 8.– Chordwise pressure distribution of the OLS/TAAT airfoil, $M = 0.54$; (a) $\alpha_c = -3.50°$, (b) $\alpha_c = -1.80°$.

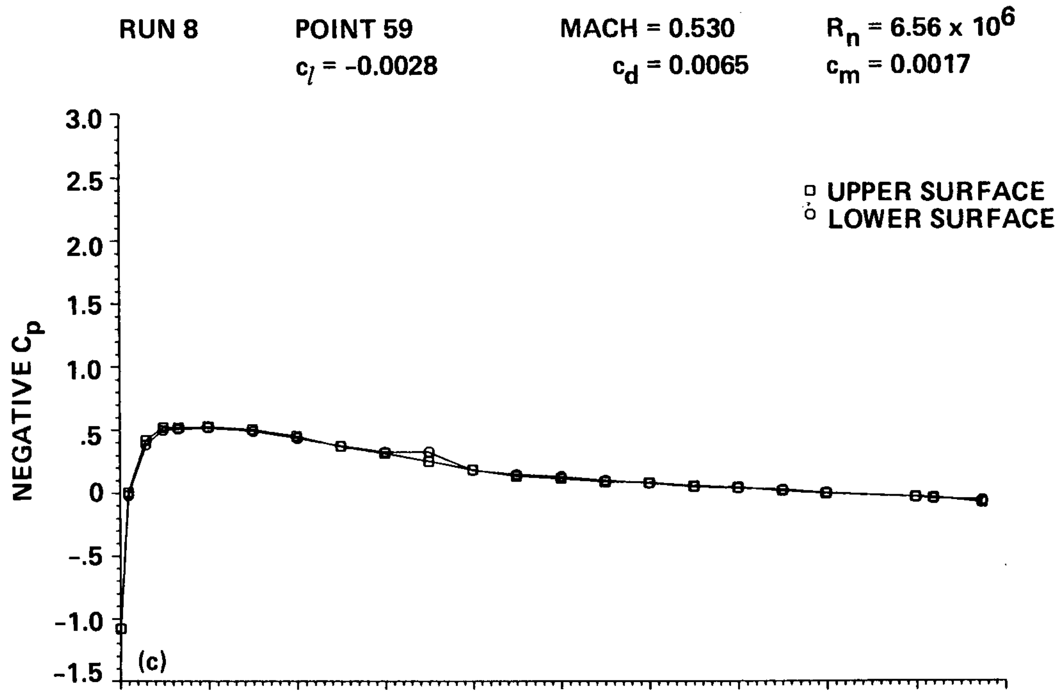

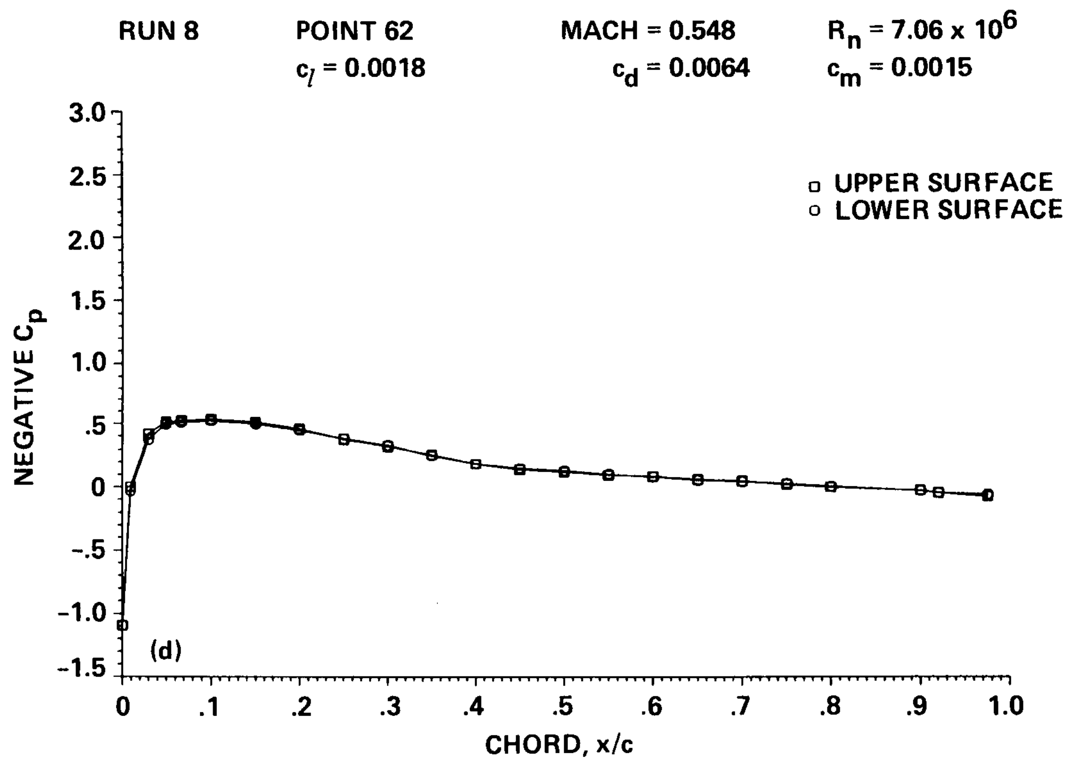

Figure 8.– Continued; (c) α_c = -0.03°, (d) α_c = -0.03°.

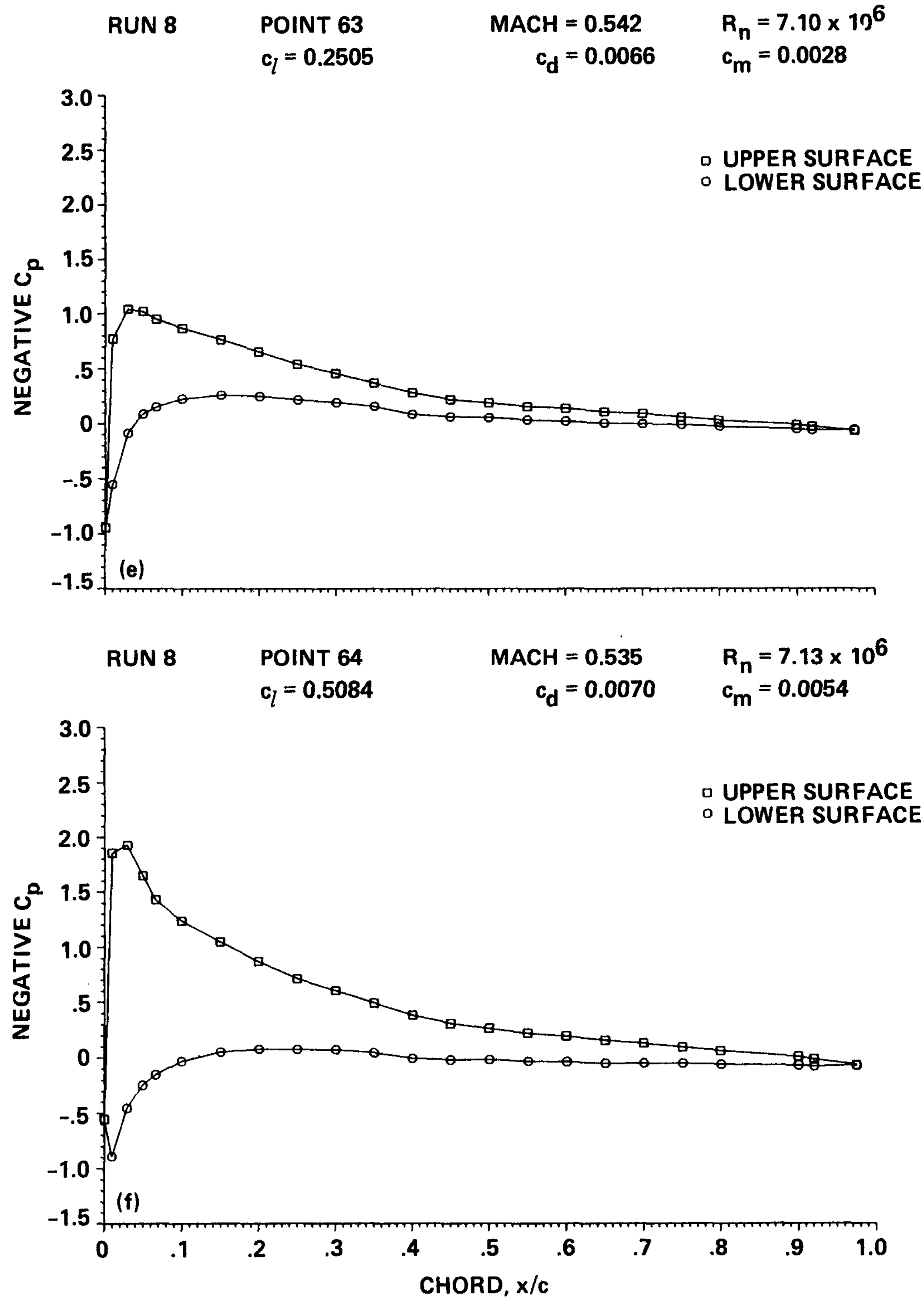

Figure 8.– Continued; (e) $\alpha_c = 1.78°$, (f) $\alpha_c = 3.61°$.

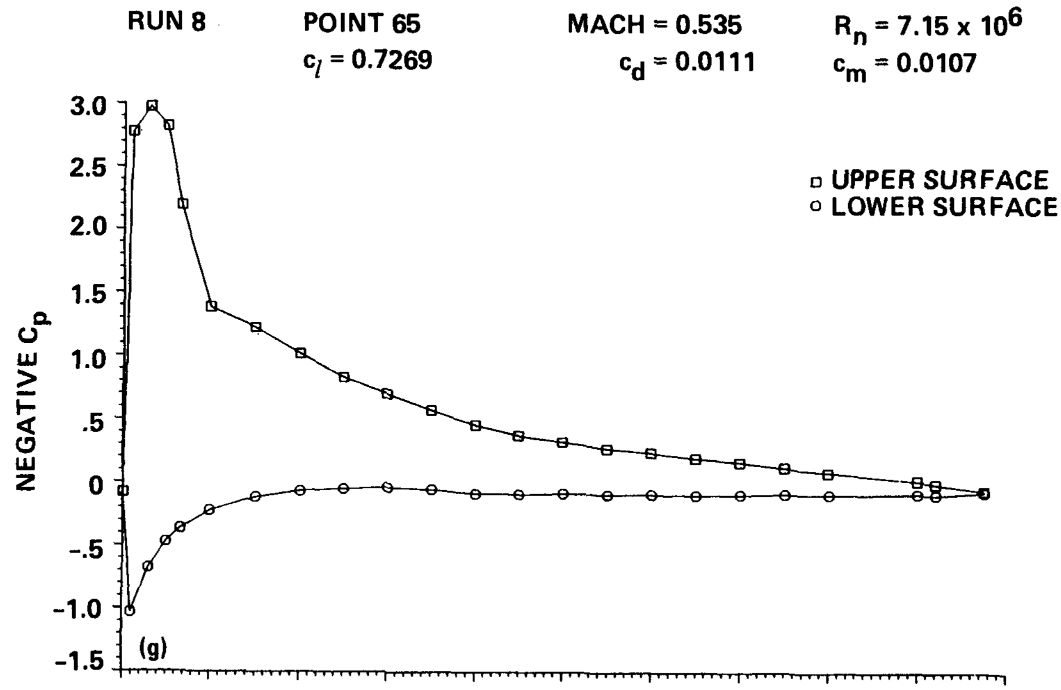

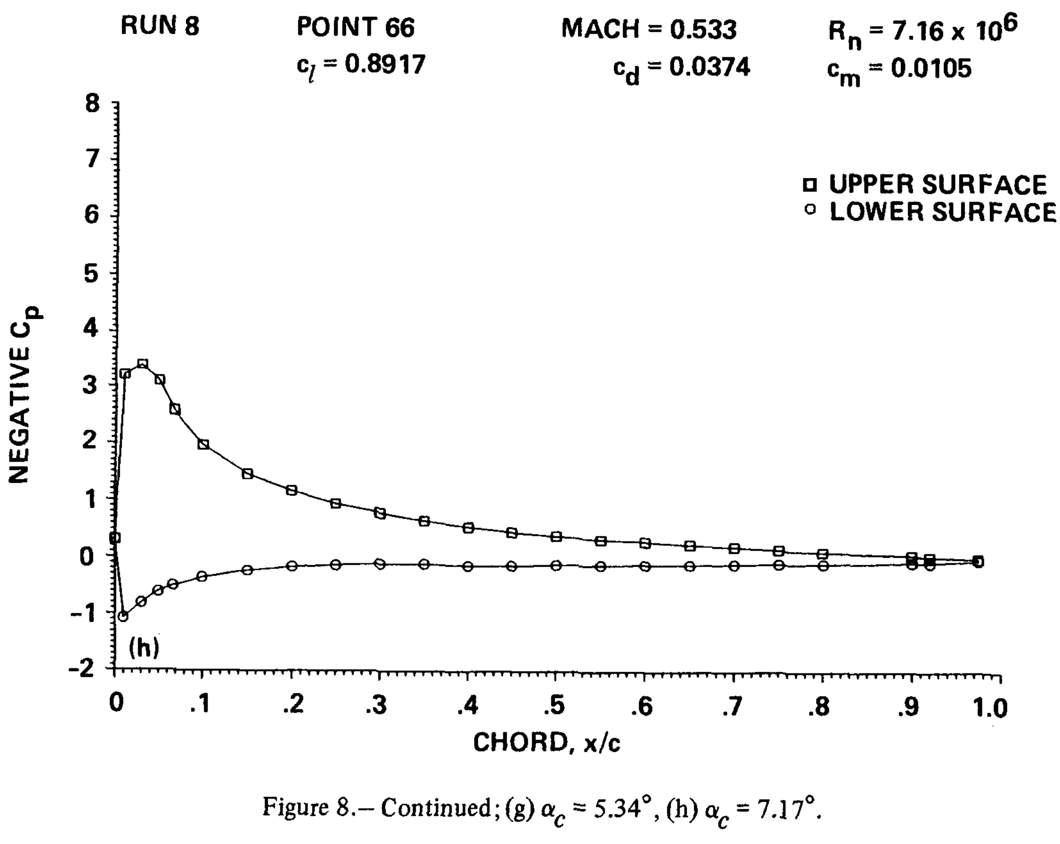

Figure 8.– Continued; (g) α_c = 5.34°, (h) α_c = 7.17°.

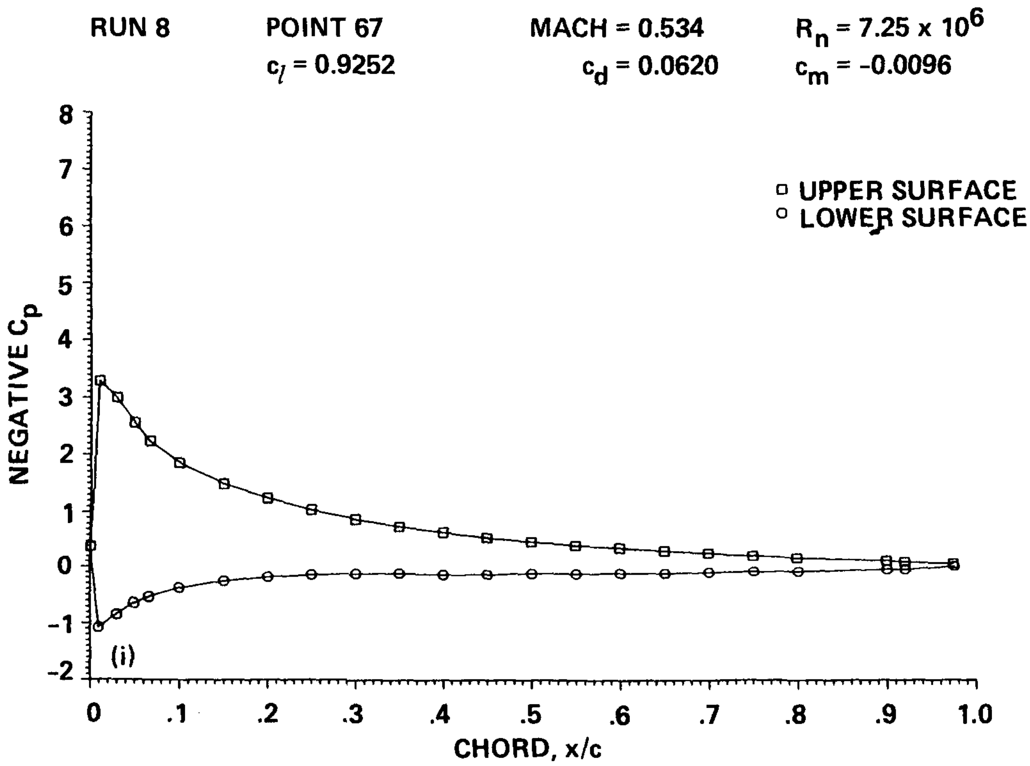

Figure 8.– Concluded; (i) $\alpha_c = 8.17°$.

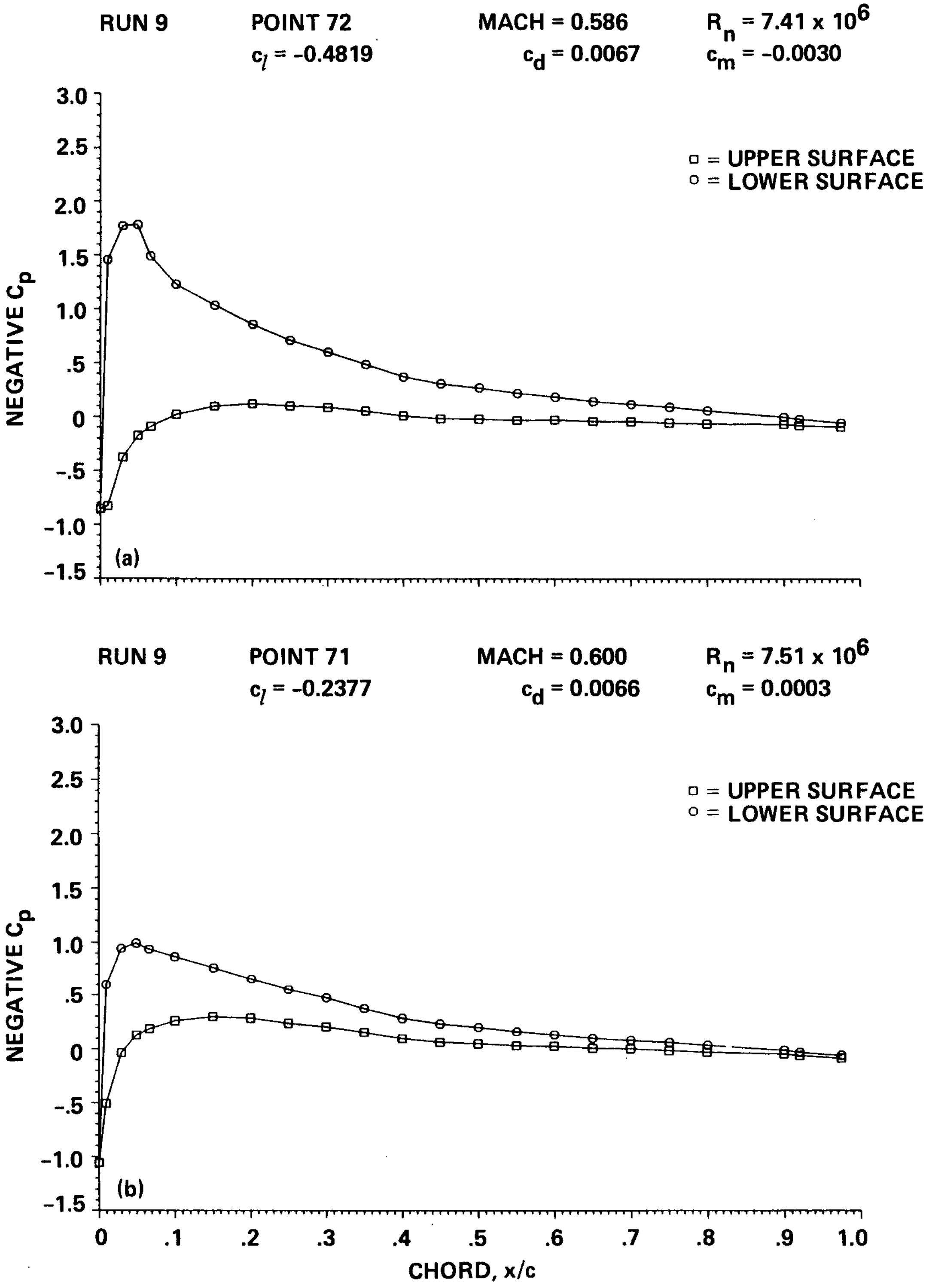

Figure 9.– Chordwise pressure distribution of the OLS/TAAT airfoil, $M = 0.59$; (a) $\alpha_c = -3.45°$, (b) $\alpha_c = -1.81°$.

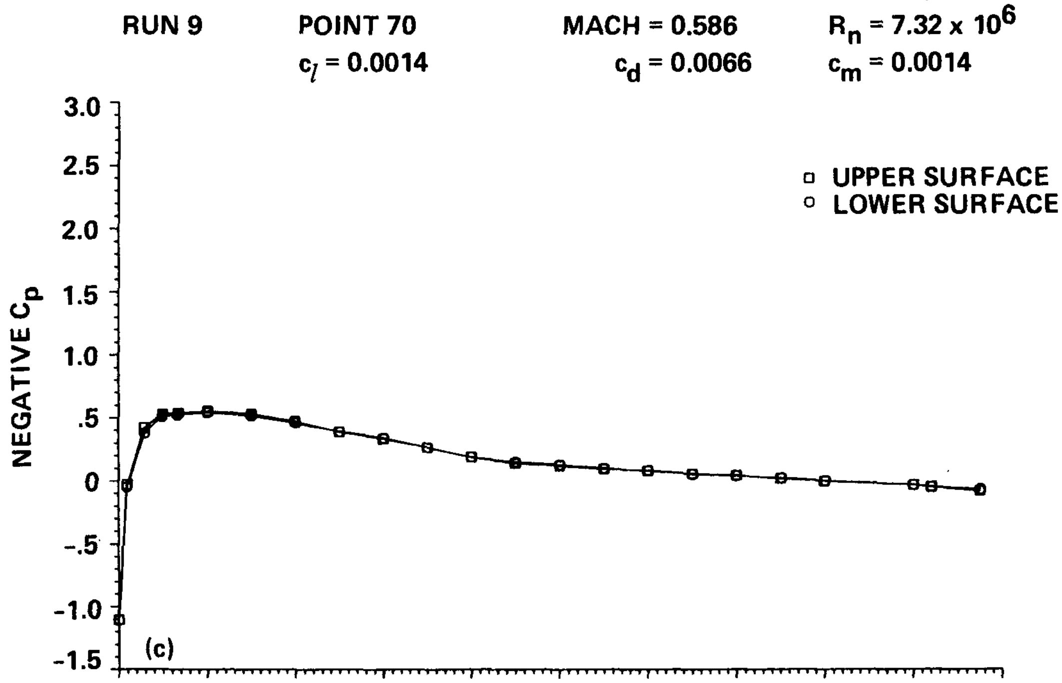

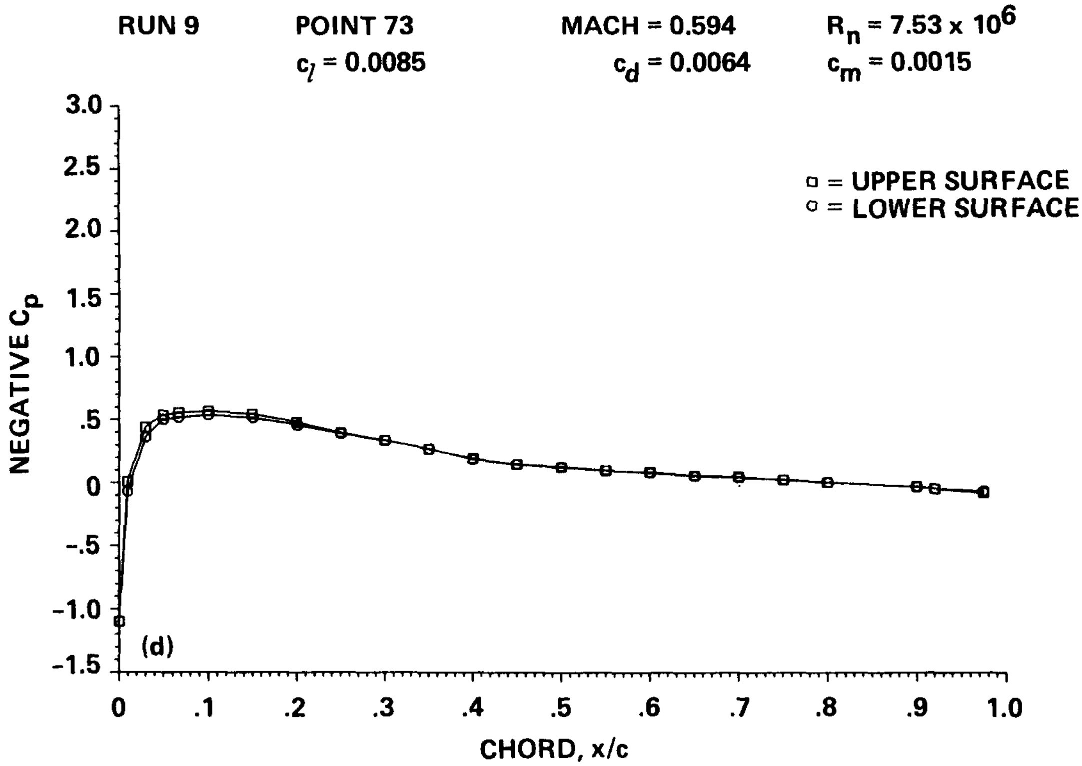

Figure 9.– Continued; (c) α_c = -0.07°, (d) α_c = -0.01°.

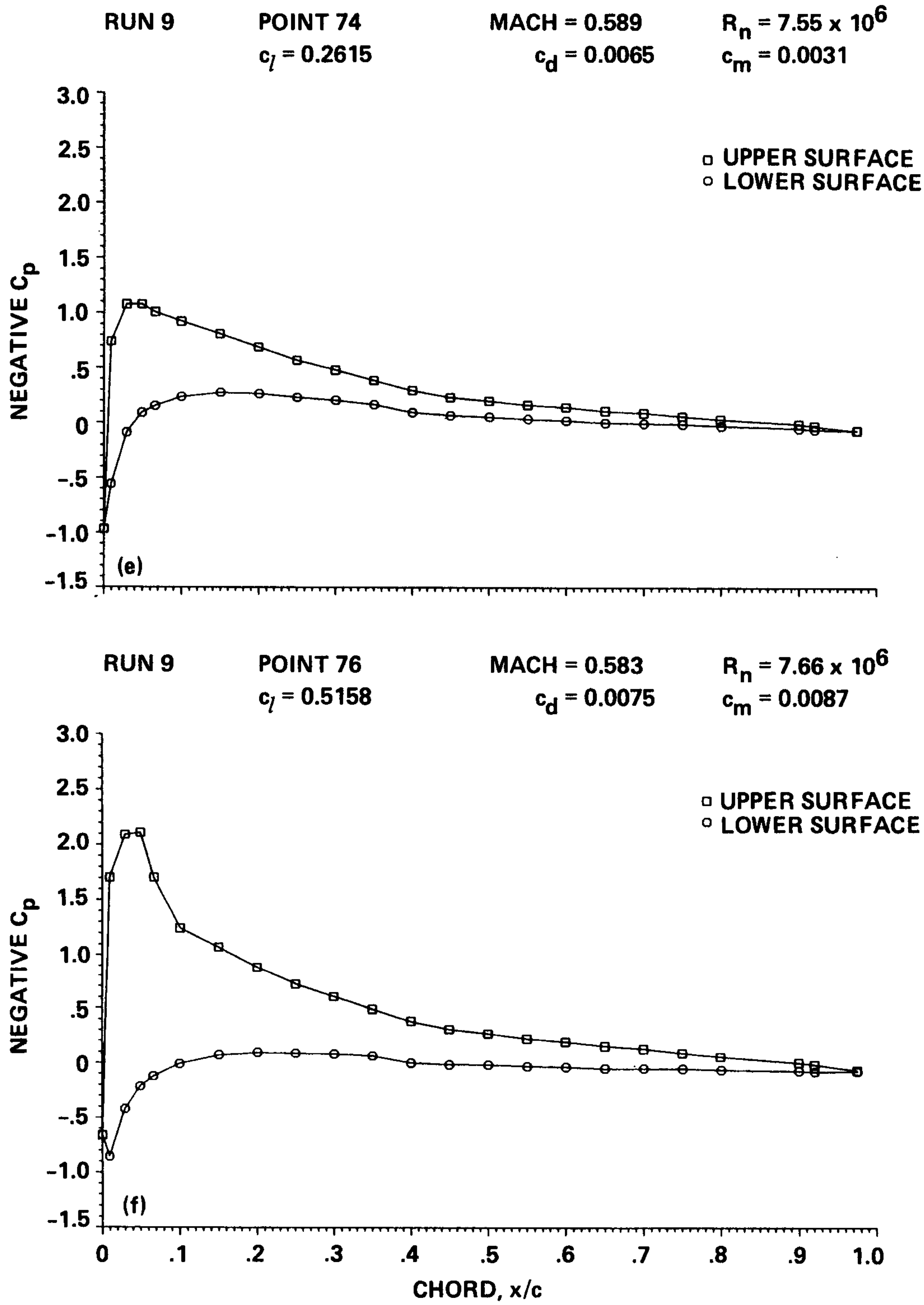

Figure 9.– Continued; (e) $\alpha_c = 1.77°$, (f) $\alpha_c = 3.45°$.

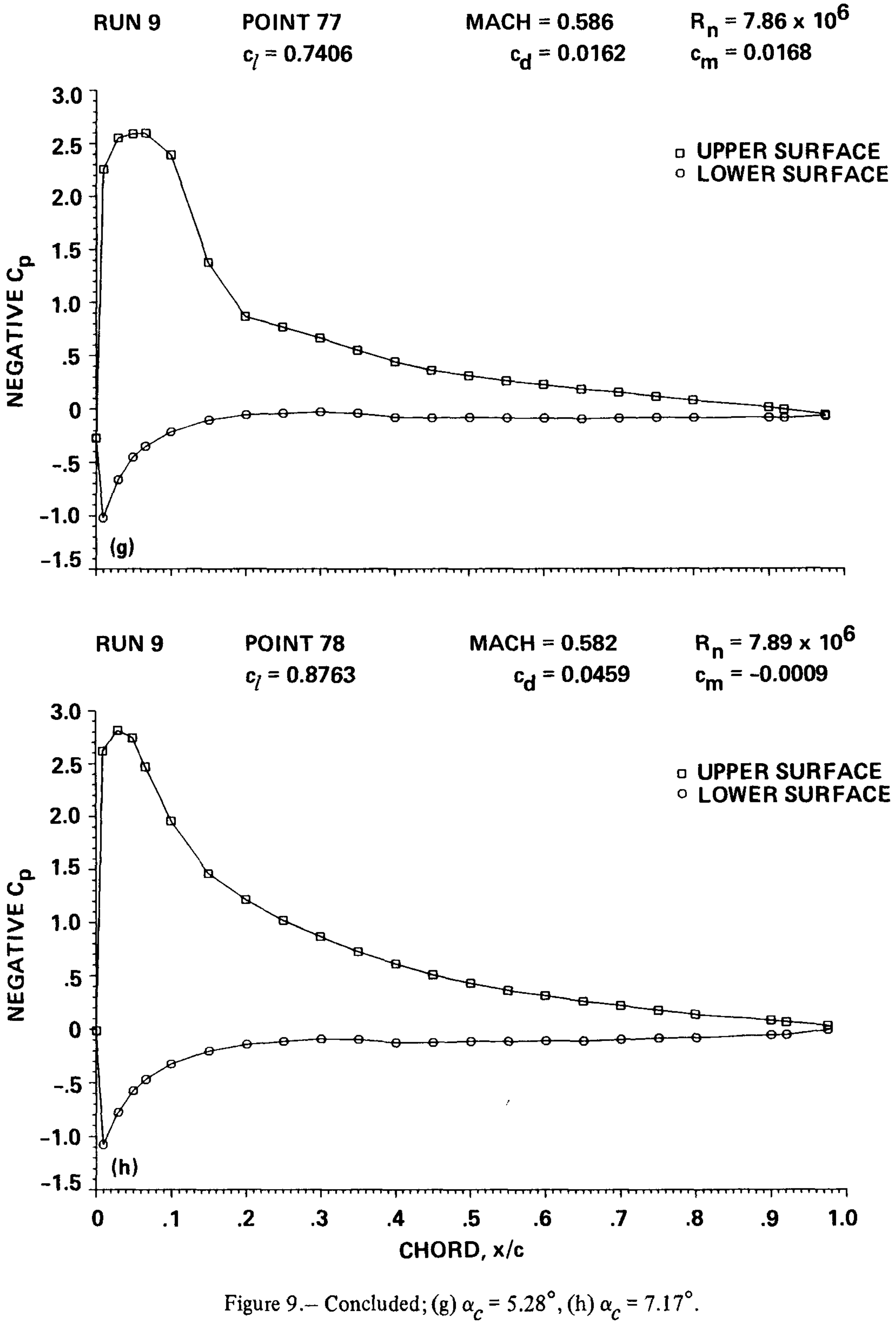

Figure 9.– Concluded; (g) $\alpha_c = 5.28°$, (h) $\alpha_c = 7.17°$.

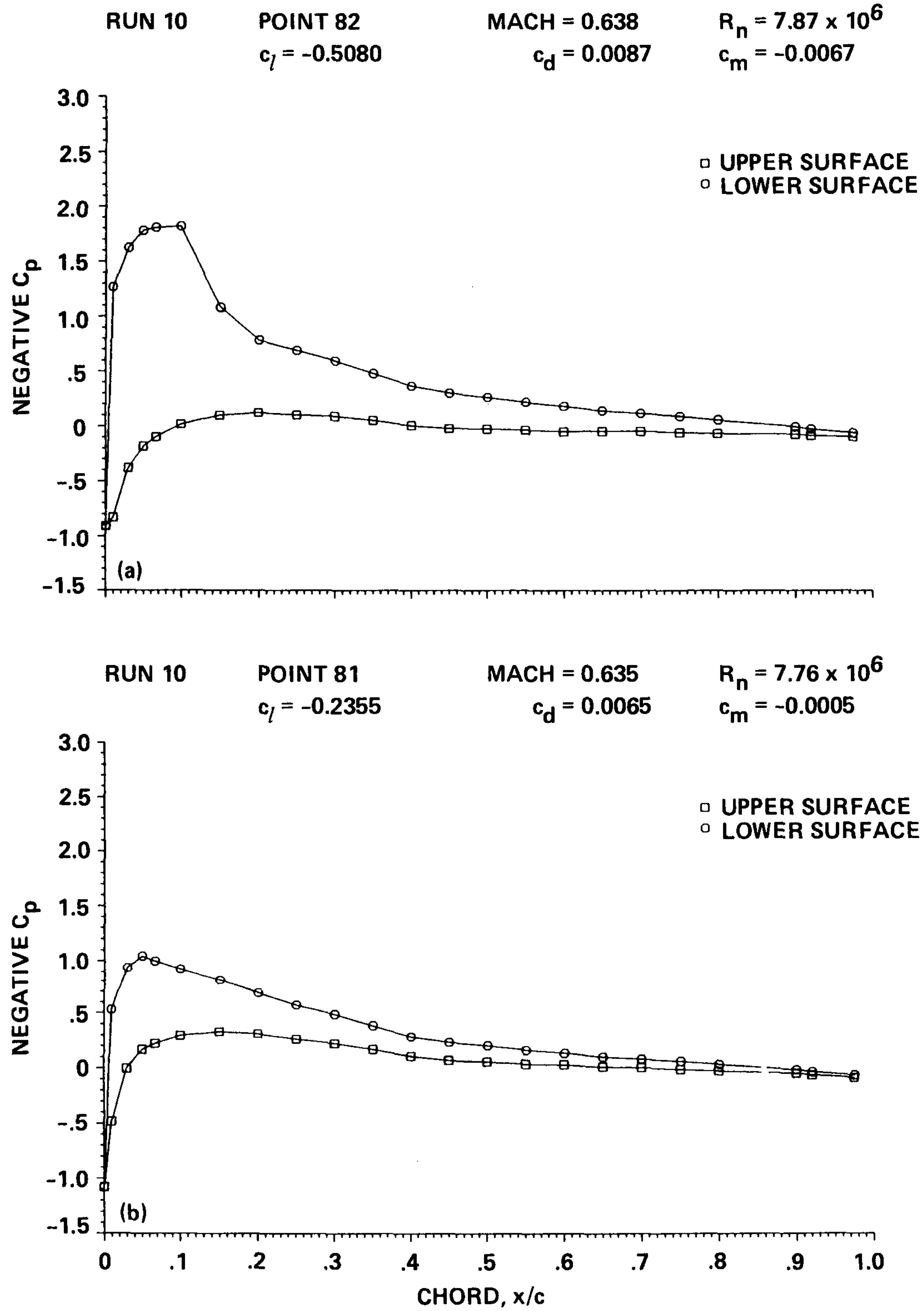

Figure 10.– Chordwise pressure distribution of the OLS/TAAT airfoil, $M = 0.64$; (a) $\alpha_c = -3.52°$, (b) $\alpha_c = -1.66°$

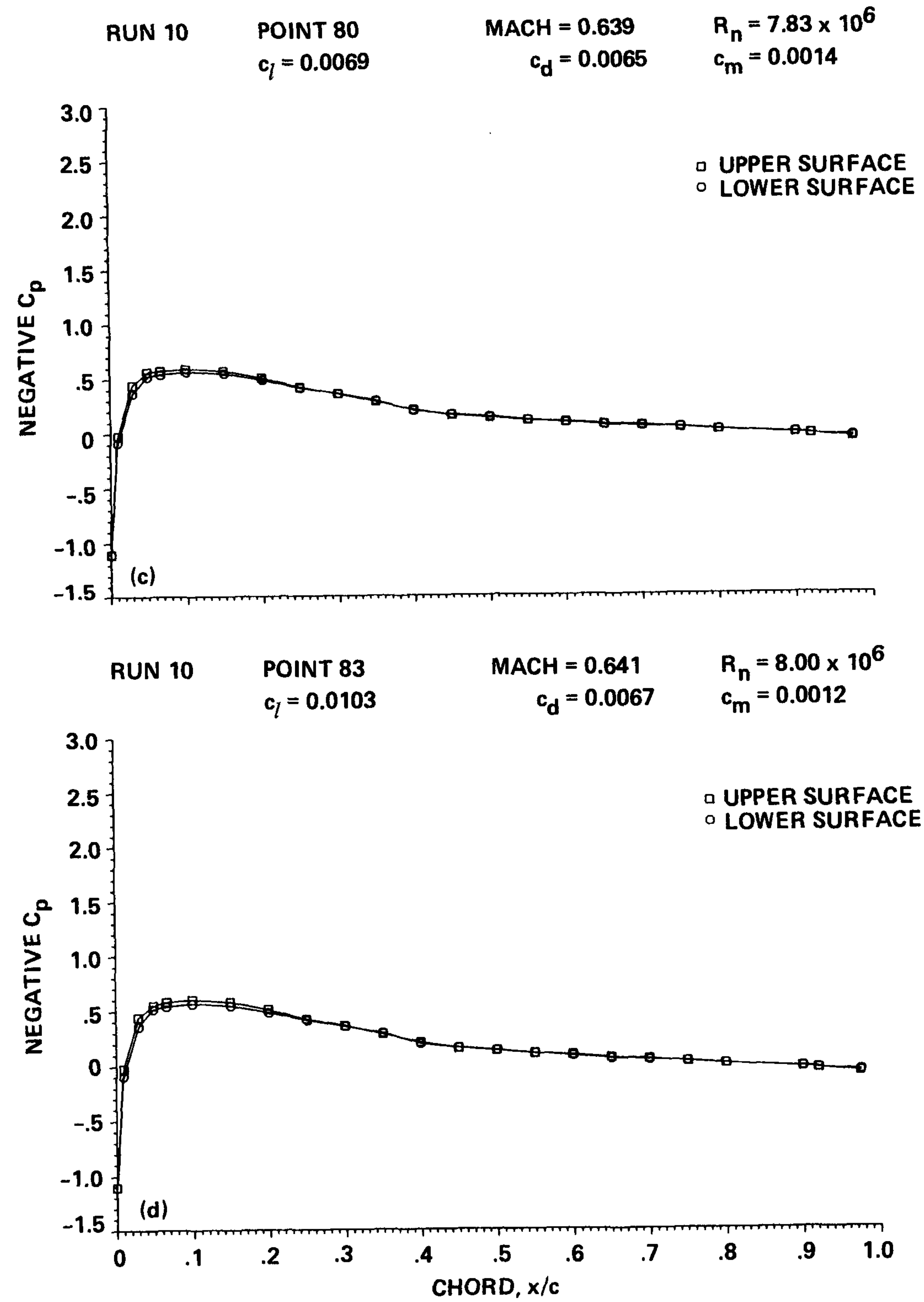

Figure 10.– Continued; (c) α_c = -0.03°, (d) α_c = 0.02°.

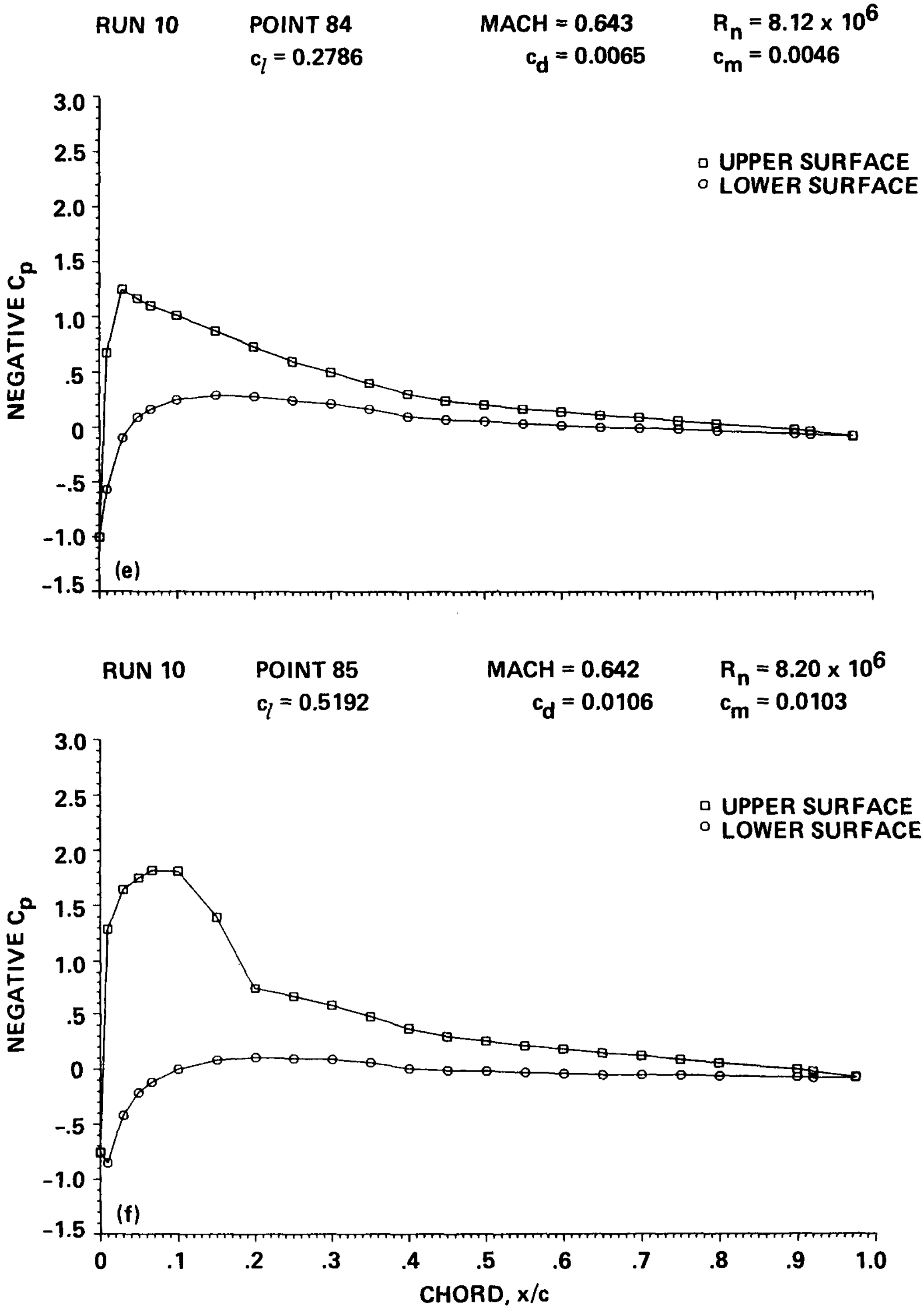

Figure 10.– Continued; (e) $\alpha_c = 1.77°$, (f) $\alpha_c = 3.51°$.

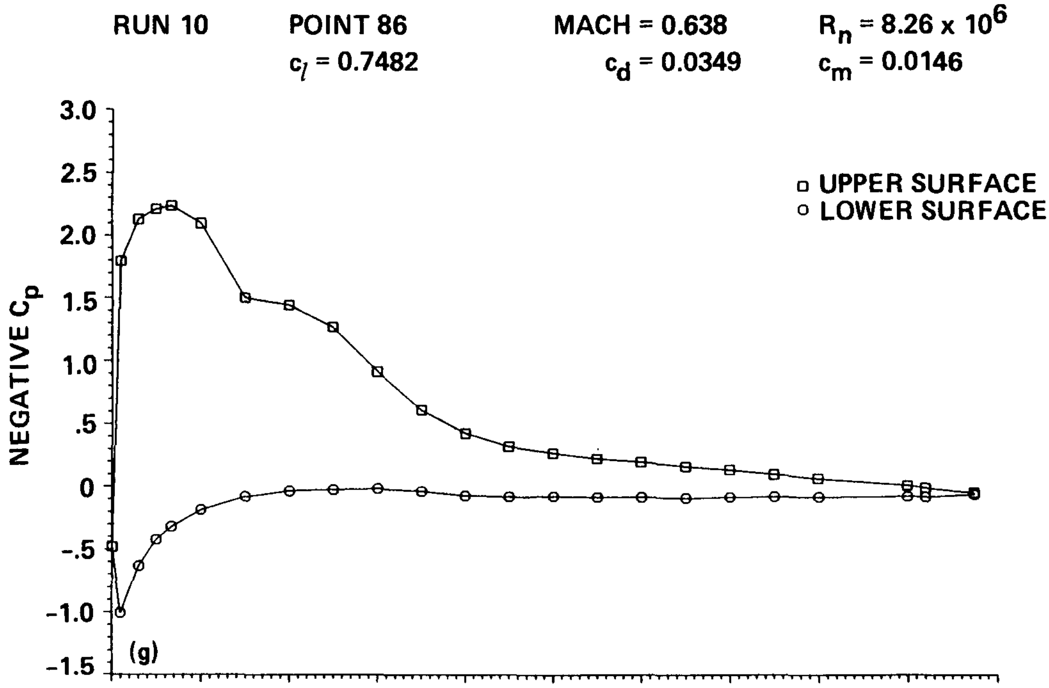

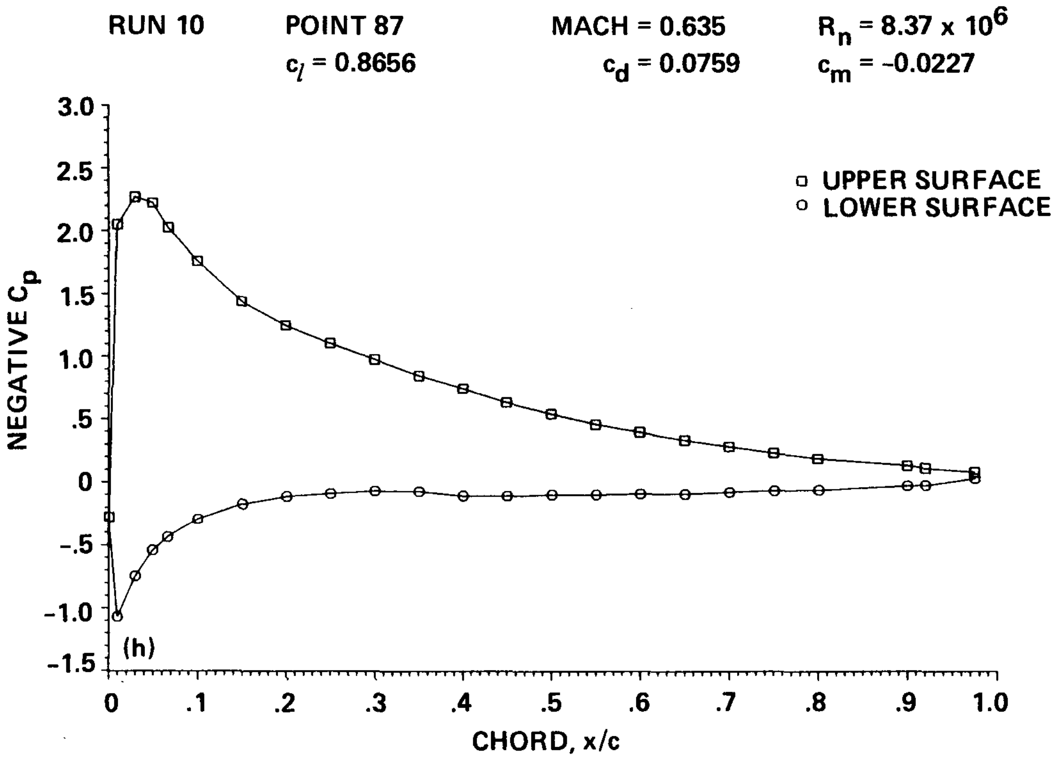

Figure 10.– Concluded; (g) $\alpha_c = 5.27°$, (h) $\alpha_c = 7.24°$.

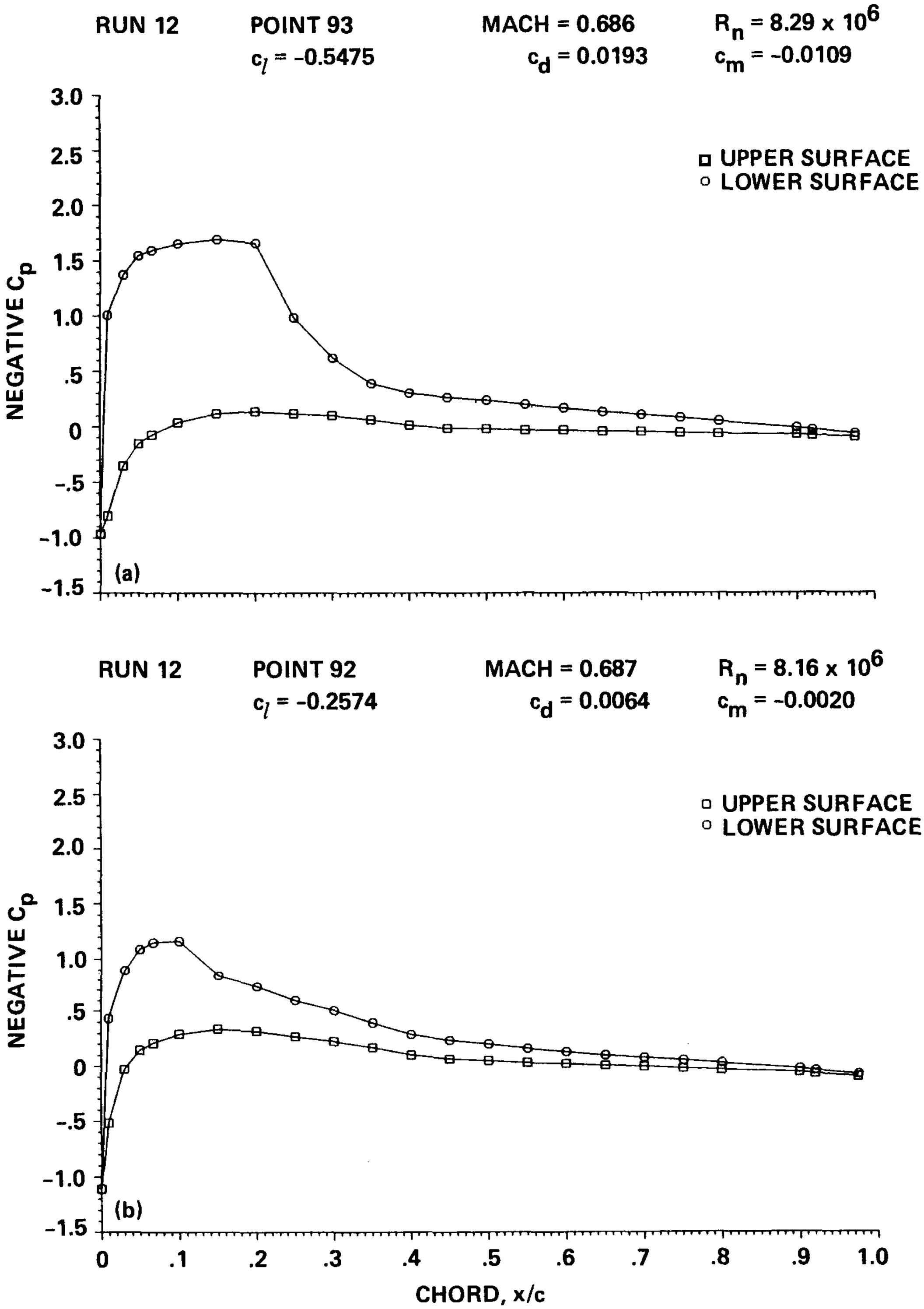

Figure 11.– Chordwise pressure distribution of the OLS/TAAT airfoil, M = 0.69; (a) α_c = -3.44°, (b) α_c = -1.71°.

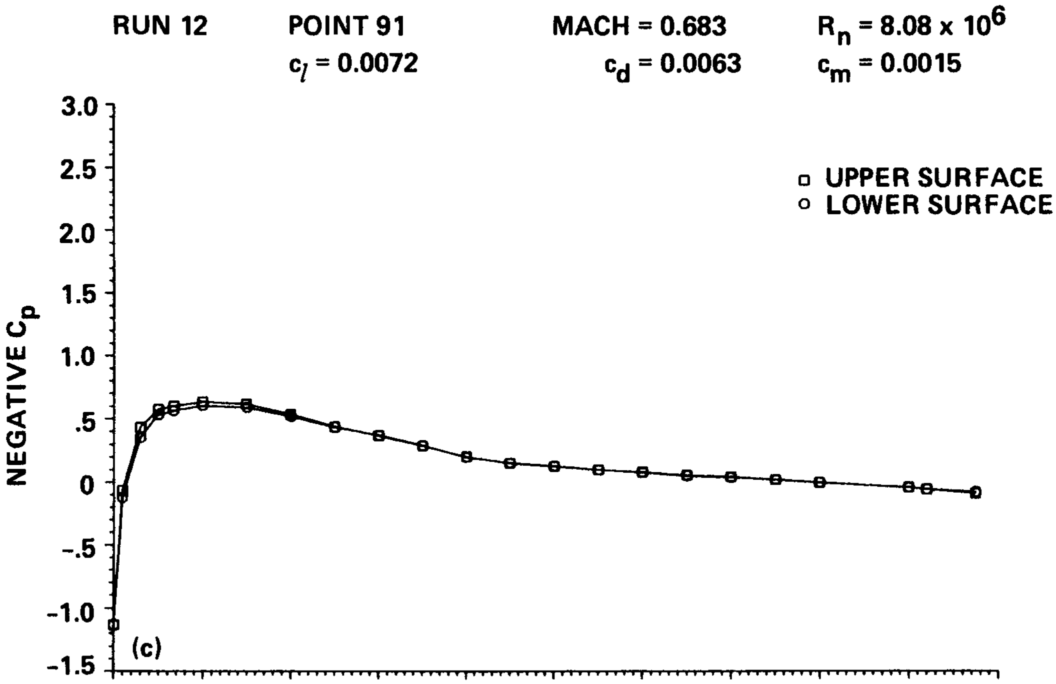

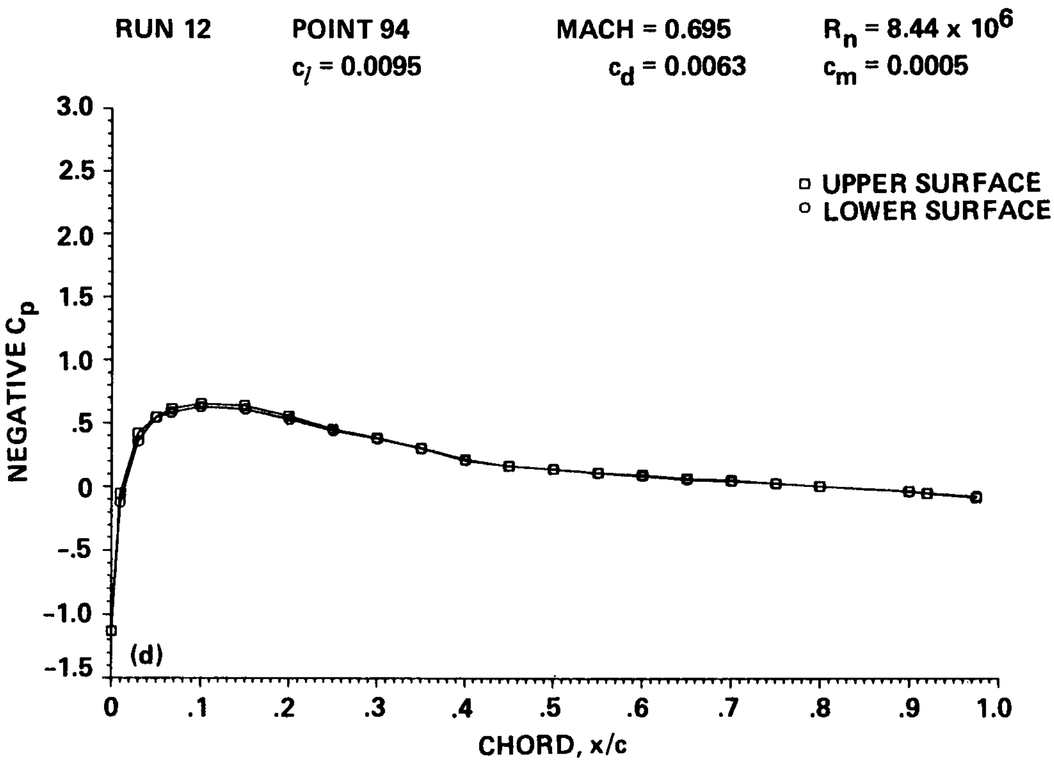

Figure 11.– Continued; (c) α_c = -0.01°, (d) α_c = 0.06°.

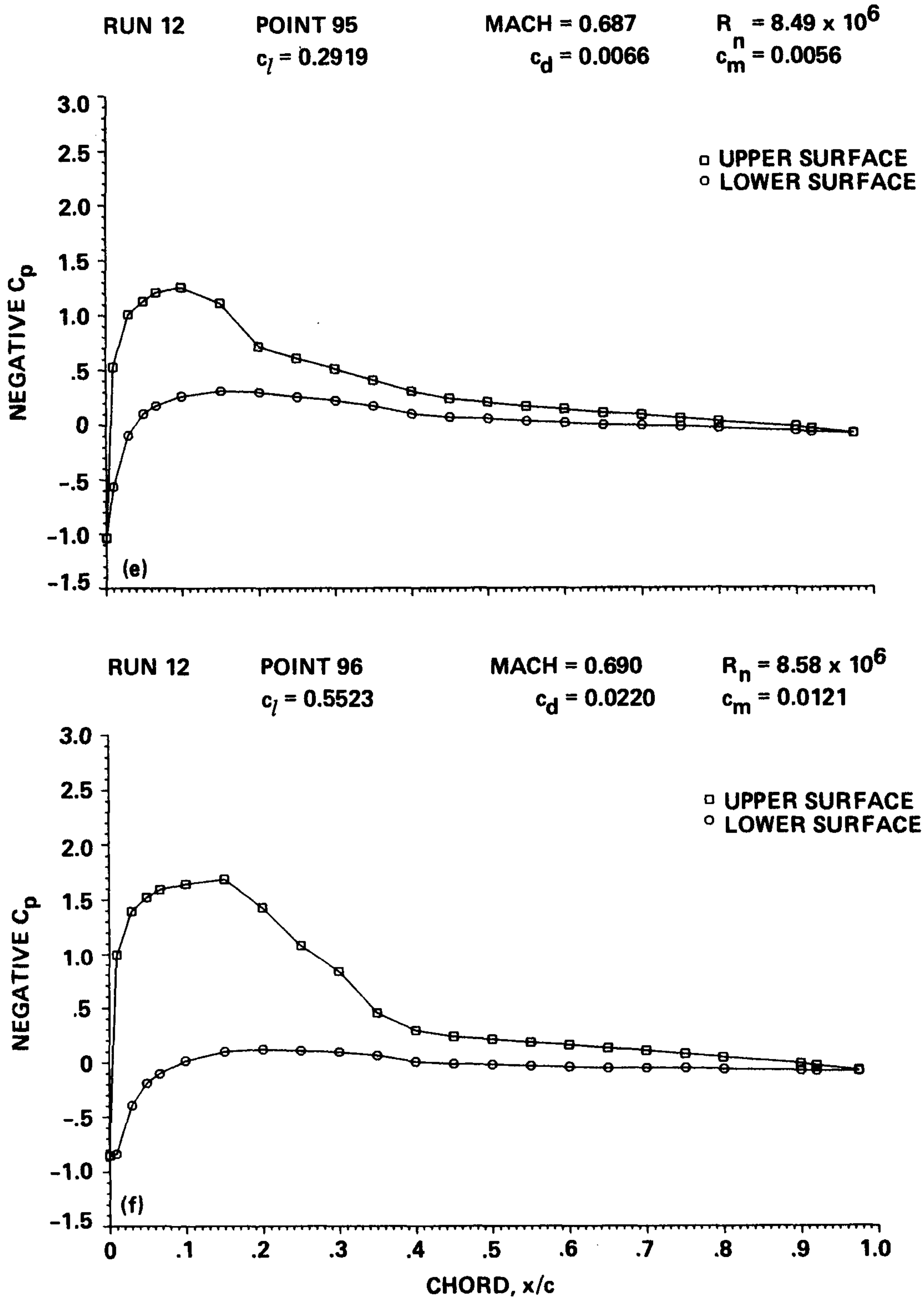

Figure 11.– Continued; (e) $\alpha_c = 1.78°$, (f) $\alpha_c = 3.49°$.

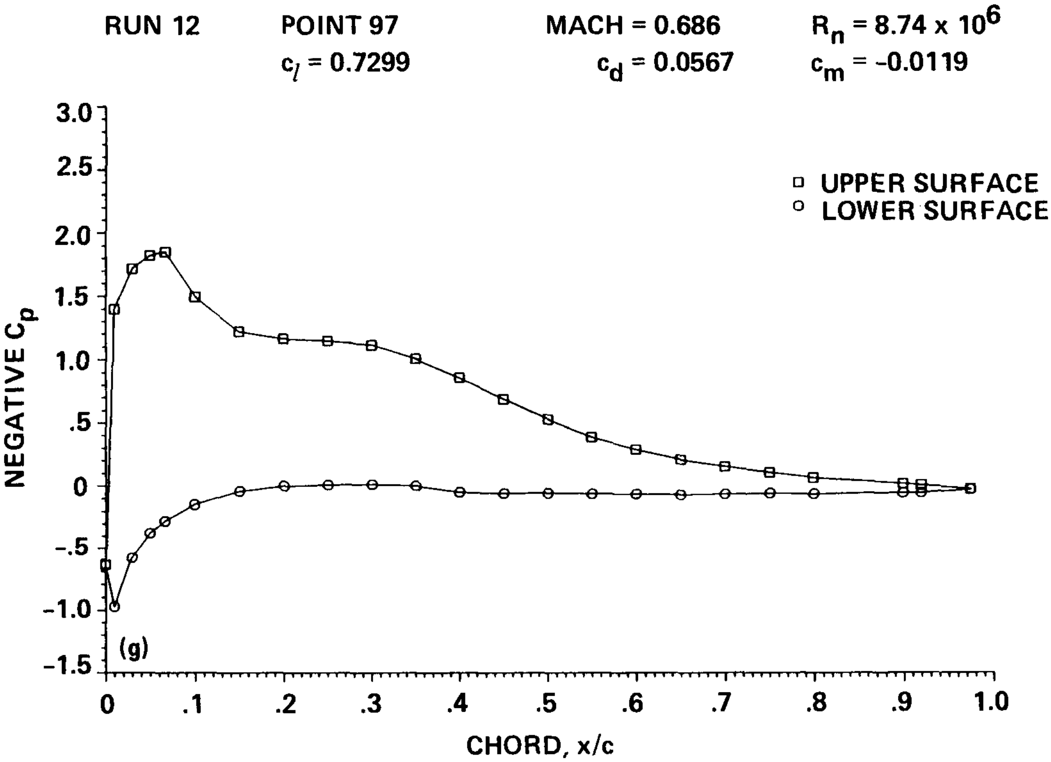

Figure 11.– Concluded; (g) $\alpha_c = 5.29°$.

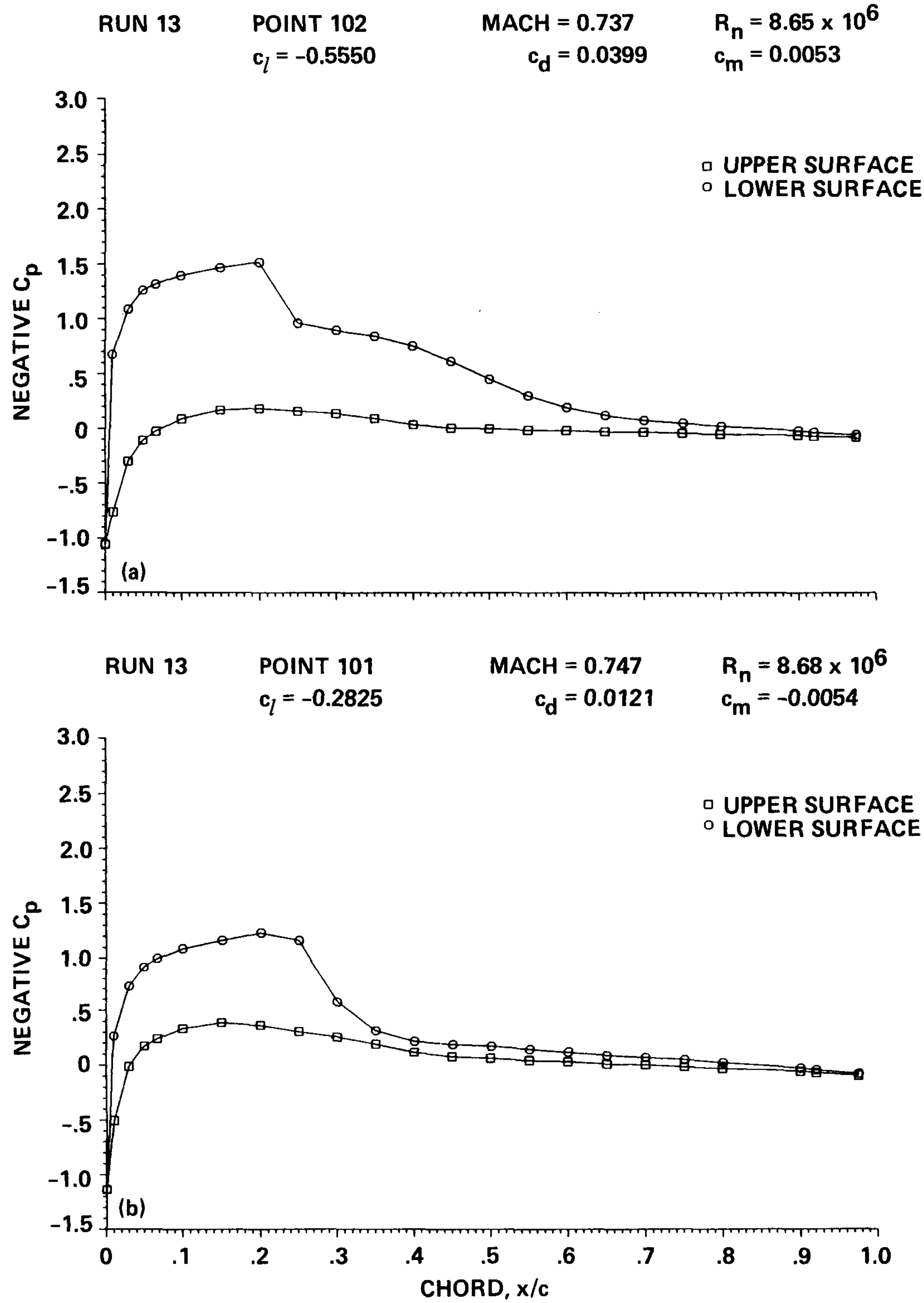

Figure 12.– Chordwise pressure distribution of the OLS/TAAT airfoil, $M = 0.74$; (a) $\alpha_c = -3.42°$, (b) $\alpha_c = -1.72°$.

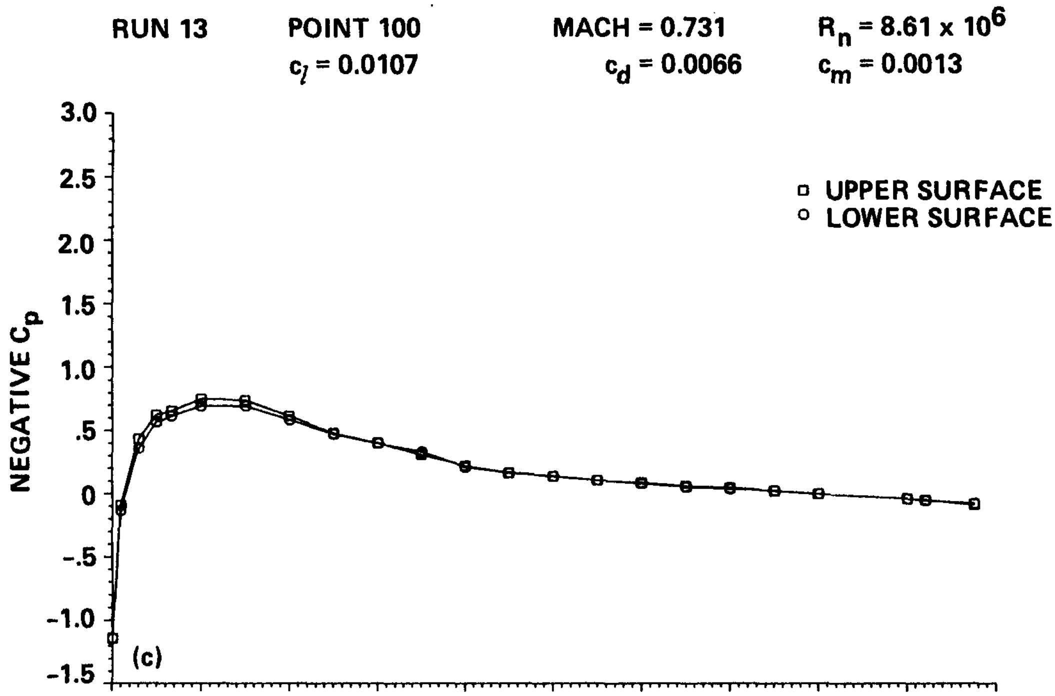

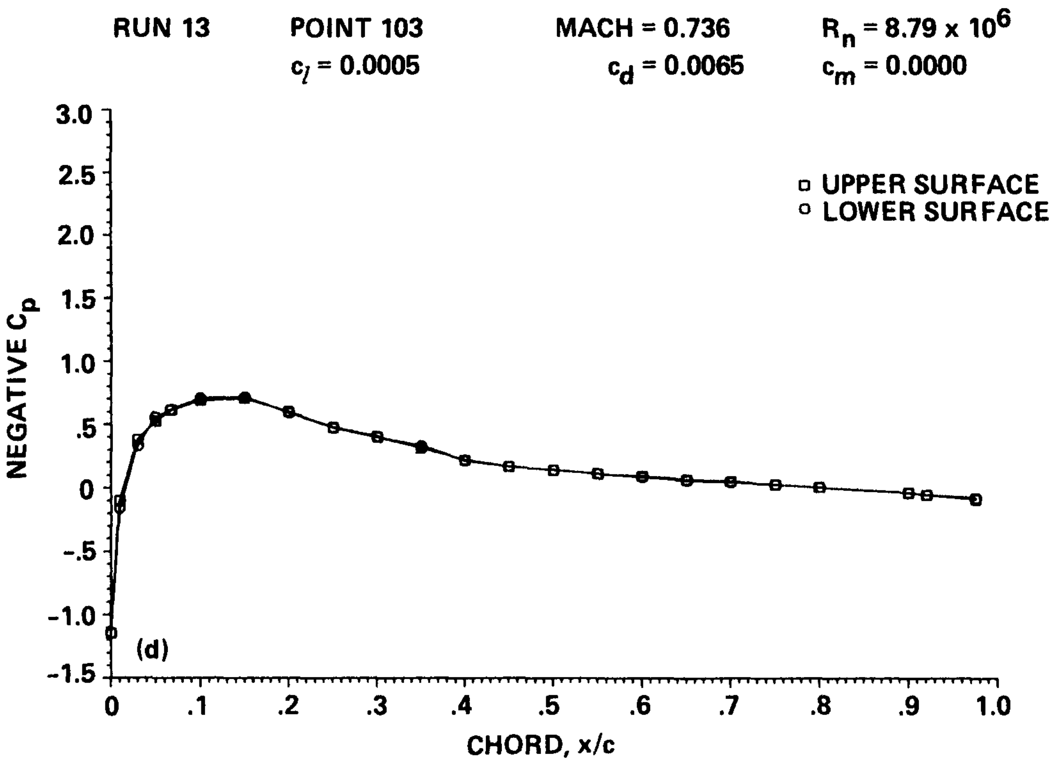

Figure 12.– Continued; (c) $\alpha_c = -0.02°$, (d) $\alpha_c = 0.00°$.

RUN 13 POINT 104 MACH = 0.735 $R_n = 8.92 \times 10^6$

$c_l = 0.3068$ $c_d = 0.0121$ $c_m = 0.0076$

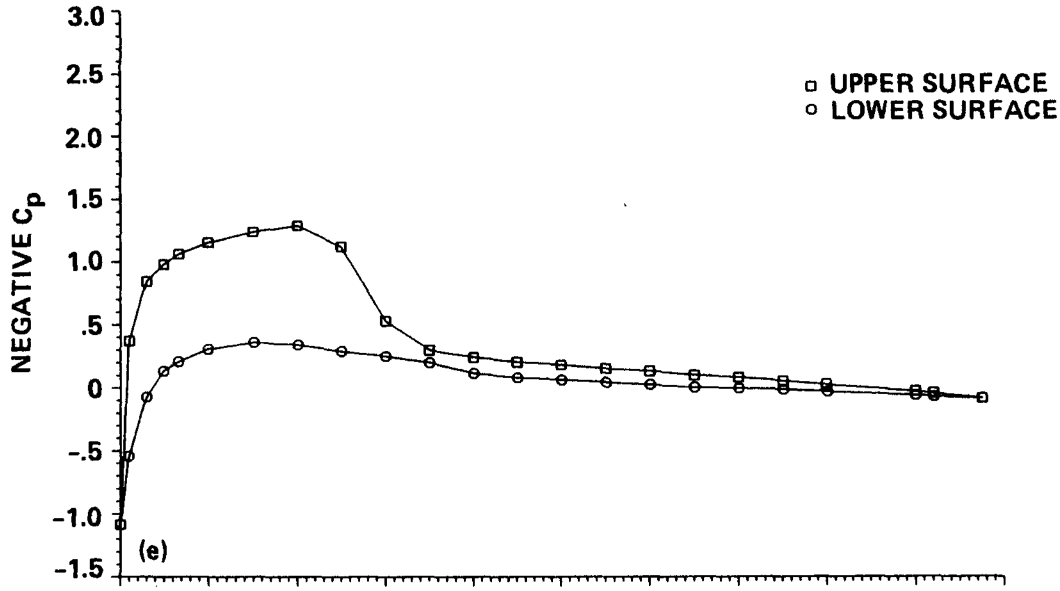

RUN 13 POINT 105 MACH = 0.732 $R_n = 9.01 \times 10^6$

$c_l = 0.5723$ $c_d = 0.0427$ $c_m = -0.0007$

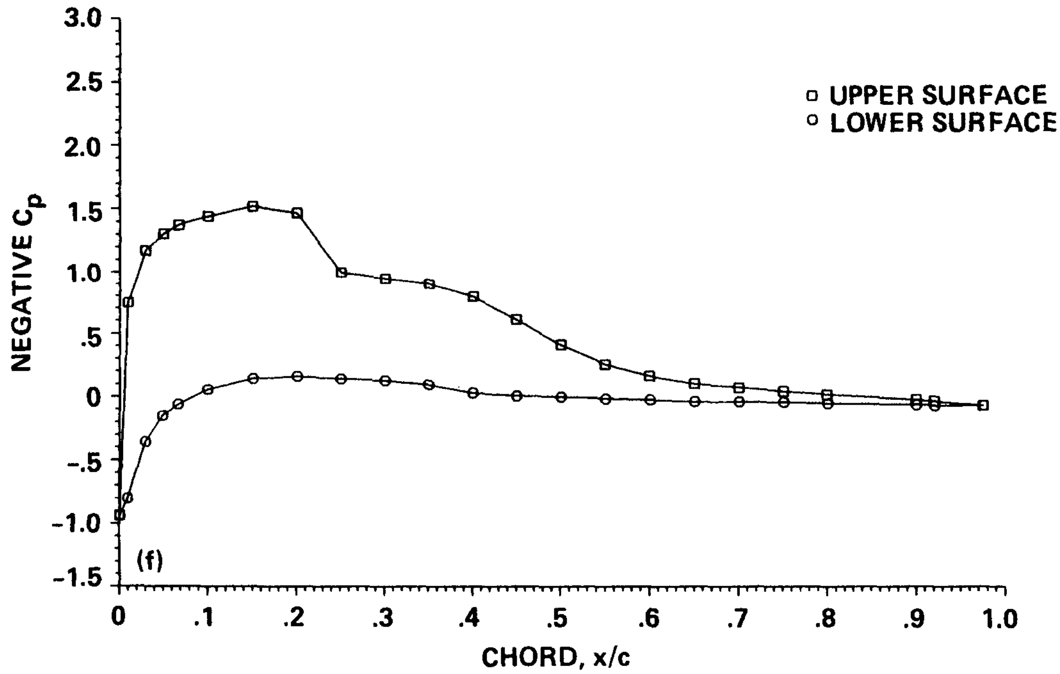

Figure 12.– Continued; (e) $\alpha_c = 1.71°$, (f) $\alpha_c = 3.45°$.

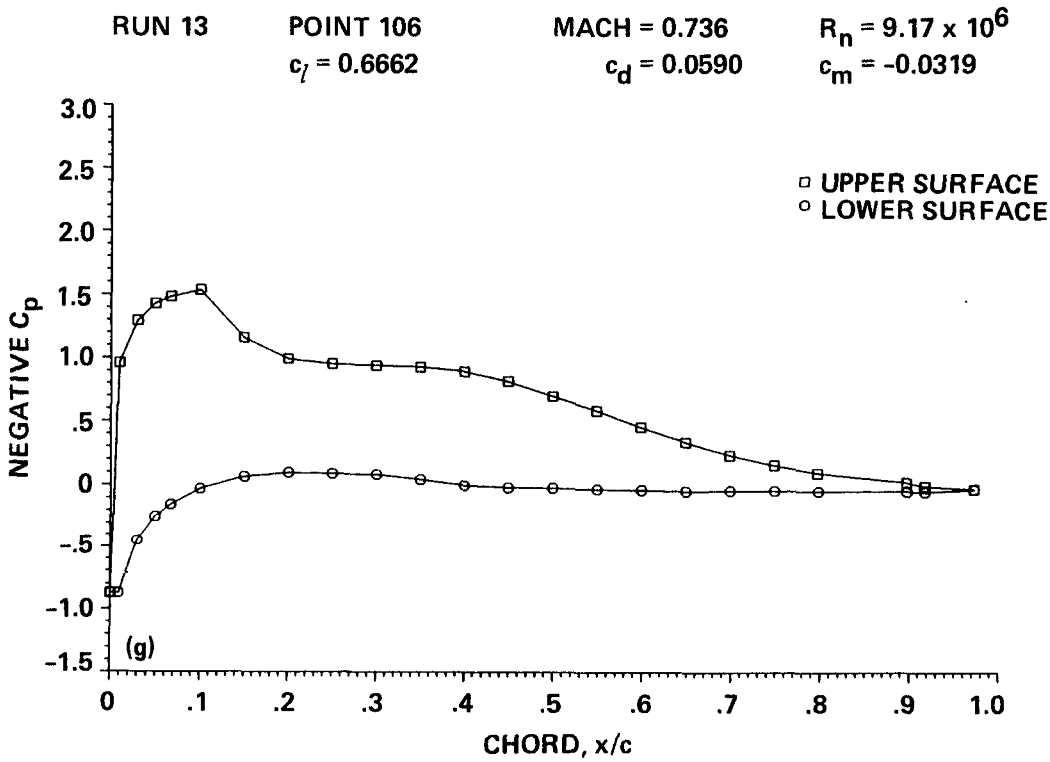

Figure 12.– Concluded; (g) $\alpha_c = 4.34°$.

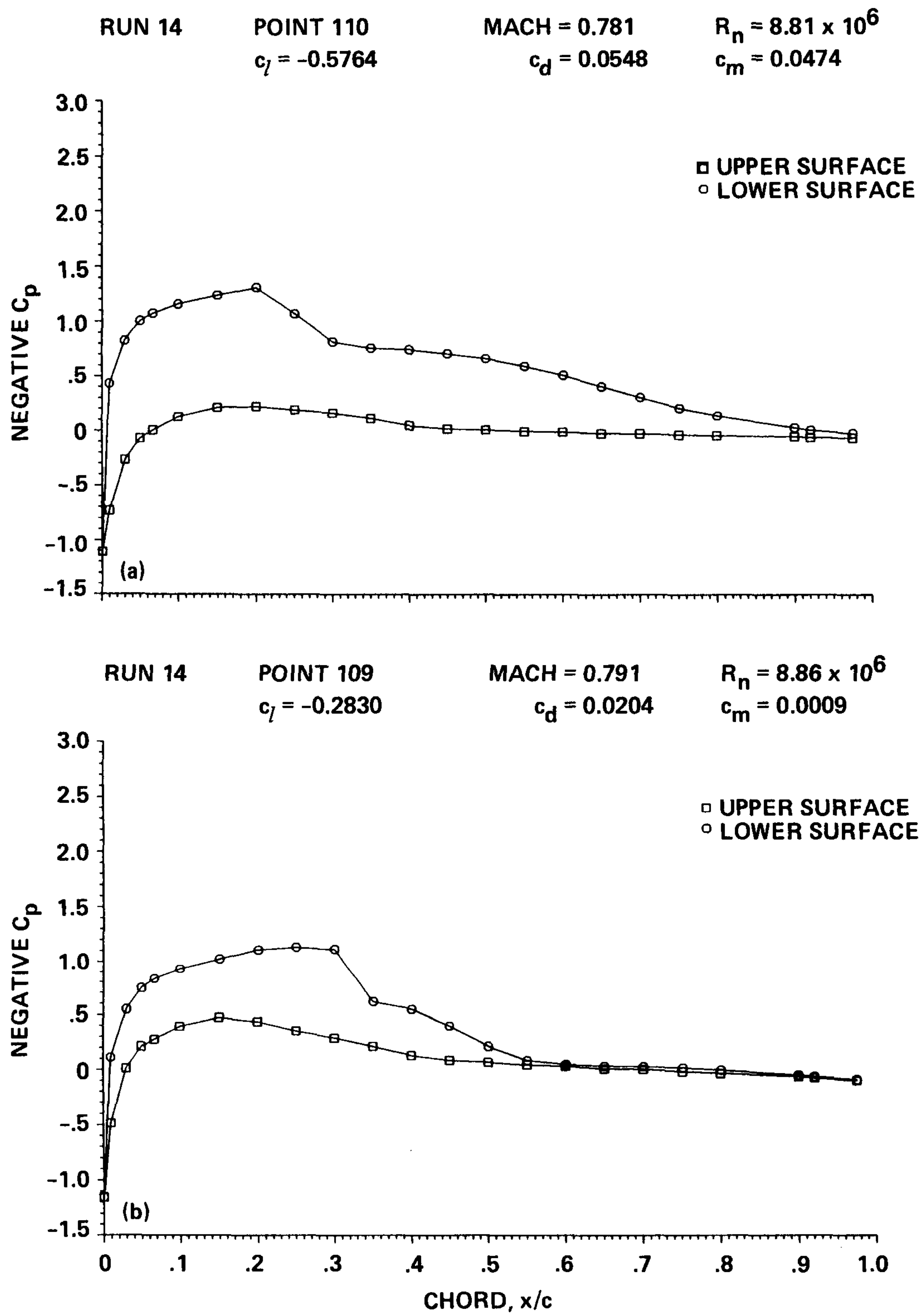

Figure 13.– Chordwise pressure distribution of the OLS/TAAT airfoil, $M = 0.79$; (a) $\alpha_c = -3.41°$, (b) $\alpha_c = -1.64°$.

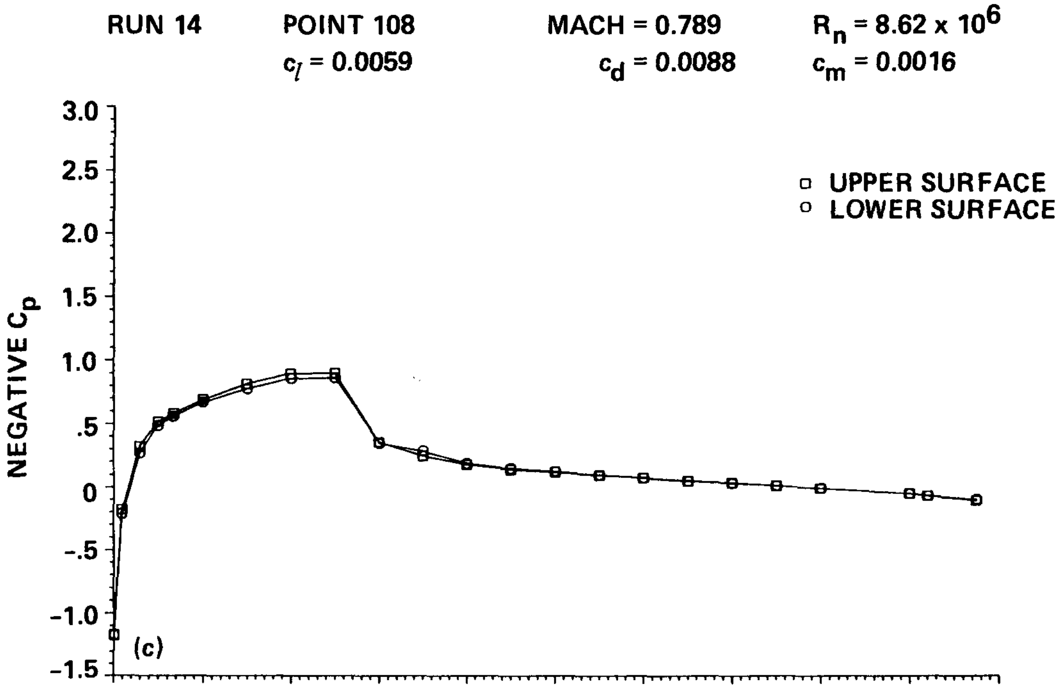

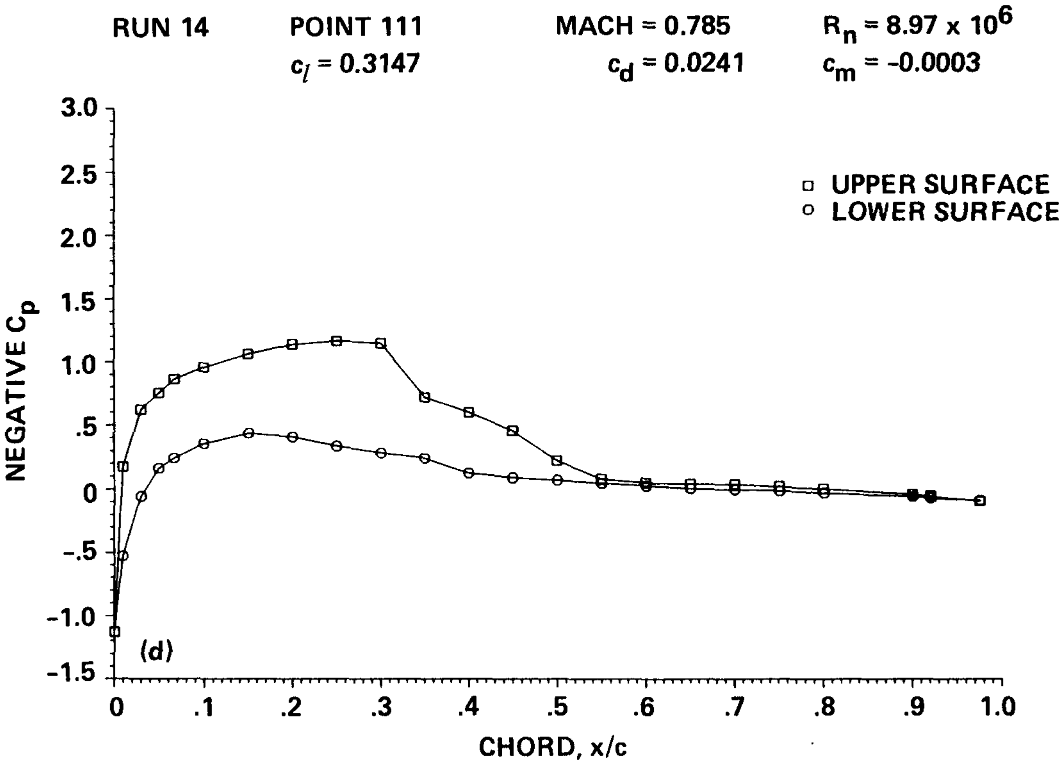

Figure 13.– Continued; (c) α_c = -0.07°, (d) α_c = 1.66°.

RUN 14 POINT 112 MACH = 0.783 $R_n = 9.11 \times 10^6$

$c_l = 0.4884$ $c_d = 0.0377$ $c_m = -0.0154$

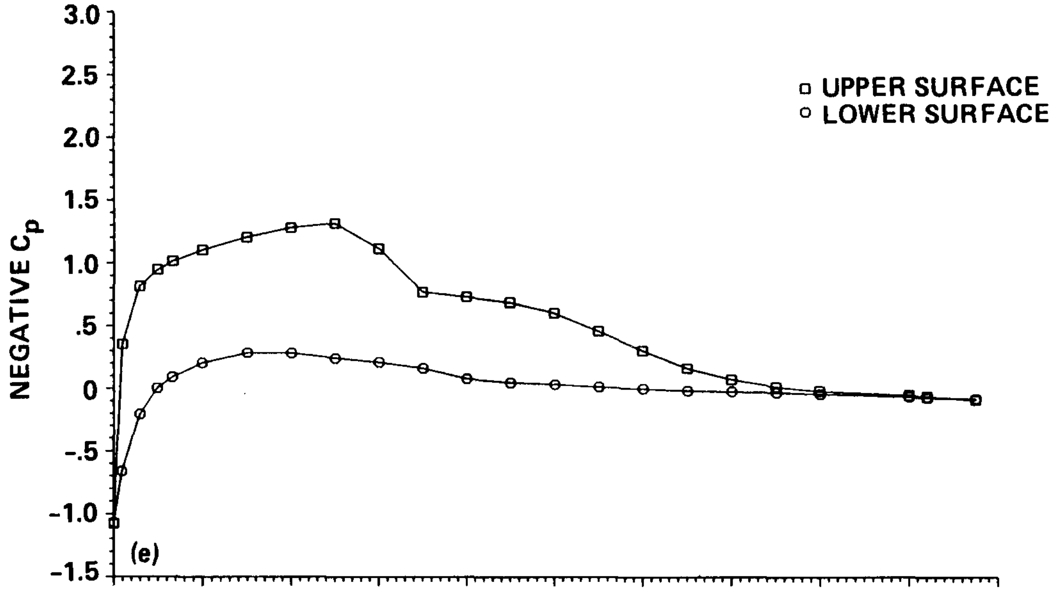

RUN 14 POINT 113 MACH = 0.781 $R_n = 9.15 \times 10^6$

$c_l = 0.6001$ $c_d = 0.0529$ $c_m = -0.0440$

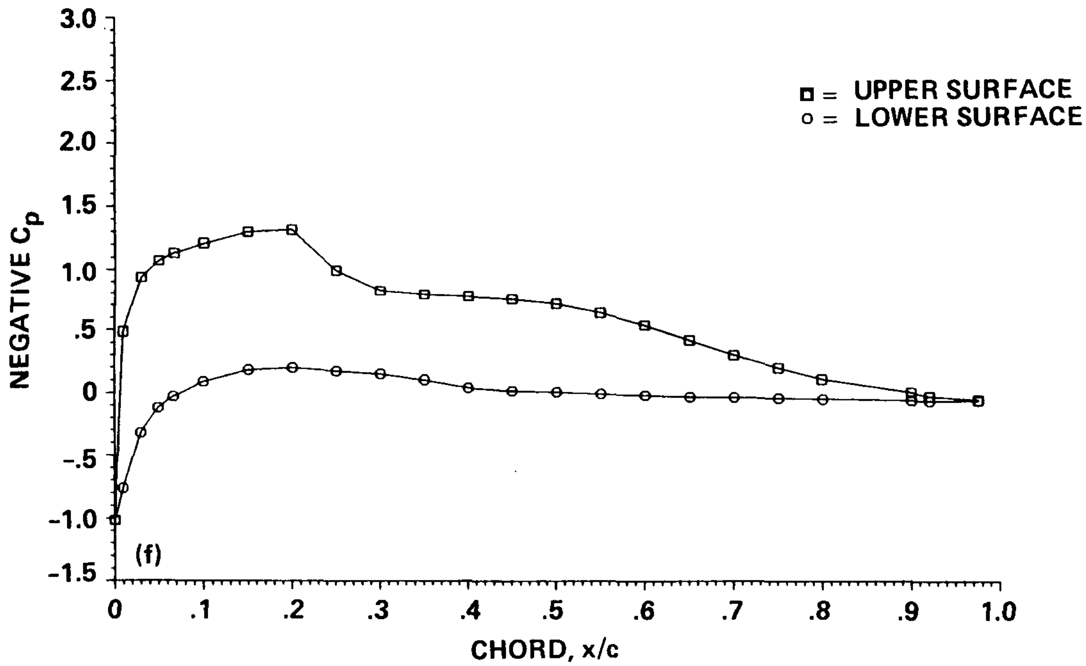

Figure 13.– Concluded; (e) $\alpha_c = 2.54°$, (f) $\alpha_c = 3.39°$.

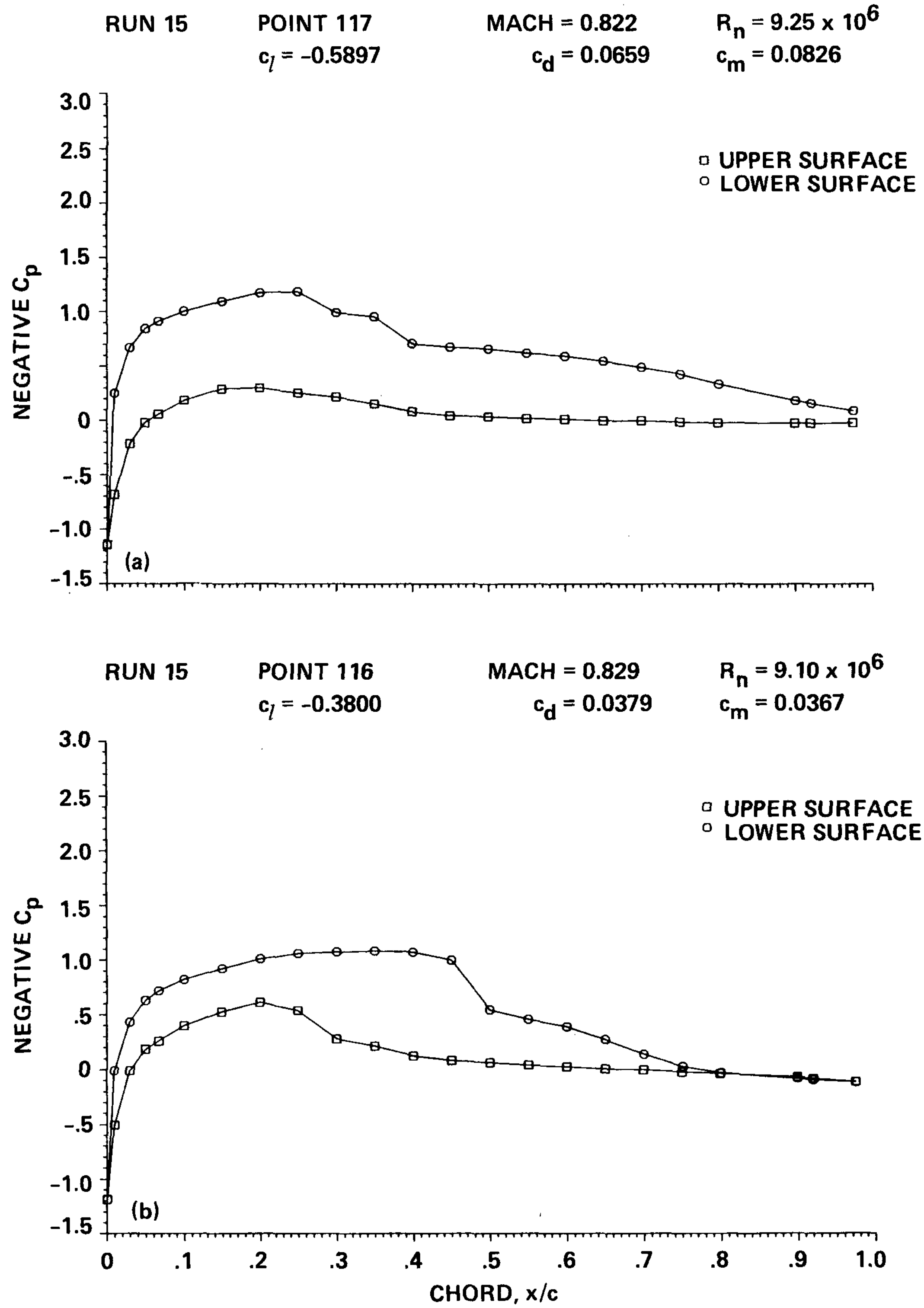

Figure 14.– Chordwise pressure distribution of the OLS/TAAT airfoil, $M = 0.84$; (a) $\alpha_c = -3.29°$, (b) $\alpha_c = -1.73°$.

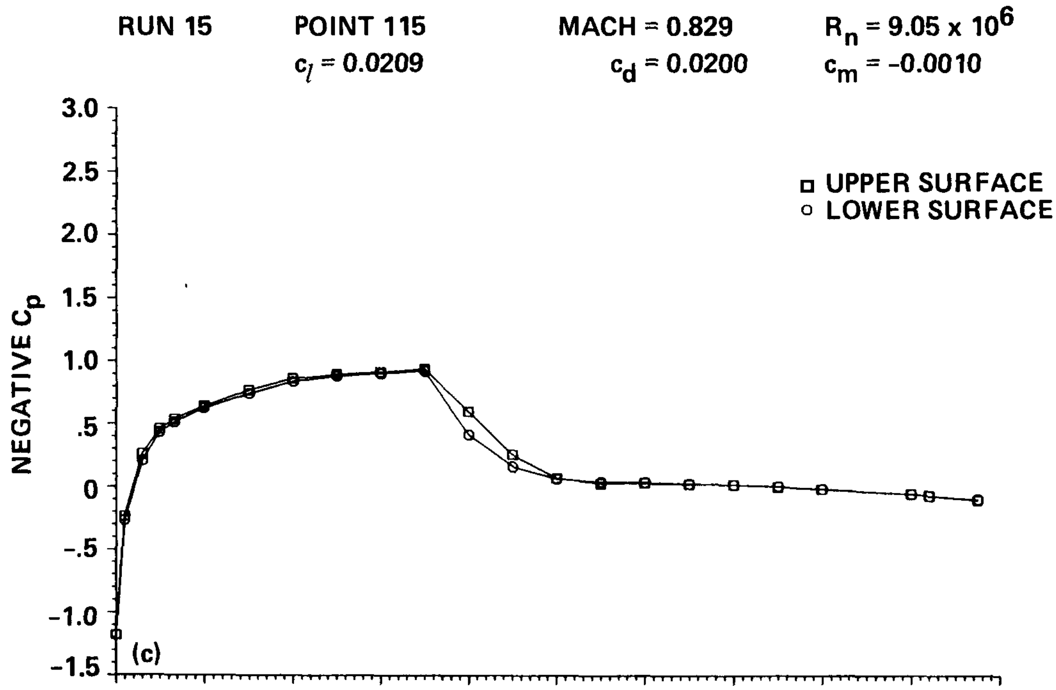

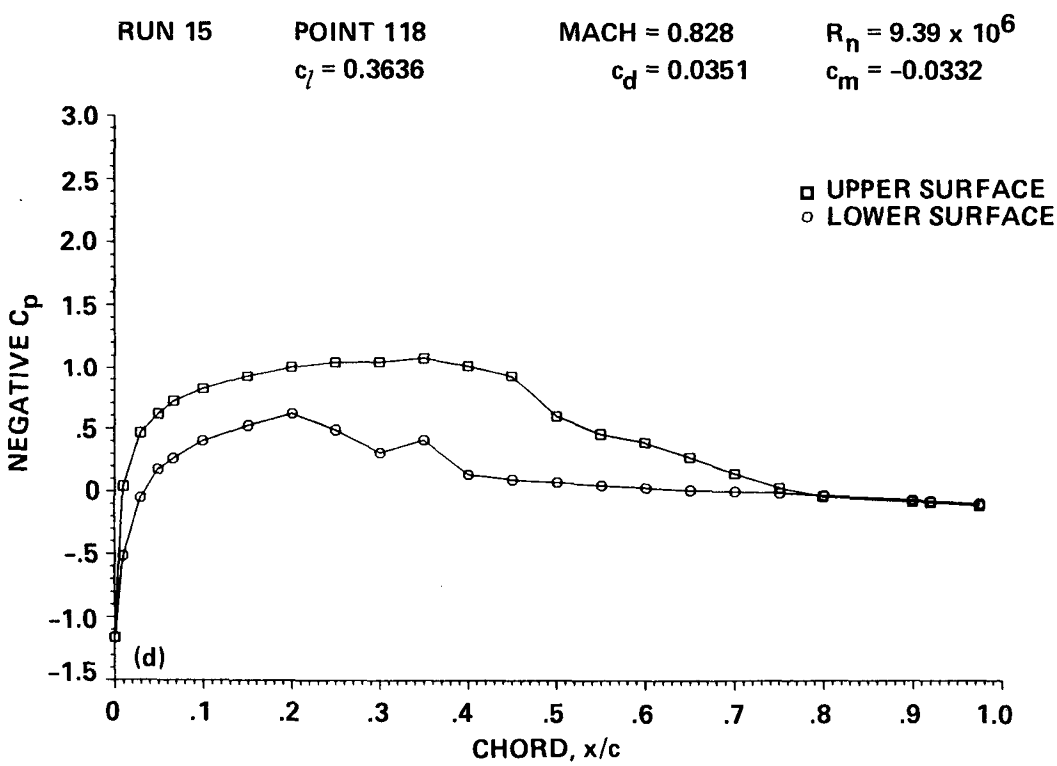

Figure 14.– Continued; (c) $\alpha_c = -0.05°$, (d) $\alpha_c = 1.64°$.

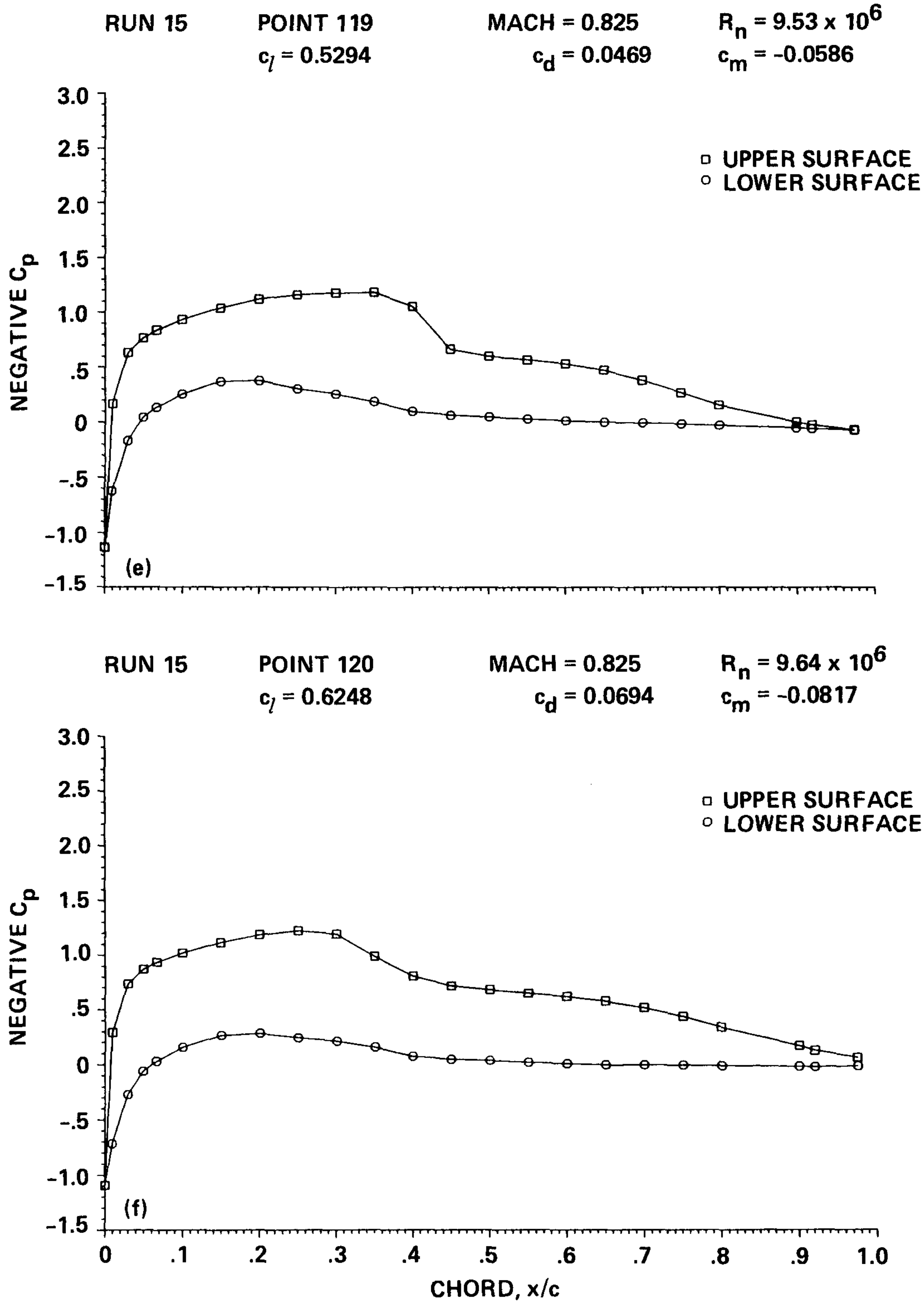

Figure 14.– Concluded; (e) $\alpha_c = 2.47°$, (f) $\alpha_c = 3.44°$.

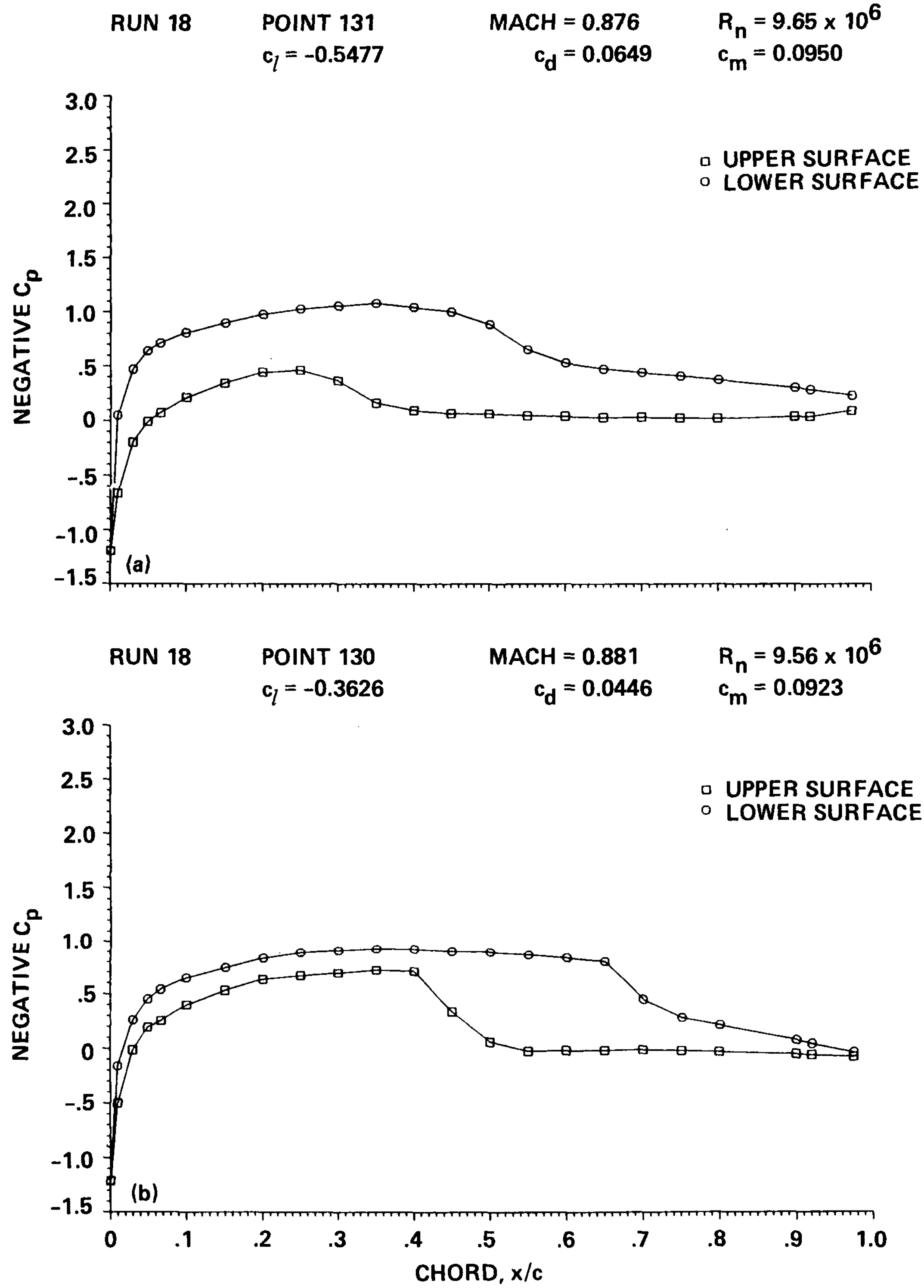

Figure 15.– Chordwise pressure distribution of the OLS/TAAT airfoil, $M = 0.88$; (a) $\alpha_c = -3.49°$, (b) $\alpha_c = -1.65°$.

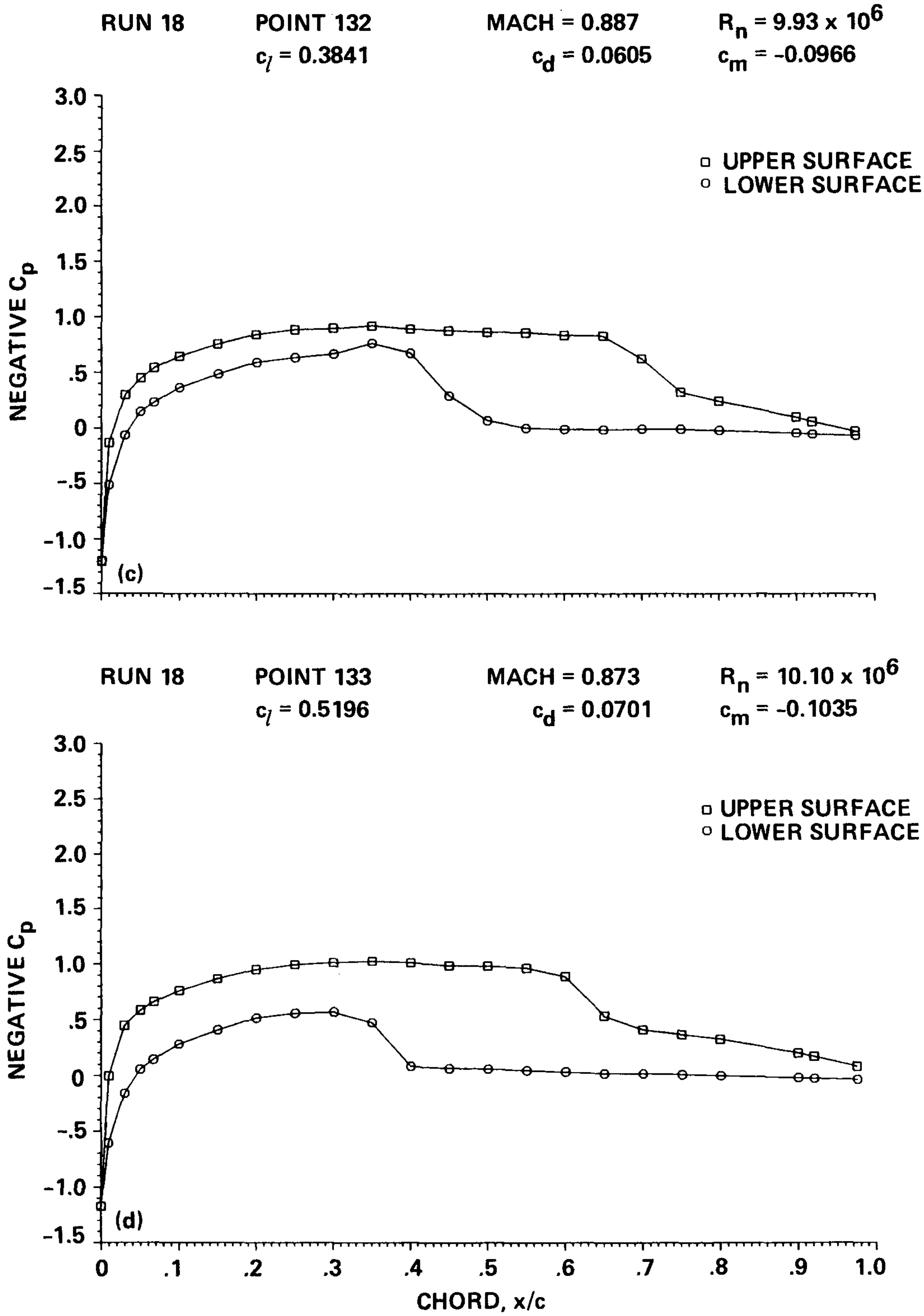

Figure 15.– Concluded; (c) $\alpha_c = 1.64°$, (d) $\alpha_c = 2.54°$.

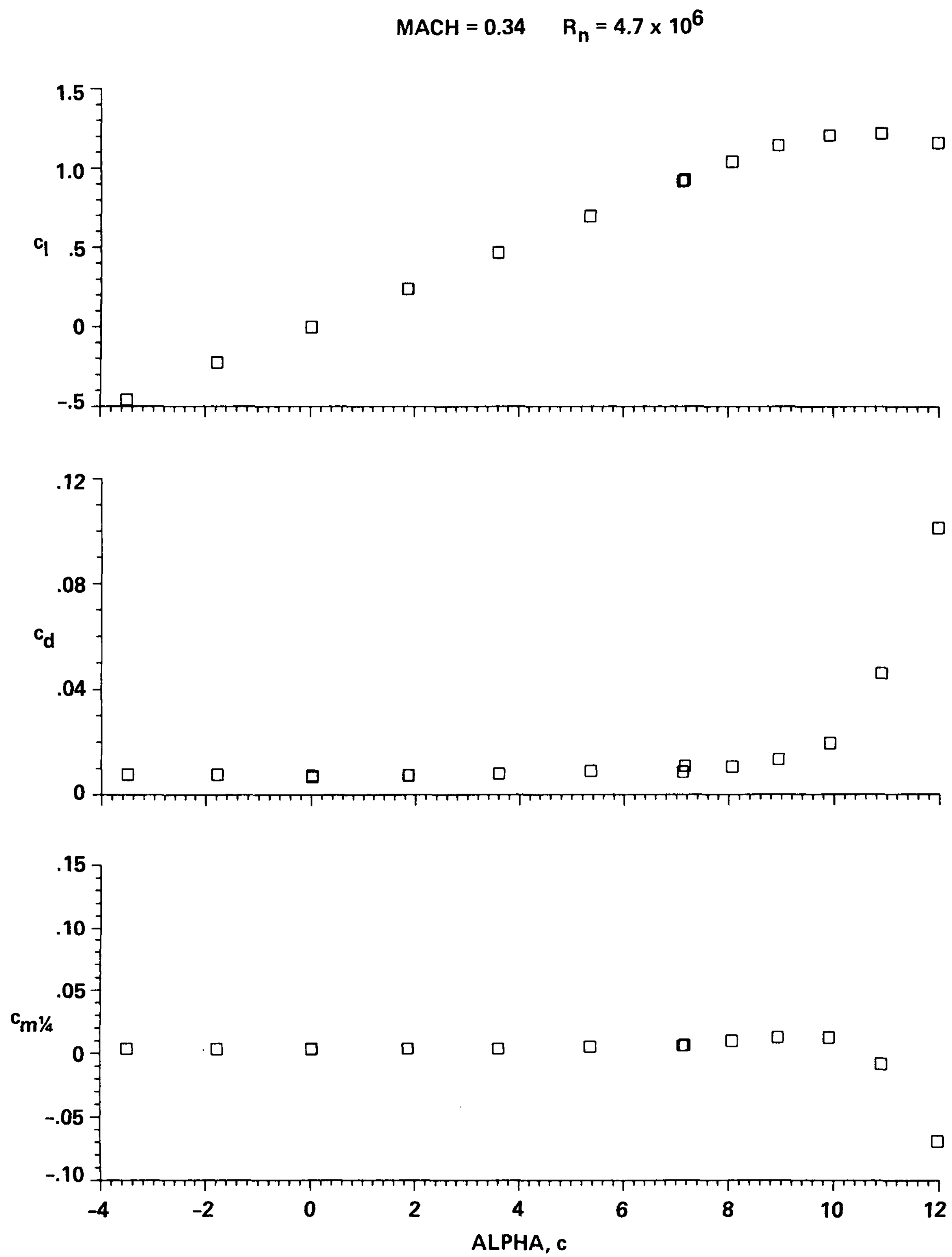

Figure 16.– Aerodynamic characteristics of the OLS/TAAT airfoil, $M = 0.34$, $R_n = 4.7 \times 10^6$.

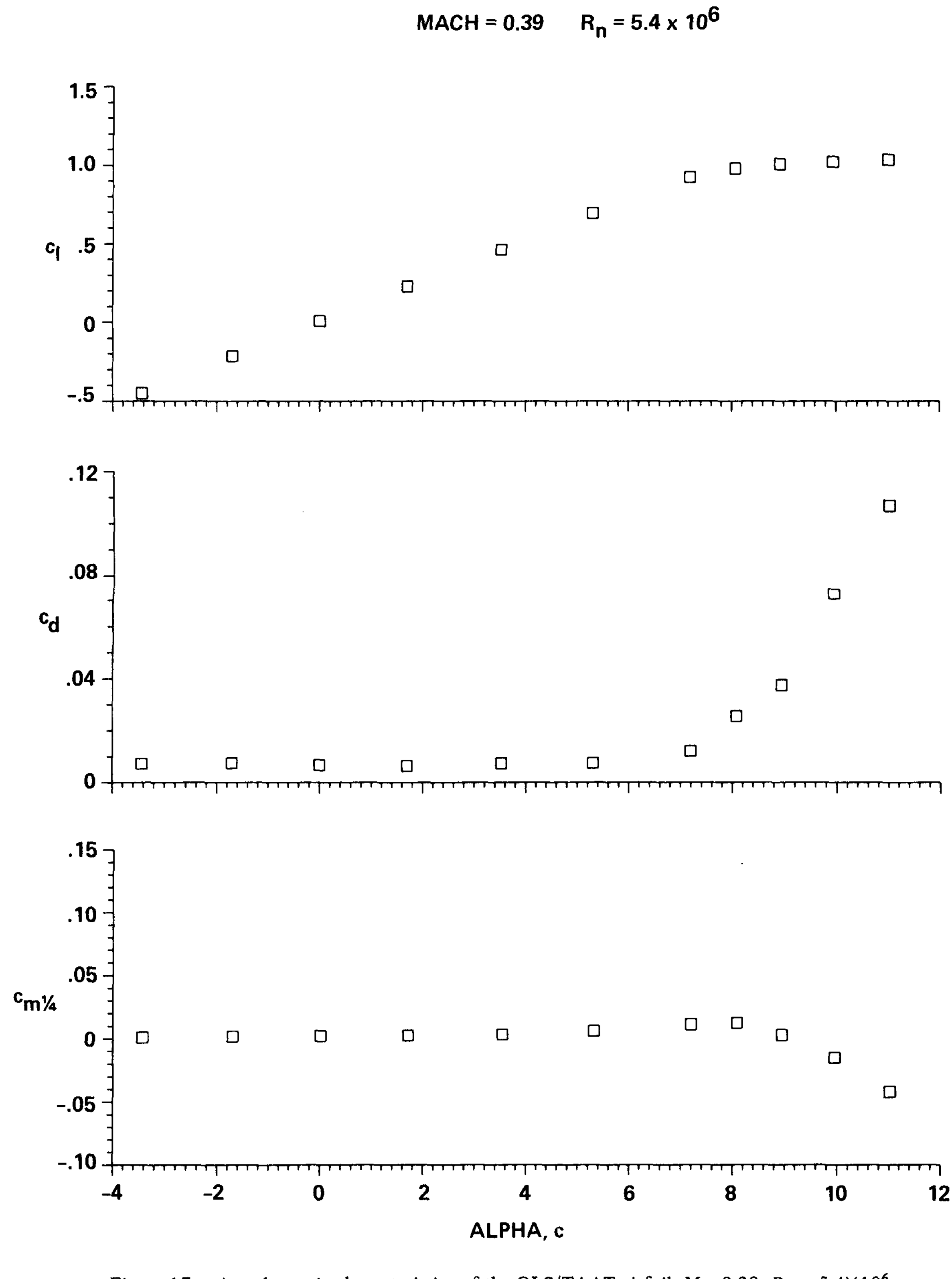

Figure 17.– Aerodynamic characteristics of the OLS/TAAT airfoil, $M = 0.39$, $R_n = 5.4 \times 10^6$.

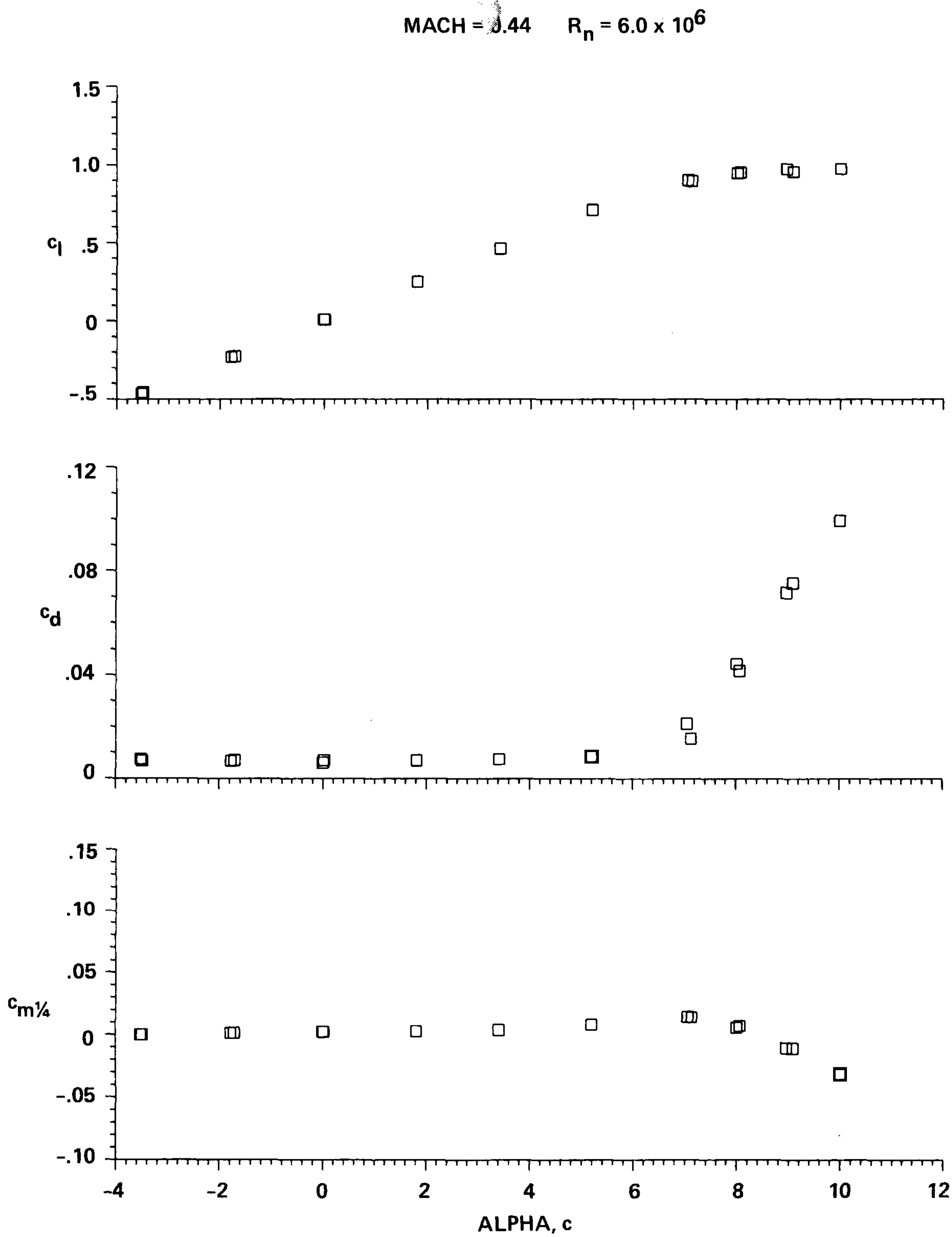

Figure 18.– Aerodynamic characteristics of the OLS/TAAT airfoil, $M = 0.44$, $R_n = 6.0\times10^6$.

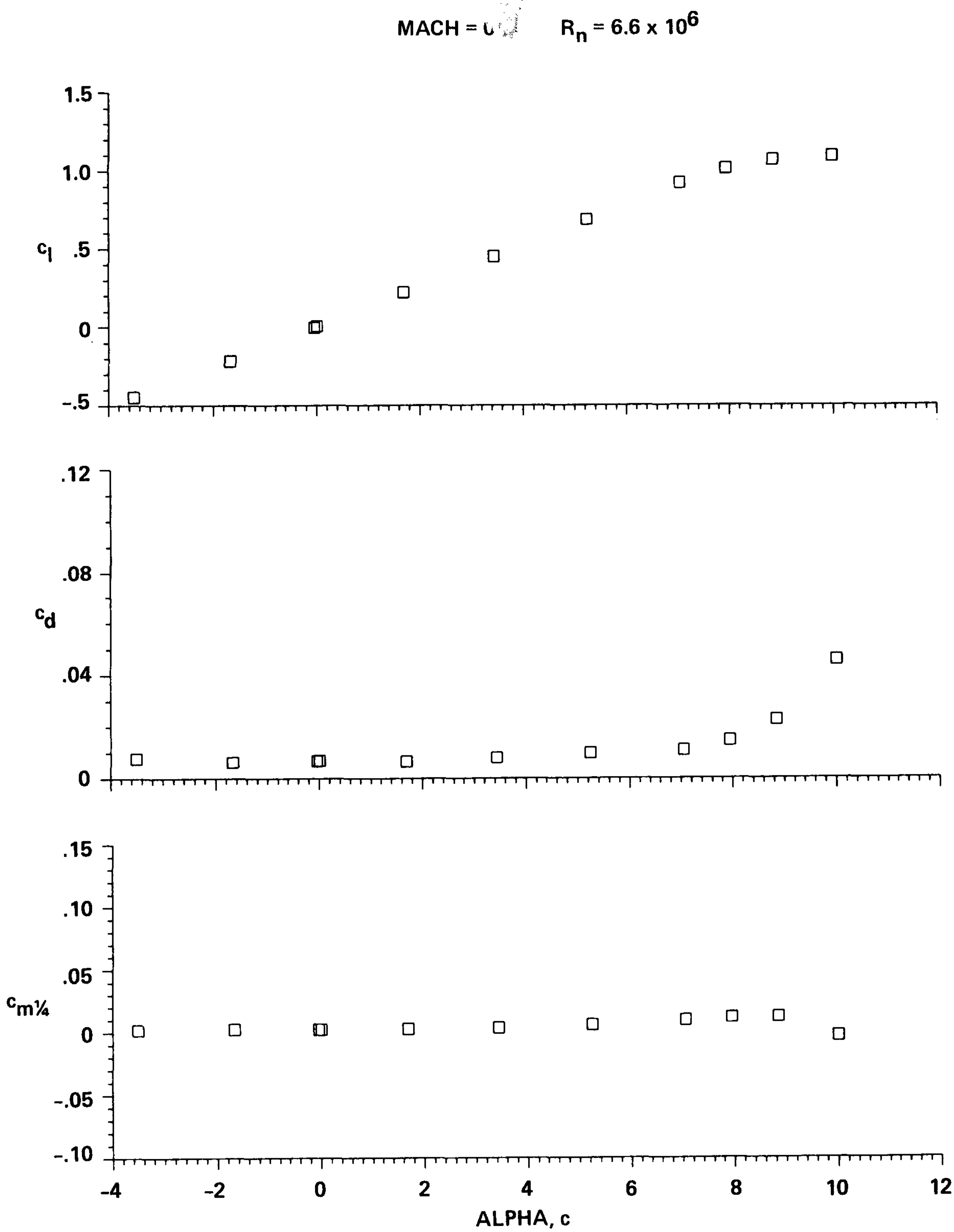

Figure 19.– Aerodynamic characteristics of the OLS/TAAT airfoil, $M = 0.49$, $R_n = 6.6 \times 10^6$.

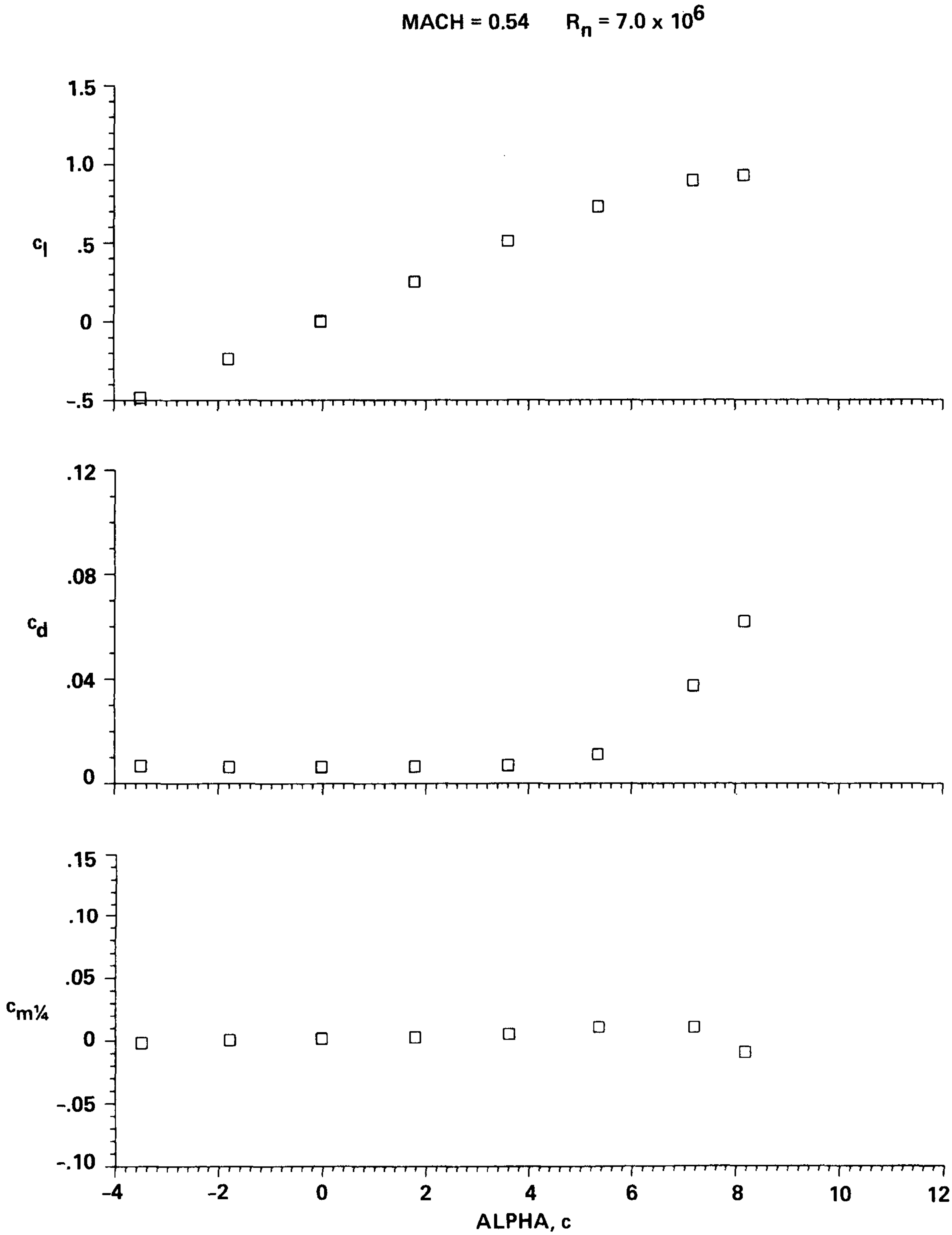

Figure 20.– Aerodynamic characteristics of the OLS/TAAT airfoil, $M = 0.54$, $R_n = 7.0 \times 10^6$.

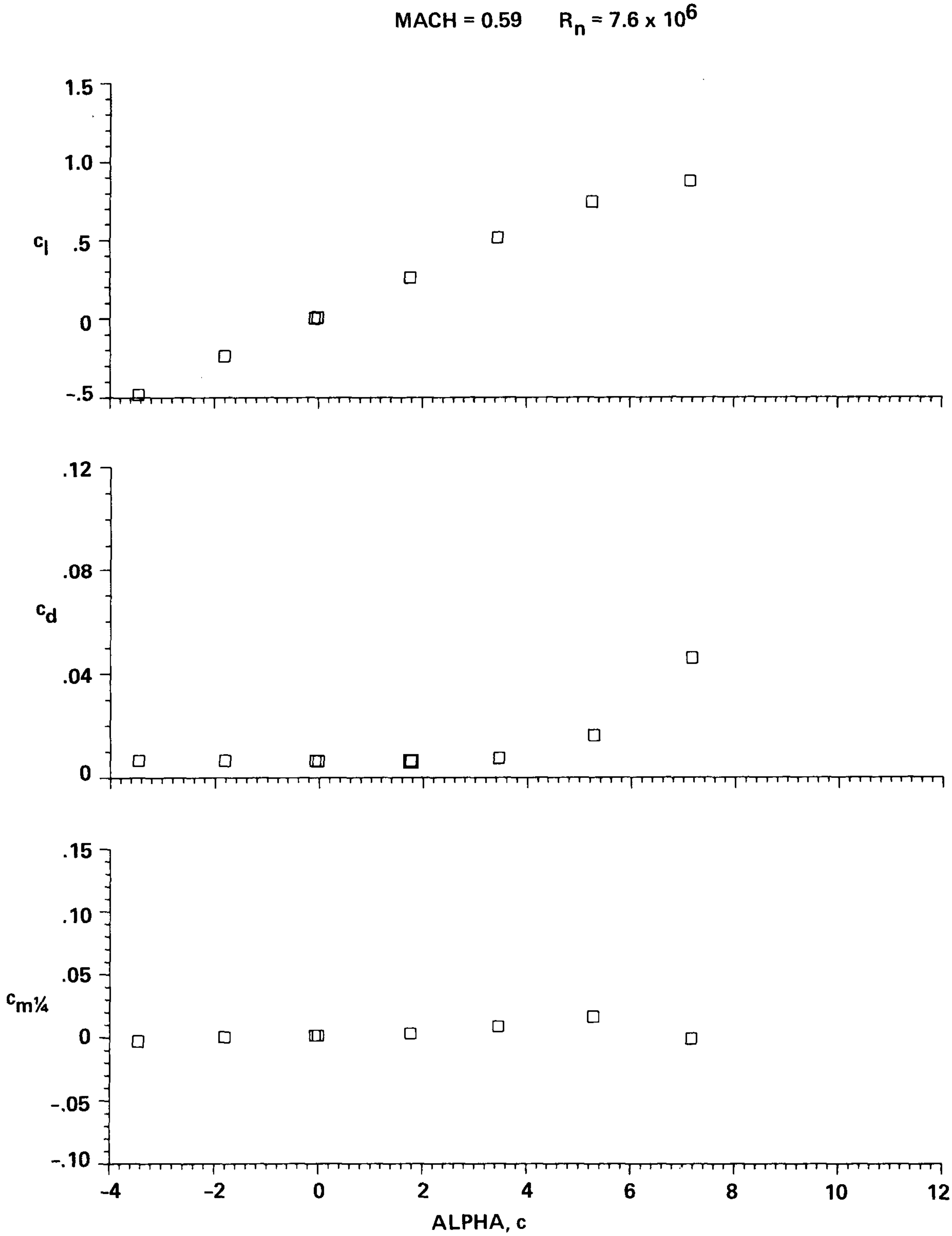

Figure 21.– Aerodynamic characteristics of the OLS/TAAT airfoil, $M = 0.59$, $R_n = 7.6 \times 10^6$.

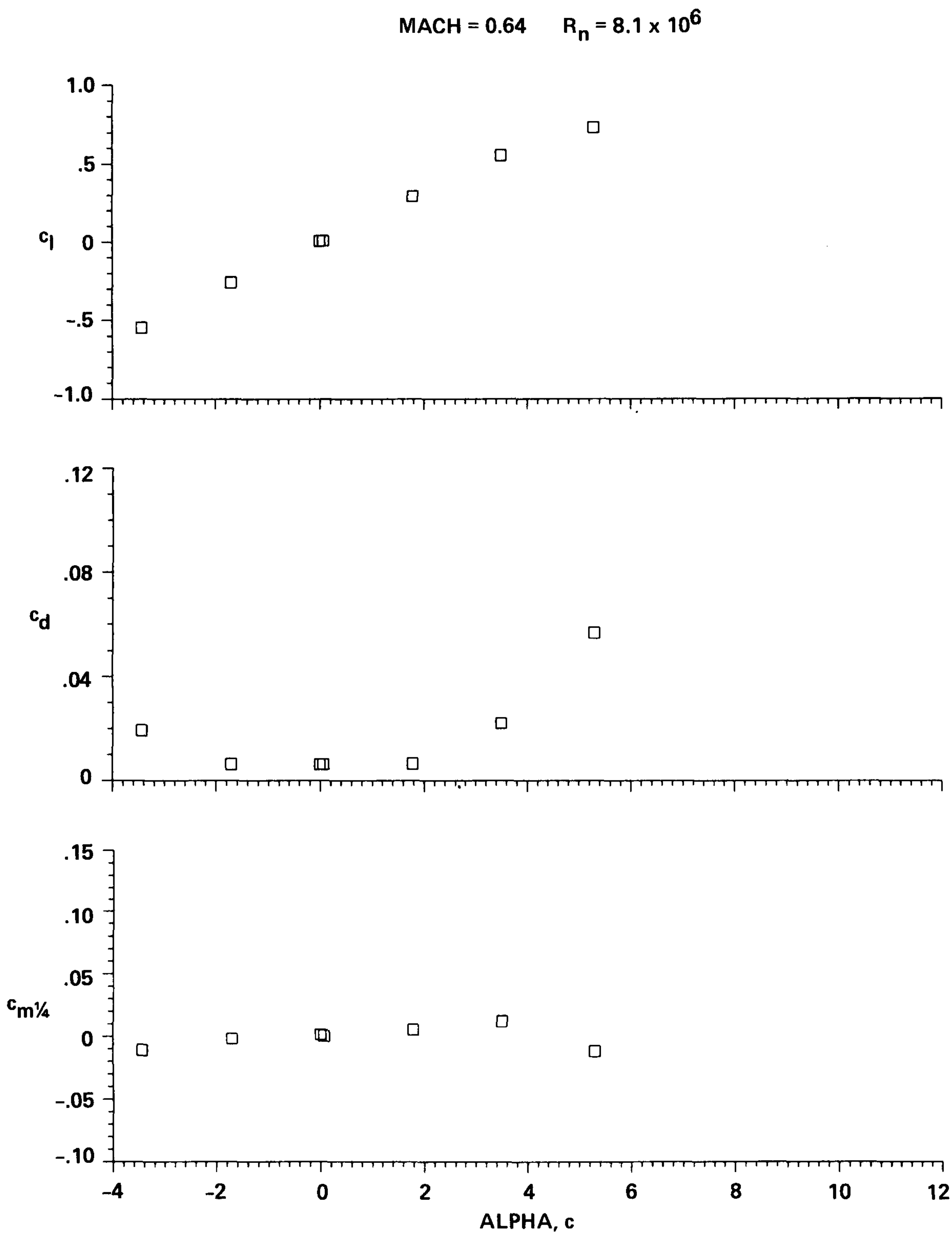

Figure 22.– Aerodynamic characteristics of the OLS/TAAT airfoil, $M = 0.64$, $R_n = 8.1 \times 10^6$.

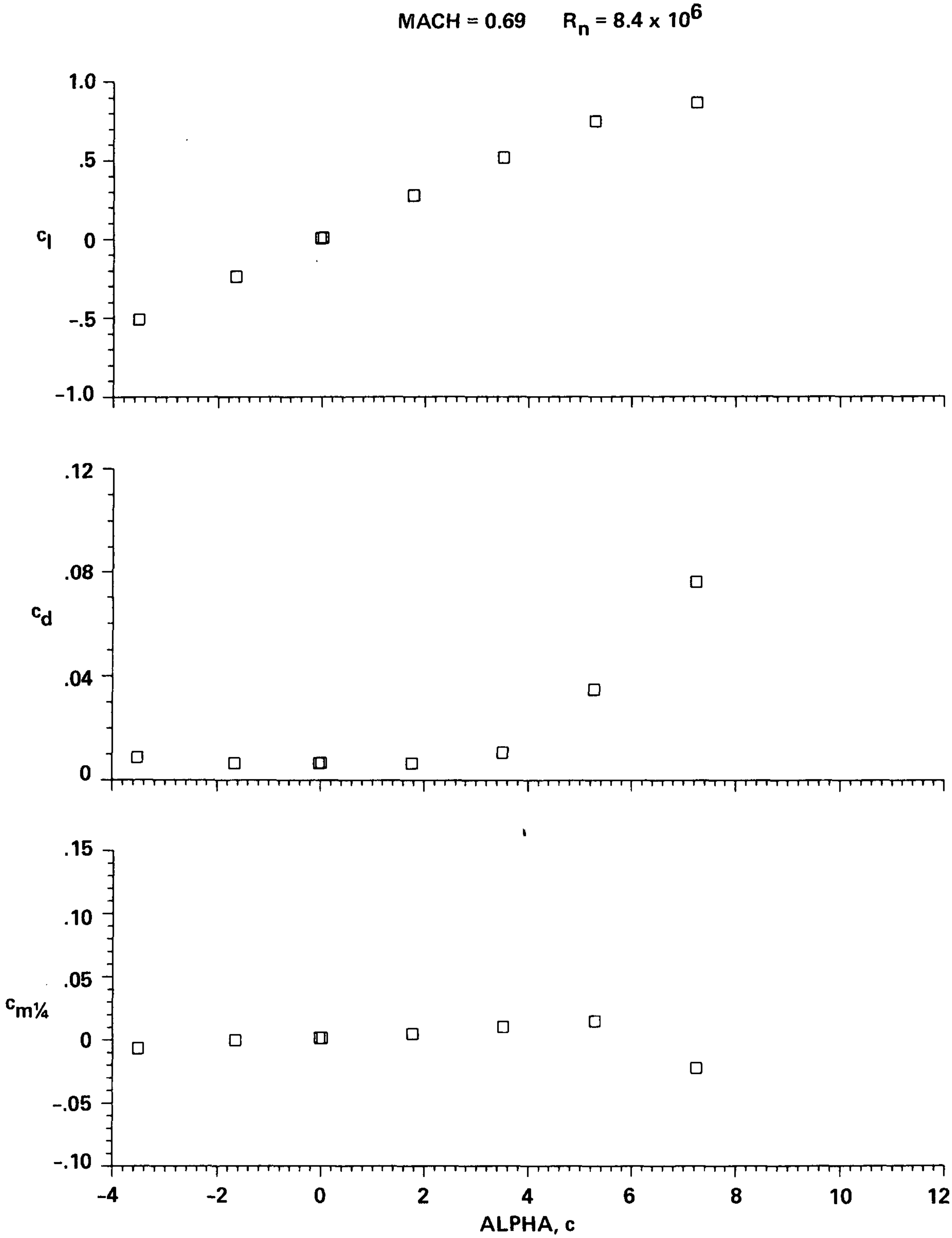

Figure 23.– Aerodynamic characteristics of the OLS/TAAT airfoil, $M = 0.69$, $R_n = 8.4 \times 10^6$.

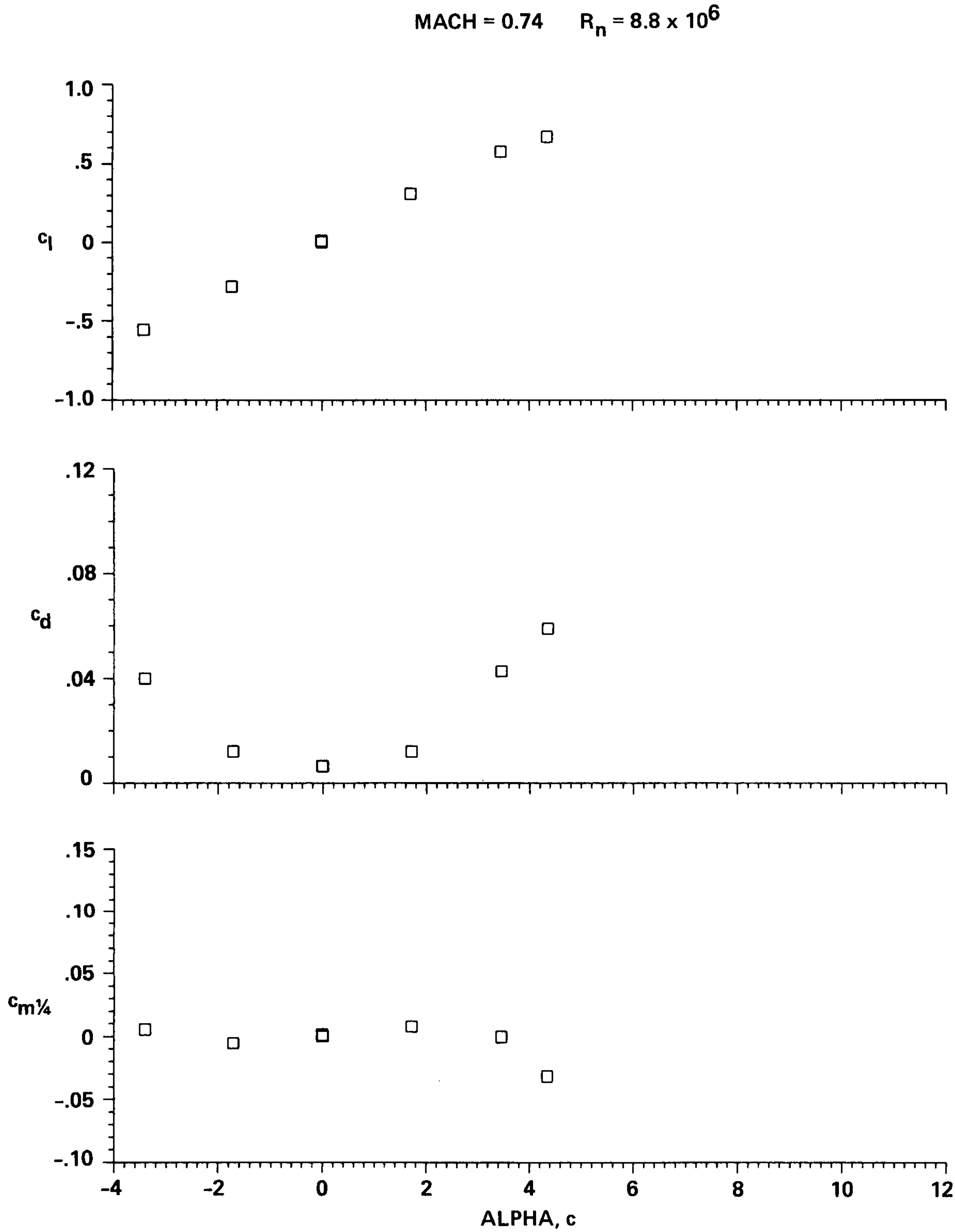

Figure 24.– Aerodynamic characteristics of the OLS/TAAT airfoil, $M = 0.74$, $R_n = 8.8 \times 10^6$.

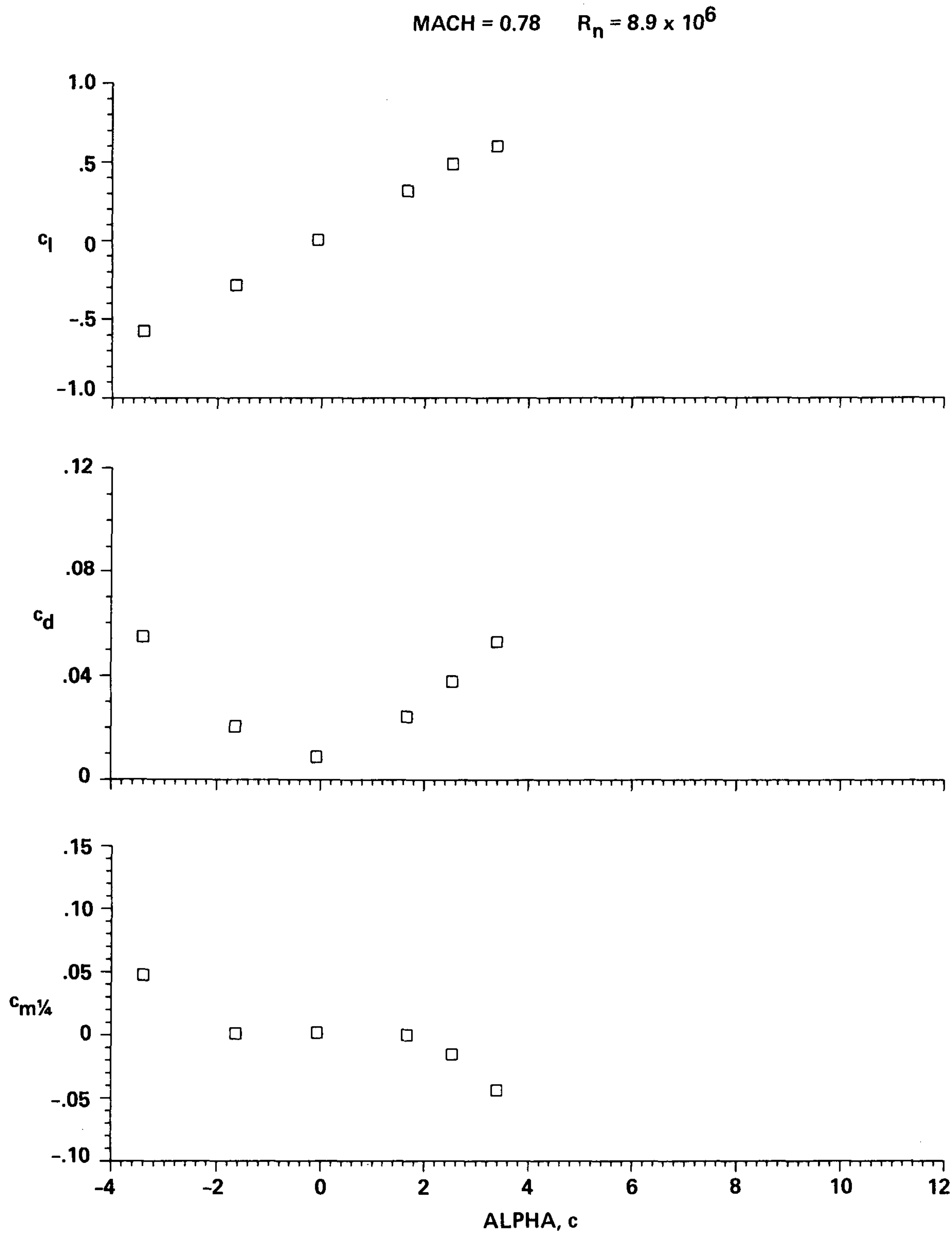

Figure 25.– Aerodynamic characteristics of the OLS/TAAT airfoil, $M = 0.78$, $R_n = 8.9 \times 10^6$.

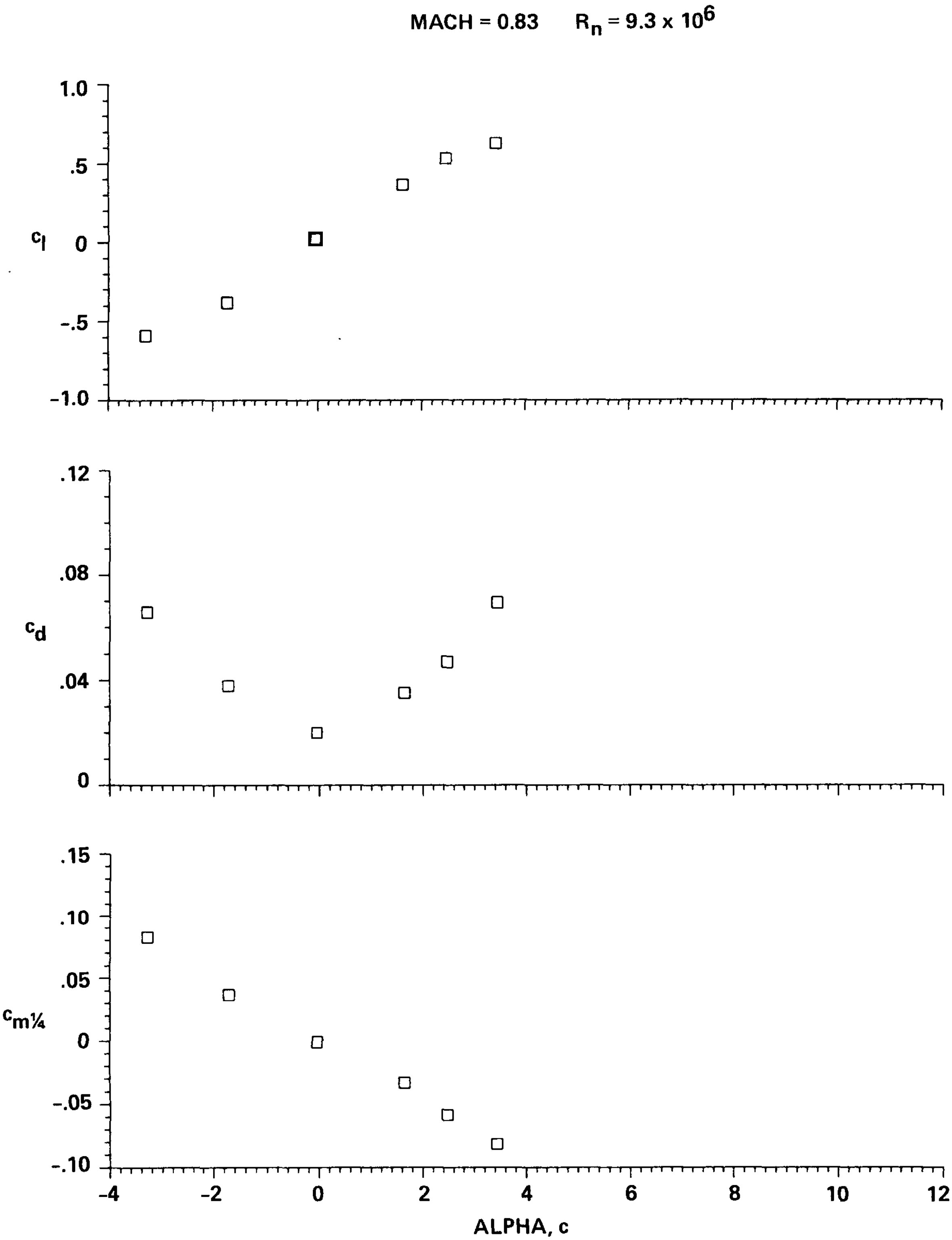

Figure 26.– Aerodynamic characteristics of the OLS/TAAT airfoil, $M = 0.83$, $R_n = 9.3 \times 10^6$.

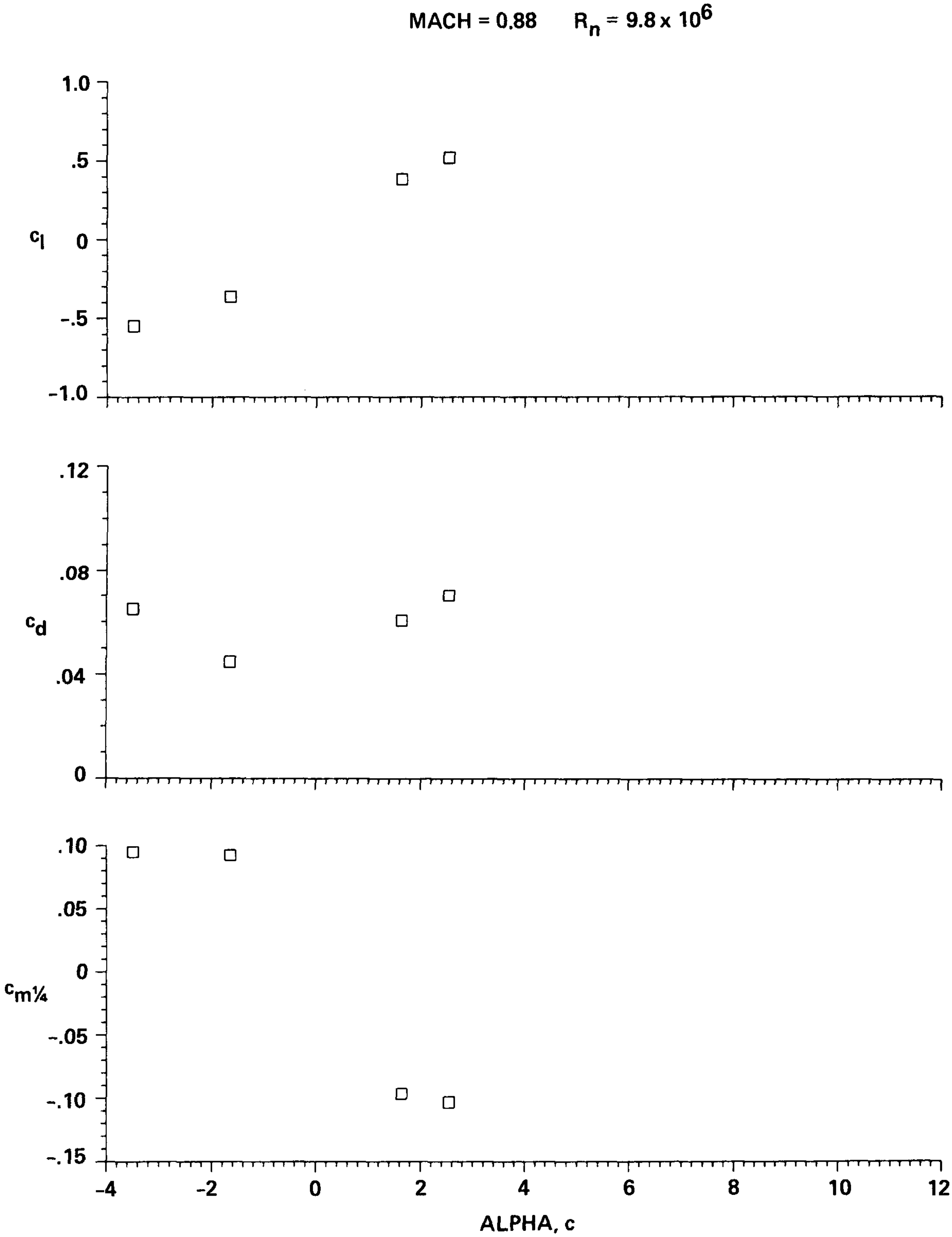

Figure 27.– Aerodynamic characteristics of the OLS/TAAT airfoil, $M = 0.88$, $R_n = 9.8 \times 10^6$.